Universitat de Girona

DYNAMICS OF HYDROTHERMAL PLUMES IN LAKE BANYOLES

Marianna SOLER ORTEGA

ISBN: 978-84-691-5678-0
Dipòsit legal: GI-1098-2008

Dynamics of hydrothermal plumes in Lake Banyoles

Universitat de Girona

Marianna Soler

2008

Na **Teresa Serra i Putellas**, i En **Jordi Colomer i Feliu**, professors titulars del Departament de Física de la Universitat de Girona,

CERTIFIQUEM que la tesi doctoral que aquí es presenta, i porta el títol de Dynamics of hydrothermal plumes in *Lake Banyoles*, ha estat realitzada sota la nostra direcció, per na **Marianna Soler i Ortega**, a fi d'optar al grau de Doctora pel doctorat en Ciències Experimentals i Sostenibilitat (línia de Física Ambiental)

Girona, 1 d'abril de 2008

Signat: Teresa Serra i Putellas Jordi Colomer i Feliu

Als meus “tres nens”

Als meus pares

Acknowledgments

Many people have contributed, in many ways, to my work. Here I would like to express my gratitude to all of them.

A la Teresa i a en Jordi els vull agrair la confiança que sempre han tingut en mi i els ànims constants. El seu ajut i coneixement han estat inestimables. Més enllà de tutors han esdevingut els meus amics.

A en Javi, qui em va ajudar a recollir les dades en les campanyes realitzades a l'estany de Banyoles i qui sempre em va ajudar quan em va fer falta.

As part of the project, I was fortunate to spend three months at the Geophysical Fluid Dynamics Laboratory, Princeton University, under the guidance of Professor Sonya Legg. This could be carried out by a financial support from the Generalitat de Catalunya , (grant 2004BE00073). Also, I would like to thanks her and her family their kindness during my stay.

A en Xavier Casamitjana, l'Esperança Gacia i en Ramon Julià per l'ajuda en les campanyes realitzades a Banyoles.

Al Capità Joan Coromines per la seva ajuda en les campanyes i el material utilitzat.

Als meus companys de despatx: Xevi, Jesús i Lluïsa. Amb qui he compartit els maldecaps i les alegries diàries en la realització d'aquesta tesi a l'hora del cafè.

A en Manuel pels dubtes de Matlab resolts i per la seva amistat.

A en Romualdo, per la seva ajuda en l'estudi de pluges i pel seu coneixement en models numèrics.

A la Farners i en Pere per la seva ajuda en els anàlisis realitzats al Laboratori d'aigües de la UdG.

A en Carles per la seva ajuda en algunes campanyes realitzades.. sobretot en els dies de vacances escolars i els ànims que m'ha donat en tot moment. A l'Albert i l'Oriol, només per ser-hi han fet que agafes forces per tirar endavant.

A la meva mare qui sempre m'ha transmès energia positiva. Als meus germans que m'han animat contínuament.

No voldria deixar-me a ningú. En certs moments, petits cops de mà són necessaris per a poder tirar endavant. A totes aquestes persones. Gràcies.

Marianna Soler, 2008

Table of contents

1 Introduction …….. 1

Reference List …… 11

2 Relationship between anomalous rainfall and sediment fluidization events in Lake Banyoles ……. …. 17

Paper 1: Anomalous rainfall and associated atmospheric circulation in the northeast Spanish Mediterranean area and its relationship to sediment fluidization events in a lake *Water Resour. Res.*, 43, W01404, doi:10.1029/2005WR004810.

Abstract ……..…… 18

Introduction ……..…… 18

Data and analysis……..…… 20

Results and discussion ……..…….. 23

Conclusions ……..……. 30

References……...… 30

3 Evolution of hydrothermal plumes in Lake Banyoles……... 33

3.1 Characterization of Buoyant jets…….. 34

3.2 Plume structure characterization…….…….... 35

3.3 Methods and Instrumentation .…… 38

3.3.1 Instrumentation

3.3.1.1 ADCP……... 40

3.3.1.2 CTD…..……. 41

3.3.1.3 LISST …….. 41

3.3.1.4 Fluoroprobe……..… 43

3.3.2 Methods

3.2.1 Sediment traps...…….... 43

3.2.2 Calibration ADCP- Backscatter ...……... 45

3.4 Water Temperature evolution……..……... 47

3.5 Fluidization events and their consequences 50
3.6 Sediment distribution 51
3.7 Temporal evolution of basins B1 and B2..... 53
3.7.1 Mixing Period. The end of the summer 54
3.7.2 Beginning the Stratified period..... 65
3.7.3 Stratified Period 66
3.7.4 Beginning the mixing Period 69
3.7.5 Mixing Period 70
3.8 Summary and Discussion
3.8.1 Basin B1..... 73
3.8.2 Basin B2 76
Reference List..... 81
Paper 2: Effects of a hydrothermal plume on the sedimentation rates in a karstic lake. *Geophysical Research Letters.* 10.1029/2002GL015368. 29 (21): 25-28. ISSN: 0094-8276..... 85
Paper 3: Sediment fluidization events in a lake caused by large monthly rainfalls, *Geophysical Research. Letters, 29*(8), doi: 10.1029/ 2001GL014299..... 89
Paper 4: Hydrothermal plumes trapped by thermal stratification, *Geophysical Research. Letters, 30*(21), 2092, doi: 0.1029/2003GL018131... 93
Paper 5: Behaviour and dynamics of a hydrothermal plume in Lake Banyoles, Catalonia, *Sedimentology 52*(4), 795-805..... 97

4 Single Plume convection in Lake Banyoles 111

Paper 5: Scaling analysis of single-plume convection from a hydrothermal source. Journal of Geophysical Research – Oceans (in press)
Abstract 112
Introduction..... 113
Methods..... 115
Model. Scale Estimates for circular convection 116
Experimental results and comparison with theory..... 117
Discussion..... 123
Appendix 125
Reference List..... 131

Tables…….….. 134
Figures……. 135

5 **Application of the MITgcm model. Localized convection source**.. 145
5.1 The Model...…….…..... 146
5.1.1 Non-hydrostatic ocean modeling ..……...… 147
5.1.2 Finite-volume methods and the representation of topography……. 148
5.1.3 High order, non-linear (scalar) advection schemes…...…….. 149
5.1.4 Model equations...……..…….. 150
5.2 Changes on the Model……..…..... 151
5.3 Running the Model……..….. 152
5.3.1 Lake stratification ...…….....… 153
5.3.2 Grid ...…….....… 154
5.4 Results of the Model……..…..... 155
5.4.1 Basin 1 and Basin 2 (behaving as B1) ……..…….. 156
5.4.1.1 Stratified period……..... 156
5.4.1.2 Mixed period……...……..... 164
5.4.2 Basin 2 (behaving as a single-plume)…...……..... 170
5.5 Conclusions...……..…..... 175
Reference List …… 177

6 **Summary and conclusions**……. 179
6.1 Relationship between sediment fluidization events and anomalous rainfall……..... 180
6.2 Basin 1…...……..…..... 181
6.3 Basin 2……..…..... 181
6.4 MITgcm numerical model..……..... 183
6.5 Suggestions for further work……..……. 184
Annex A …… 187
Annex B…….. 191

1 Introduction

Convection from isolated sources has received much attention because of its application to geophysical and engineering flows. Relevant examples include plumes (continuous sources of buoyancy) and thermals (fixed volumes of buoyant fluid). Man-made plumes include waste outfalls in oceans and chimney stacks in the atmosphere (List, E.J., 1982; Turner, J.S., 1973). In devices that eject buoyant fluid with some momentum, as the flow evolves, the buoyancy becomes the dominant driving force and can be defined as buoyant jets. Oceanic hydrothermal vents are an example of a natural flow driven by isolated buoyancy sources. They are formed in regions where upwelling magma from the Earth's interior solidifies at mid-ocean ridges to form new crust, thus transferring heat from magma to surrounding waters to create turbulent plumes (Lupton et al., 1985; Speer and Rona, 1989). Another case of geophysical interest is deep ocean convection, wherein predisposed regions of high-latitude oceans (known as "chimneys") become unstable due to intense

surface cooling and generate turbulent convection that can penetrate to depths of 2-4 km. Deep water in the oceans is cold, and the deepest water is the coldest, although salinity can complicate this simple picture (Veronis, 1972). In general, the oceans are stably stratified everywhere, except in top and bottom mixed layers; even polar oceans, which at first glance have only slight stratification, have stable stratification that has a valuable function: to form dense water masses that sink downward and spread out to low latitude regions with the purpose of redistributing the ocean heat.

Observations suggest that there are certain features and conditions that predispose a region to deep reaching convection. First, there must be strong atmospheric forcing because of thermal and/or haline surface fluxes. Thus open-ocean regions adjacent to boundaries are favoured, where cold and dry winds from land or ice surfaces blow over water, inducing large sensible heat, latent heat and moisture fluxes. Second, the stratification beneath the surface-mixed layer must be weak. And third, the weakly stratified underlying waters must be brought up toward the surface so that they can be readily and directed exposed to intense surface forcing. Whether and when the deep convection then occurs depends on the seasonal development of the surface buoyancy flux with respect to the initial stratification at the beginning of the winter period and on the role of lateral advection (Marshall and Schott, 1999). There are only a handful of rather small sites where open-ocean deep convection is known to occur: the Labrador, Weddell, and Greenland Seas and the northwestern Mediterranean Sea. In the open ocean the convective plumes entrain ambient fluid and, if deep enough, become affected by rotational effects and any pre-existing stratification. In shelf regions the convective plumes reach the sloping bottom, spread along it toward deeper locations, and are diverted by the Coriolis force as appropriate. In polar regions, especially in wintertime, high salinity water from brine rejection under a forming ice sheet sinks, and convective turbulent plumes form (Kowalik and Matthews, 1983; Stössel and Kim, 2001). In the Gulf of Lions, north of Spain, deep convection like that near Greenland and in the Labrador Sea occurs as a result of cooling by the cold

Mistral, a wind that blows out of the Rhone Valley, and to a lesser degree by the Tramontane. This was detected by the MEDOC field experiments (MEDiterranean Ocean Convection) during the winters of 1969-75. The horizontal scale of the homogeneous convection layer itself was on the order of tens of kilometres (MEDOC group 1970; Killworth 1976), however eddies on the order of about 5 km in diameter were found to detach from the front around this more or less homogeneous convective layer (Gascard, 1978; Maxworthy and Narimousa, 1994). Strong vertical currents of the order of 10 cms^{-1} were observed for the first time by Stommel et al. (1971). Low air temperatures of 5 ^{o}C blowing over a surface of 12 ^{o}C result in large values of the latent and sensible heat fluxes that are responsible for the surface energy loss of 1000 $W m^{-2}$ or more (Leaman and Schott, 1991). Also, convection cells of horizontal scale between a few hundred meters and 1 km have been observed by direct measurements at all three major convection sites (Gulf of Lions and Labrador and Grenland Seas, because in Weddell Sea open-ocean deep convection only occurs occasionally). The downward flow velocities for the different experiments carried out are between 7 cms^{-1} from the Labrador Sea (early 1990s) and 12 cms^{-1} of the Gulf of Lions, where the most intense vertical velocities are reported.

Convection dynamics and flow features have also been studied in many laboratory and numerical experiments. Turbulent localized convection has been generated in laboratory tanks, for both laterally confined and unconfined domains issuing into a homogeneous, nonrotating, environment (Kaimal et al., 1976; Boubnov and Van Heijst, 1994; Colomer et al., 1998a; Colomer et al., 1999) and into a homogeneous, rotating fluid (Maxworthy and Narimousa, 1994; Boubnov and Van Heijst, 1994; Dai et al., 1994; Narimousa, 1996; Whitehead et al., 1996, Narimousa, 1997; Jacobs and Ivey, 1998). The experiments have led to the prediction of a physical scaling of length and velocity of the convective chimney under gravity and rotation with a resulting dependency on the buoyancy, B_o, the Coriolis parameter, f, and the chimney height, h. As an alternative to laboratory experiments, localized open ocean convection has been

examined by high-resolution numerical models (Morton et al., 1956; Legg et al., 1966; Julien et al., 1999; Fannelop and Webber, 2003) to investigate a relationship between the convection process and the external parameters (Phillips, 1996; Okada et al., 2004). Also, numerical experiments have allowed studies of the growth as well as of the scaling laws of buoyant plumes (Speer and Marshall, 1995) and megaplumes (Lowell and Germanovich, 1995; Palmer and Ernst, 1998), and analysis of the rotation effect of the heat source (Leaman et al., 1991; Pham et al., 2006).

In convection processes, the vertical movement is both upward and downward, and the individual convection cells, known as plumes, act to efficiently "mix" the layer. A *thermal plume* is generated by an underlying heat source. If the heating is confined to a finite area, a vertical thermal plume and associated circulation will develop as a result of the temperature (density) difference between the plume and its environment. The plume stops rising as the temperature difference between the plume and its ambient vanishes due to entrainment or fluid from a stable environment. Therefore, the height/depth of a plume is determined by a balance between the strength and size of the heat source (Lu et al., 1997a,b) and the strength of the ambient stratification.

A case example of the natural occurrence of convective plumes, which will be the focus of our study, is the hydrothermal plume developing in Lake Banyoles.

Lake Banyoles (42º07'N, 2º45'E), in the eastern Catalan pre-Pyrenees, is a small multibasin lake (surface area of 1.12 km^2) of mixed tectonic-karstic origin, composed by six basins (B1–B6, indicated by the boxes areas in Figure 1.1). The lake can be divided into the northern and the southern lobes, separated by a shallow sill. Basins B1 and B2 are the largest and deepest (73.5 m depth and 77 m depth, respectively, Canals et al., 1990) and are situated in the southern lobe of the lake with the remainder situated in the northern lobe. The main supply of water to the lake is through subterranean springs located at the bottom of the basins of the lake (Abella, 1980; Casamitjana and Roget, 1993;

Colomer et al., 1998). An underlying fault (at the East of the lake), which acts as a barrier to ground water movement in a complex series of confined aquifers, forces the vertical discharge of the ground water flow through the bottom of the basins, Moreno-Amich and Garcia-Berthou, 1989 (Figures 1.2 –bottom-). The aquifers are supplied by the percolation of precipitation in two watersheds, located between 15 and 40 km to the northwest of Banyoles (Sanz, 1985); mainly through B1, which supplies 500 Ls^{-1}, 85 % of the total incoming water to the lake (Roget and Casamitjana, 1987). The discharged volume by several creeks situated on the western shore of the lake is much smaller and is subject to seasonal variations (Casamitjana et al., 1988; Roget et al., 1994; Colomer et al., 1998). As a result of cumulative episodes of land subsidence, the most recent being in 1978 (Julià, 1980) all basins have cone-shape structures (Figures 1.3).

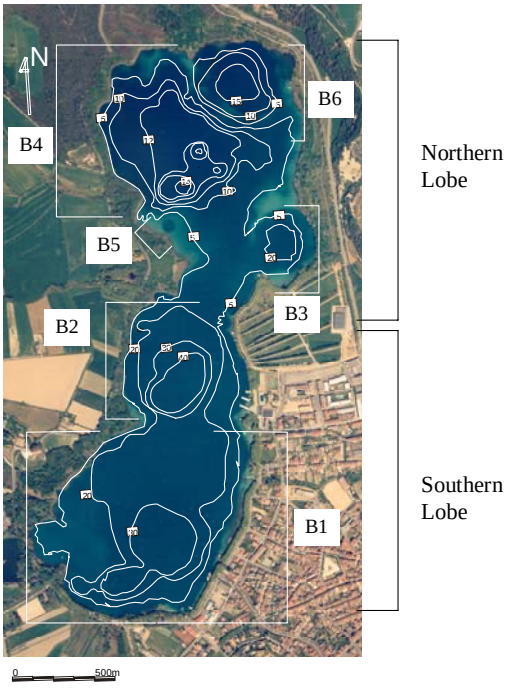

Figure 1.1 Aerial photograph of Lake Banyoles. The lake is divided into six basins. Basin B1 is located in the southern lobe, basin B2 in the central lobe and B3, B4, B5 and B6 in the northern lobe, some of them clearly seen in the photograph. This photograph was kindly provided by the Institut Cartografic de Catalunya.

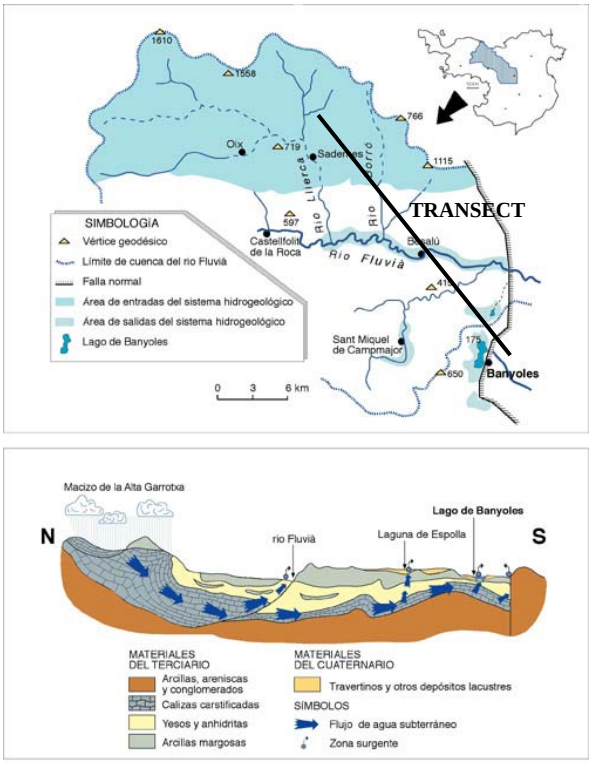

Figure 1.2 (top) General location map of Lake Banyoles and schematic representation for the hydrological system in the Lake Banyoles region. (bottom) Path of karstic water, along the transect marked in the top panel (Sanz, 1985 and redrawn by Brusi et al., 1 990).

The subterranean springs mix the sediments above up to a fairly sharp interface known as the lutocline. The lutocline is a strong gradient in density that divides the water column into two zones: a V-shaped zone below, full of sediments in suspension, and a zone of clearer water above. The lutocline is well detected by seismic profiling (Figure 1.3-top-) and is located at a depth Z_L from surface (Figure 1.3-bottom-). During periods of high precipitation in the recharge area, situated at the North of La Garrotxa (see Figure 1.2 –top-), the lutocline can migrate upward.

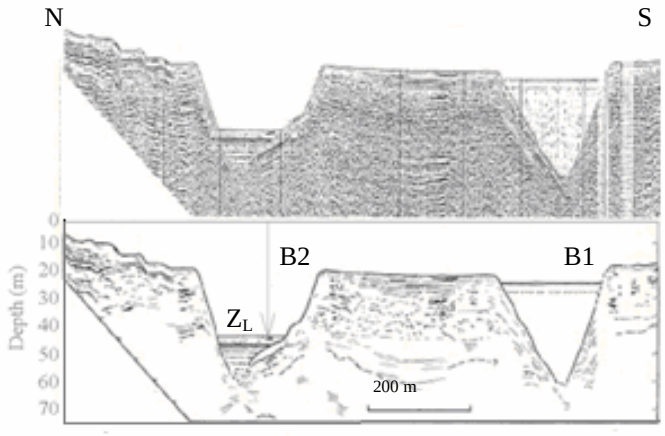

Figure 1.3 (top) South-North seismic transect and (bottom) schematic interpretation of the section from B2 to B1 (Canals et al. 1990); the lutocline is well detected by the seismic profile and is located at a depth Z_L from the surface.

The chronic hydrothermal plume in the main basin (B1) of Lake Banyoles was described by Colomer et al. (2001) for the first time. This phenomenon develops in the same way that turbulent convective plumes developed from localized sources (Maxwhorty, 1997) in oceanic and atmospheric deep convection (Schott et al., 1993, 1996), atmospheric microbursts (Lundgren et al., 1992), having the same behaviour of low-aspect-ratio plumes such as urban heat islands (Lu et al., 1997a, b). As much as 90% of the total underground inflow enters the lake through this basin (Roget et al., 1994). The temperature of the water at the lutocline level is warmer (~19^{o}C, constant throughout the year) than the hypolimnetic water immediately above it, and this difference in temperature generates a convective hydrothermal

plume. In contrast to the ocean convection plumes, in which the source of the convection is situated at the top of the water column where surface water cools and dense water is formed, in Lake Banyoles, the source is situated at the bottom of the lake, where warm water, rich in sediments, heats the hypolimnetic water and the bottom water becomes less dense and therefore buoyant. The plume develops upwards and entrains particles from the lutocline up to an equilibrium depth (Casamitjana et al., 1993; Serra et al., 2002a). At the equilibrium depth, the water spreads laterally (see Figure 1.4) forming a mesopycnal turbidity current, following the classification of Mulder and Alexander (2001) for a volume sediment concentration < 10%. This turbidity current is ~0.02 K warmer than the surrounding water and has a typical thickness of ~1 m (Colomer et al., 2001). Sedimentation from turbidity currents and density interfaces has been found to be an effective mechanism for the transport of suspended material through the bottom of the water column, thereby determining the bottom sedimentary records in the whole lake (Serra et al., 2005). This sedimentation process has been attributed mainly to double diffusive sedimentation rather than to single particle sedimentation rates at the southern lobe of the lake (Serra et al., 2002b; Zamora et al., 2002).

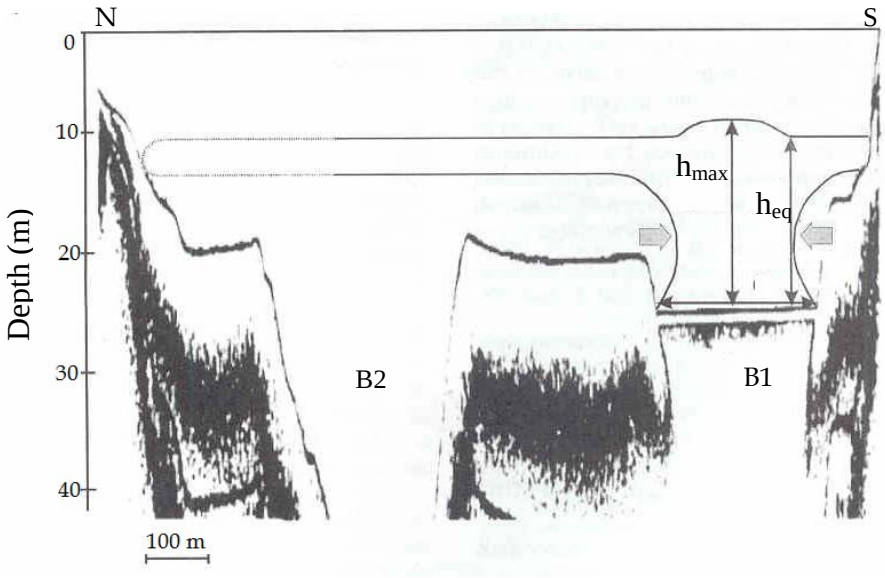

Figure 1.4
Schematic view of the hydrothermal plume in B1. The plume reaches an equilibrium height, h_{eq}, and the vertical excursion stops at height h_{max}.

The vertical structure of the plume depends on the stratification of the water column, which in turn depends on seasonal meteorological conditions. During the stratified period of the lake, the plume is constricted to the hypolimnetic zone. At the beginning of the summer season the plume reaches the bottom of the metalimnion, but at the end of this season the strong stratification overcomes the plume buoyancy and the plume does not reach it. In the mixed period of the lake, the plume develops in the whole water column and reaches the surface of the lake, where particles accumulate and spread around the centre (Serra et al., 2002a). The maximum height that the sediments can rise to is also affected by the formation of aggregates (Casamitjana et al., 1996). Experiments dealing with the vertical distribution of fishes in the water column in the stratified season of the lake showed that the increase in the particle concentration due to the presence of the turbid plume can constrain their habitat (Serra et al., 2002a).

For high precipitation periods in the recharge area, the aquifer increases the pressure enough to resuspend the confined sediments of basin B2, usually compacted at the bottom of the lake (Colomer et al., 2003); this resuspension results in a displacement of the lutocline (Canals et al., 1990; Casamitjana and Roget, 1993; Colomer et al., 2002). During the fluidization events a hydrothermal plume also develops in B2 (Colomer et al., 2003). This finite hydrothermal plume, first studied in 2002, could not be well described because it did not extend far vertically in the water column and remained trapped in a small region below the strong thermal stratification.

Records show that the sediment fluidization in basin B2 of the lake develops episodically (episodic fluidization) as a function of the amount of rainfall in the recharge aquifer area (Colomer et al., 2002). Sediment fluidization is of great limnological interest because it is a mechanism that carries particles in suspension from the sediment interface upward into the lake water column (Colomer et al., 1998b), affecting water quality and fish distribution (Serra et al., 2002a). Differences in sedimentation records are also observed in the cores taken from the lake floor (Serra et al., 2005) caused by the differences in

sedimentary rates between the two lobes of the lake during the period of lake stratification, attributed to the fact that then, the turbidity current depth generated by the hydrothermal plume in B1 is deeper than the shallow sill zone and it remains constrained to the southern lobe.

The aim of this PhD thesis is to acquire a better understanding of the dynamics of the hydrothermal plumes in the lake and to gain more insight into the interrelationship between meteorology and fluidization. This study, therefore, has several objectives:

1) Time-series of historical observations of fluidization events in basin B2 (basin depth) will be compared to the atmospheric patterns that supply the largest amount of rain to the area under study in order to find the atmospheric patterns that generate the fluidization events, as well as their frequency. This is crucial to determining the water quality of Lake Banyoles. For this purpose rainfall data taken from the European Centre for Medium-Range Weather Forecasts (ECMWF) ERA-40 have been analyzed. This study has already been published in the journal *Water Resources Research* **(Chapter 2)**.

2) To study the spatial inhomogeneity of the chronic thermal plume found in basin B1 as well as the spatial inhomogeneity of the episodic thermal plume found in basin B2. Frequent field campaigns have been undertaken to have temperature, particles concentration and three dimension velocity data in the whole water column. The campaigns have been undertaken from July 1998 till October 2004. Results found during campaigns undertaken from July 1998 to July 2002 can be read in three articles: two of them published in the journal *Geophysical Research Letters* and one in the journal *Sedimetology* **(Chapter 3)**.

3) To characterize the structure of the episodic thermal plume in B2 and compare it with the chronic plume developed in B1. It has been used experimental data undertaken from intensive field work carried out from October 2003 to November 2004, during the presence of a

hydrothermal plume in B2. The results of this study have been published in the *Journal of Geophysical Research –Oceans-* **(Chapter 4)**.

4) The experimental data collected have a two-spatial dimensional scale, as they were taken in a longitudinal transect along the lake over time and over the whole water column depth. In order to know the three-dimensional variations and the evolution under different ambient conditions it has been used a numerical model: **MIT G**eneral **C**irculation **M**odel (**MITgcm)** designed to study the atmosphere, ocean, and climate. As convection in model is supposed to develop in ocean, it has been necessary to modify the buoyancy source from the top of the water surface to the bottom. After, experimental data undertaken from the field campaigns, they have been included all the variable characteristics of the case of the hydrothermal plume of Lake Banyoles. With this model we will be able to determine the dynamics of the forcing parameters that mimic the hydrothermal plume in the lake **(Chapter 5)**.

Finally, in Chapter 6, all the main discussions and conclusions of this PhD will be summarized.

Reference List

Abella, C.A., 1980. Comparative population dynamics of planktonic phototrophic bacteria, PhD. Disertation, U.A.B., Bellaterra, Spain, 1980.

Boubnov, B. M. and G. F. V. Van Heijst, 1994. Experiments on convection from a horizontal plate with and without background rotation, *Experiments in Fluids*, 16, 155-164.

Canals, M., H. Got, R. Julia and J. Serra, 1990. Solution-collapse depressions and suspensates in the limnocrenic lake of Banyoles (NE Spain). *Earth Surface Processes and. Landforms,* 15, 243-254.

Casamitjana, X. and E. Roget, 1993. Resuspension of sediment by focused groundwater in Lake Banyoles, *Limnology and Oceanography*, 38(3), 643-656.

Casamitjana, X., G. Schladow and E. Roget, 1993. The seasonal cycle of a groundwater dominated lake, *Journal of Hydraulic Research*, 31 (3), 293-306.

Casamitjana, X., J. Colomer, E. Roget and T. Serra, 1996. On the presence of aggregates in the basin of Lake Banyoles, *Geophysical Research Letters*, 23 (20), 2737-2740.

Casamitjana, X., E. Roget, D. Jou and J. E. Llebot, 1998. Effect of suspended sediment on the heating of lake Banyoles, *Journal of Geophysical Research-Oceans*, 93 (C8), 9332-9336.

Casamitjana, X. and E. Roget, 1993. Resuspension of sediment by focused groundwater in Lake Banyoles, *Limnology and Oceanography*, 38(3), 643-656.

Colomer, J., L.D. Zieren and H. J. S. Fernando, 1998a. Comment on "Localized convection in rotating stratified fluid" by J. A. Whitehead et al., *Journal of Geophysical Research-Oceans, 103* (C6), 12 891-12 894.

Colomer, J., J. A. Ross and X. Casamitjana, 1998b. Sediment entrainment in karst basins, *Aquatic. Science.* 60 (4), 338-358.

Colomer, J., B. M. Boubnov, and H. J. S. Fernando, 1999. Turbulent convection from isolated sources. *Dynamics of Atmospheres and Oceans,* 30, 125-148.

Colomer, J., T. Serra, J. Piera, E. Roget and X. Casamitjana, 2001. Observations of a hydrothermal plume in a karstic lake, *Limnology and Oceanography,* 46**,** 197-203.

Colomer, J., T. Serra, M. Soler and X. Casamitjana, 2002. Sediment fluidization events in a lake caused by large monthly rainfalls, *Geophysical Research. Letters, 29*(21), doi:10.1029/2001GL014299.

Colomer, J., T. Serra, M. Soler and X. Casamitjana, 2003. Hydrothermal plumes trapped by thermal stratification, *Geophysical Research. Letters, 30*(21), 2092, doi:10.1029/2003GL018131.

Dai, Z., L. K. Tseng and G. M. Faeth, 1994. Structure of round, fully developed, buoyant turbulent plume, *Journal of Heat Transfer*, 116, 409-417.

Fannelop, T. K. and D. M. Webber, 2003. On buoyant plumes rising from area sources in a calm environment, J*ournal of Fluid Mechanics*, 497, 319-334.

Gascard, J.C., 1978. Mediterranean deep water formation – Baroclinic instabilities and oceanic eddies, *Oceanologica Acta,* 1, 315-330.

Jacobs, P. and G.N. Ivey, 1998. The influence of rotation on shelf convection, J*ournal of Fluid Mechanics*, 369, 23-48.

Julia, R., 1980. Catchment area of Banyoles-Besalu (in Catalan). Ph. D. Thesis, Centre d'Estudis Comarcals de Banyoles, 275 p.

Julien, K., S. Leff, J. McWilliams and J. Werne, 1999. Plumes in rotating convection. Part 1. Ensemble statistics and dynamical balances, J*ournal of Fluid Mechanics,* 391, 151.

Kaimal, J.C., J. C. Wyngaard, D. A. Haugen, O. R. Coté, Y. Izumi, S. J. Caughey and C. J. Readings, 1976. Turbulence structure in the convective boundary layer. *Journal of Atmospheric Sciences,* 33, 2 152-2 169.

Killworth, P. D., 1976. The mixing and spreading phase of MEDOC 1969, Vol. 7, *Progress in Oceanography*, Pergamon, 59-90.

Kowalik Z. and J. B. Matthews, 1983. Numerical study of the water movement driven by brine rejection from nearshore Arctic ice, *Journal of Geophysical Research*, 88(C5), 2 953-2 958.

Leaman, K. D. and F. A. Schott, 1991. Hydrographic Structure of the Convection Regime in the Gulf of Lions: Winter 1987, *Journal of Physical Oceanography*, 21, 575-597.

Legg, S., H. Jones and M. Visbeck, 1996. A heton perspective of baroclinic eddy transfer in localized open ocean convection. *Journal of Physical Oceanography*, 26, 2 251-2 266.

List, E. J., 1982. Turbulent jets and plumes, Annual Review of Fluid Mechanics, 14, 189-212.

Lowell, R. P. and L. N. Germanovich, 1995. Dike Injection and the Formation of Megaplumes at Ocean Ridges, *Science,* 269, 1 804-1 807.

Lu, J., S. P. Arya, W. H. Snyder and R. E. Lawson Jr., 1997a. A laboratory study of the urban heat island in a calm and stably stratified environment. Part I: Temperature field. *Journal of Applied Meteorology,* 36(10), 1 377-1 391 .

Lu, J., S. P. Arya, W. H. Snyder and R. E. Lawson Jr., 1997b. A laboratory study of the urban heat island in a calm and stably stratified environment. *Part II: Velocity field. Journal of Applied Meteorology,* 36(10), 1 392-1 402.

Lundgren, T. S., J. Yao and N. N. Mansour, 1992. Microburst modelling and scaling, *Journal of Fluid Mechanics*. 239, 461-488.

Lupton, J. E., J. R. Delaney, H. P. Johnson and M. K. Tivey, 1985. Entrainment and vertical transport of deep-ocean water by buoyant hydrothermal plumes, *Nature,* 316, 621-623.

Marshall, J. and F. Schott, 1999. Open-ocean convection: observations, theory, and models. *Reviews of Geophysics*, 37 (1), 1-64.

Maxworthy, T. and S. Narimousa, 1994. Unsteady, turbulent convection into a homogeneous, rotating fluid, with oceanographic applications. *Journal of Physical Oceanography*, 24, 865-887.

Maxworthy, T., 1997. Convection into domains with open boundaries, *Annual Review of Fluid Mechanics,* 29, 327-371.

MEDOC Group, 1970. Observations of formation of deep water in the Mediterranean Sea, 1969. *Nature*, 227, 1 037-1 040.

Moreno-Amich, R. and E. Garcia-Berthou, 1989. A new bathymetric map based on echosounding and morphological characterization of the Lake Banyoles, *Hydrobiologia*, 185, 83-90.

Morton, B. R., G. Taylor and J. S. Turner, 1956. Turbulent gravitational convection from maintained and instantaneous sources, *Proceedings of the Royal Society of London (A)*, 234, 1-32.

Mulder, T. and J. Alexander, 2001. The physical character of subaqueous sedimentary density flows and their deposits, *Sedimentology*, 48, 269-299.

Narimousa, S., 1996. Penetrative turbulent convection into a rotating two-layer fluid, *Journal of Fluid Mechanics*, 321, 299-313.

Narimousa, S., 1997. Dynamics of mesoscale vortices generated by turbulent convection at large aspect ratios, *Journal of Geophysical Research*, 102 (C3), 5615 -5624.

Okada, N., M. Ikeda and S. Minobe, 2004. Numerical experiments of isolated convection under polynya, *Journal of Oceanography*, 60, 927-943.

Palmer M. R. and G. G. J. Ernst, 1998. Generation of hydrothermal megaplumes by cooling of pillow basalts at mid-ocean ridges, *Nature*, 393, 643-647.

Pham, M. V., F. Plourde, S. D. Kim and S. Balachandar, 2006. Large-eddy simulation of a pure thermal plume under rotating conditions. *Physics of Fluids, 18,* (1), 015101.1-015101.15.

Phillips, O. M., 1966. On turbulent convection currents and the circulation of the Red Sea, *Deep-Sea Research,* 13, 1 149-1 160.

Roget, E. and X. Casamitjana, 1987. Hydric balance of Lake Banyoles (in spanish). Paper presented at the "IV Congreso Español de Limnología", Universidad de Sevilla, Sevilla, Spain.

Roget, E., X. Casamitjana, and J. E. Llebot, 1994. Calculation of the flow into a lake through an underground spring with suspensions, *Netherland Journal of Aquatic Ecology*, 28, 135-141

Sanz, M., 1985. Estudi Hidrogeològic de la Conca Banyoles-La Garrotxa. Quaderns del Centre d'Estudis Comarcals de Banyoles 1980-84, separata

pp. 171-250. redrawn by D. Brusi a Brusi, Maroto and Vila (1992) in "L'Estany de Banyoles" into "El Medi Natural de les Terres gironines" (Pallí i Brusi, eds.). Universitat de Girona. pp. 117-133.

Schott, F., M. Visbeck and J. Fischer, 1993. Observations of vertical currents and convection in the central Greenland Sea during the winter of 1988/89, *Journal of Geophysical Research*, 98, 14 401-14 421.

Schott, F., M. Visbeck, U. Send, J. Fischer, L. Stramma and Y. Desaubies, 1996. Observations of deep convection in the Gulf of Lions, Northern Mediterranean, during the winter of 1991/92, *Journal of Geophysical Research*, 26, 505-524.

Serra, T., J. Colomer, Ll. Zamora, R. Moreno-Amich and X. Casamitjana, 2002a. Seasonal development of a turbid hydrothermal plume in a lake, *Water Research, 36*(11), 2 753-2 760.

Serra, T., J. Colomer, E. Gacia, M. Soler and X. Casamitjana, 2002b. Effects of a hydrothermal plume on the sedimentation rates in a karstic lake, *Geophysical Research Letters.* 10.1029/2002GL015368. 29 (21): 25-28. ISSN: 0094-8276.

Serra, T., J. Colomer, R. Julià, M. Soler and X. Casamitjana, 2005. Behaviour and dynamics of a hydrothermal plume in Lake Banyoles, Catalonia, *Sedimentology 52*(4), 795-805.

Speer, K. G., and P. A. Rona, 1989. A model of an Atlantic and Pacific hydrothermal plume, *Journal of Geophysical Research*, 94, 6213-6220.

Speer, K. G. and J. Marshall, 1995. The growth of convective plumes at sea floor hot springs, *Journal of Marine Research,* 53, 1025-1057.

Stommel, H., A. Voorhis, and D. Weeb, 1971. Submarine clouds in the deep ocean, *American Science*, 59, 716-723.

Stössel, A. and S. J. Kim, 2001. On the role of sea ice and convection in a global ocean model, *Journal of Physical Oceanography*, 32, 1194-1208.

Turner, J. S., 1973. Buoyancy effects in fluids. Cambridge University Press, New York, 165-206.

Veronis, G., 1972. On properties of seawater defined by temperature, salinity and pressure, *Journal of Marine Research*, 30, 227–255.

Whitehead, J. A., J. Marshall and G. E. Hufford, 1996. Localized convection in rotating stratified fluid, *Journal of Geophysical Research, 101* (C10), 25, 705- 25 721.

Zamora, L. and R. Moreno-Amich, 2002. Quantifying the activity and movement of perch in a temperate lake by integrating acoustic telemetry and a geographic information system, *Hydrobiologia*, 483, 1-3, 209-218.

2 Relationship between rainfall and sediment fluidization events

To have a general knowledge of the hydrothermal plumes dynamics in Lake Banyoles, the fluidization events in basin B2 have been related to the characteristic rainfall in the recharge area that supplies water to the Lake Banyoles. This has been done in view of finding the most important atmospheric patterns that develop fluidization events, as well as their frequency.

This study can be found in the paper published in the journal Water Resources Research.

Marianna Soler, Teresa Serra, Jordi Colomer, Romualdo Romero. “Anomalous rainfall and associated atmospheric circulation in the northeast Spanish Mediterranean area and its relationship to sediment fluidization events in a lake”. *Water resources research*. Vol. 43, W01404, 2007

http://dx.doi.org/10.1029/2005WR004810

Received 15 December 2005; accepted 31 August 2006; published 9 January 2007

Abstract

Changes in the dynamics of sediment transport in a Mediterranean lake (sediment fluidization events) are linked to atmospheric circulations patterns (trough monthly precipitation). In the basins of Lake Banyoles, located in the northeast of Spain, water enters mainly through subterranean springs, and associated fluctuations in the vertical migration of sediment distribution (fluidization events) present episodic behavior as a result of episodic rainfall in the area. The initiation of the fluidization events takes place when the monthly rainfall is 2.7 times greater than the mean monthly rainfall of the rainiest months in the area, especially in spring (April and May), October, and December. The duration of these events is found to be well correlated with the accumulated rainfall of the preceding 10 months before the process initiation. The rainfall, in turn, is mainly associated with six atmospheric circulation patterns among the 19 fundamental circulations that emerged in an earlier study focused on significant rainfall days in Mediterranean Spain. Among them, accentuated surface lows over the northeast of Spain, general northeasterly winds by low pressure centered to the east of Balearic Islands and short baroclinic waves over the Iberian Peninsula, with easterly flows over the northeastern coast of Spain, are found the most relevant atmospheric circulations that drive heavy rainfall events. .

Keywords: atmospheric patterns; fluidization; lake; rainfall; sediment.

3 Evolution of Hydrothermal Plumes in Lake Banyoles

As water in Lake Banyoles is supplied mainly through two subterranean springs located at the bottom of basin B1 (Abella, 1980; Casamitjana and Roget, 1993; Colomer et al., 1998), rainfall quantities in the recharge area can change the amount of the water supplied, strengthening the amount of water supplied by the spring in B1 and activating in certain situations some of the springs situated in the other basins. All this phenomena provides a more complicated picture of the very variable dynamics of Lake Banyoles.

3.1 Characterization of buoyant jets

To understand the general dynamics of Lake Banyoles, the characteristics and development of large volume discharges of warm water in an ambient fluid, and the consequent mixing in the environment, will be evaluated.

Although many discharges into the environment are classified as buoyant jets, they are derived from sources of both momentum and buoyancy. At the beginning, the initial flow is driven by the momentum of the fluid, but the effluent is more or less dense than its surroundings and the resulting jet is thus acted upon by buoyancy forces. Near the source the flow is usually controlled entirely by the initial conditions, which include the geometry of the source, the outflow velocity and the initial difference between the discharge and the ambient fluid. It would be interesting to define the primary variables governing the dynamics of the buoyant jets.

The **momentum flux** for a round jet is

$$M = \frac{1}{4}\pi D^2 w^2, \tag{3.1}$$

where D is the jet diameter and w is the mean outflow velocity assumed uniform across the jet.

The **buoyancy flux** for a round source is

$$B = g_o' \frac{1}{4}\pi D^2 w, \tag{3.2}$$

where g_o' is the initial apparent gravitational acceleration, $g_o' = g\frac{\Delta\rho_o}{\rho}$, with $\Delta\rho_o$ as the difference between the density of the environment and the discharged fluid.

The stratification of the environment is given by the frequency of oscillation of a water parcel vertically displaced adiabatically from its rest position. The **Brünt-Väisäla frequency** is then

$$N^2 = g\alpha\frac{\Delta T}{\Delta z} \tag{3.3}$$

where $\Delta T/\Delta z$ is the vertical temperature gradient in the water column, α is the thermal expansibility coefficient (Chen and Millero, 1986) and g is the gravity constant.

A buoyant jet is a flow caused by a potential energy source that provides the fluid with positive or negative buoyancy relative to its surroundings. In our case the discharge is vertical and upward because it is less dense than the surroundings and therefore continues to travel upward. A buoyant jet has jetlike characteristics depending on its initial volume and momentum fluxes, and plumelike characteristics depending on its initial buoyancy flux, but far enough from the source it will always turn into a plume.

The controlling parameter for whether a buoyant jet is *jetlike* or *plumelike* is the ratio of the height of the flow, z, and the **characteristic length** for a round jet, l_M, (Fischer et al., 1979) that results from the balance between the momentum flux and the total buoyancy flux, and is given by

$$l_M = M^{3/4} B^{-1/2} , \tag{3.4}$$

If $z >> l_M$ the flow is like a plume and if $z << l_M$ it is like a jet.

3.2 Plume structure characterization

To see the effect of the stratification on the plume, it would be necessary to introduce the **Richardson number** which is the ratio of the buoyancy force

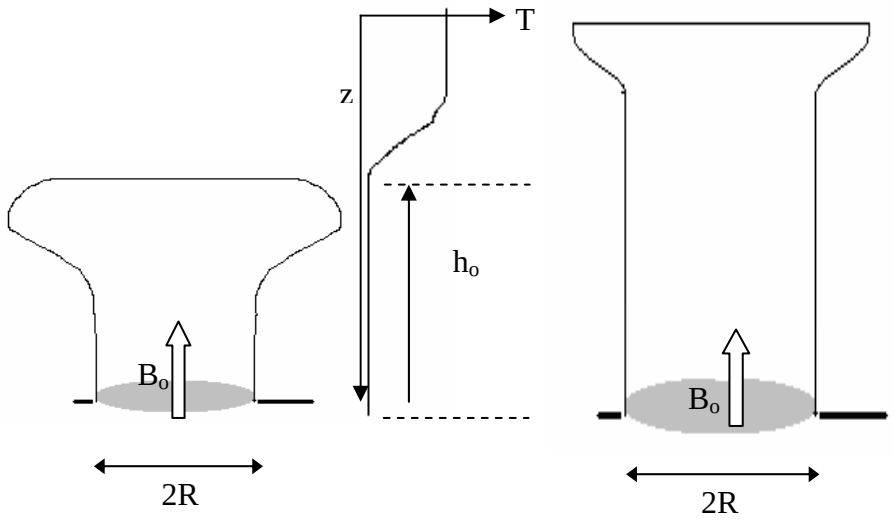

Ri > 11 *Ri < 11*

Figure 3.1
Diagram of the variables needed for the Richardson number calculation. Vertical development of a hydrothermal plume depending on its Richardson number value, over or under the critical value Ri_c=11.

across the density interface to the inertia force,

$$Ri = \frac{g'_i \, h_o}{(B_o R)^{2/3}}, \tag{3.5}$$

where h_o is the depth of the convective layer and the apparent gravitational acceleration in the interface, B_o is the buoyancy flux per area and g'_i is calculated by the density difference caused by the temperature variation in the thermocline, as can be seen in Figure 3.1. This dimensionless number can be used to determine whether the plume will penetrate through the thermocline or not (Narimousa, 1996). The critical Richardson number is: Ri_c ~11. Above that it is found that convective flows do not penetrate through density interfaces but propagate radially along the base of the mixed layer (Narimousa, 1996).

Knowing whether the plume develops as a single vortex column or several vortices is determined by the **Rossby plume number**,

$$R_o^* = \left(\frac{B_o}{f^3 h_o^2} \right)^{1/2}. \tag{3.6}$$

If it is found that $R_o^* > 3$, a single source vortex forms around the source; at values $0.5 < R_o^* < 3$ two vortices are formed; and at values $R_o^* < 0.5$ three or more vortices are formed around the source. The number of vortices formed by the baroclinic instability can be calculated using a formula from Whitehead et al. (1996):

$$N_V = 0.7\left(D^2 / B_o\right)^{1/3} f \ , \tag{3.7}$$

where f is the Coriolis parameter.

Assuming that the input of unstable buoyancy flux at a surface or diameter D is balanced by the lateral removal of flux by eddies ejected out of the convective region, Whitehead et al. (1996) and Visbeck et al. (1996) were able to determine the vertical extension of the convection. Similarly, Colomer et al. (1998) found that the depth of convection is determined by the inhibition of vertical growth due to the stratification of the water column. For both

hypotheses, the **maximum height** to which a plume migrates has been found to be a function of the source diameter, D, the buoyancy flux (Eq. 3.2) per unit area, B_o, the stratification of the water column (Eq.3.3), N, and independent of the rotation rate, *f* (Whitehead et al., 1996),

$$h_{\max} = \frac{3.7\left(B_o D\right)^{1/3}}{N}. \tag{3.8}$$

The **height** at which the plume reaches its level **of neutral buoyancy** and spreads laterally is

$$h_{eq} = \frac{2.6\left(B_o D\right)^{1/3}}{N}, \tag{3.9}$$

and this height is the one that conforms to h_{eq}/h_{max}=0.694 (Lu et al., 1997).

The maximum height (Eq. 3.8) of the plume will then depend on its internal buoyancy, but the stratification of the water column can act as a barrier to its development. The Richardson number (Eq. 3.5) will evaluate whether or not the plume buoyancy is stronger than the background stratification (for Ric>11) and if therefore the plume penetrates through the density interface (thermocline). If not, the rise of the plume would be constrained by the hypolimnion of the lake.

The quantities D, h_{eq} and h_{max} have been illustrated in Figure 3.2. Horizontal gray arrows represent the lateral entrainment of cold water into the hydrothermal plume. Here, we have only considered the hydrothermal plume in B1 and that sediment in B2 is consolidated at the bottom.

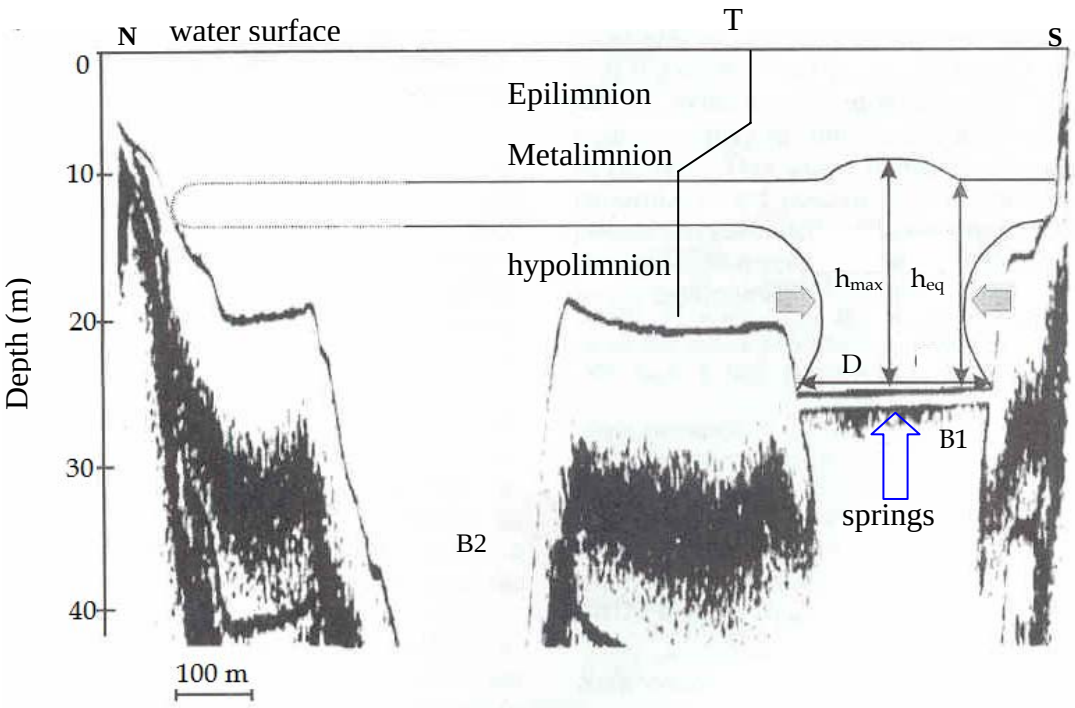

Figure 3.2
Schematic view of the hydrothermal plume in B1, with a source diameter, D, plotted on the seismic profile done by Canals et al., 1990. The plume reaches an equilibrium height, h_{eq}, and the vertical excursion stops at height h_{max}.

3.3 Methods and Instrumentation

Several campaigns have been undertaken from July 1998 till October 2004 in order to understand the dynamics of the hydrothermal plume of B1 in Lake Banyoles. Seven field surveys were undertaken from July 1998 to July 2002 along the main axis for measuring particle size distribution (PSD) and particle volume concentration (PVC), temperature, oxygen concentration, and the flow velocity and direction. Also, two cores were collected in 2000 each one from each of the two lobes of the Lake. Sediment traps were also deployed in different stations of measurement during 2000 for a period of 5 days (Serra et al., 2002, Serra et al., 2005). From May to September 2002, fourteen surveys were made along the main axes of the Lake, measuring at each station: PSD, PVC and conductivity, temperature and depth (Colomer et al., 2003).

An intensive field work was carried out during the period of the presence of a hydrothermal plume in B2. The field work started in October 2003 and finished in October 2004. Measurements were undertaken with a mean periodicity of a week during the beginning of the fluidization event (the first 4 months), and a periodicity of a month for the rest of the campaign.

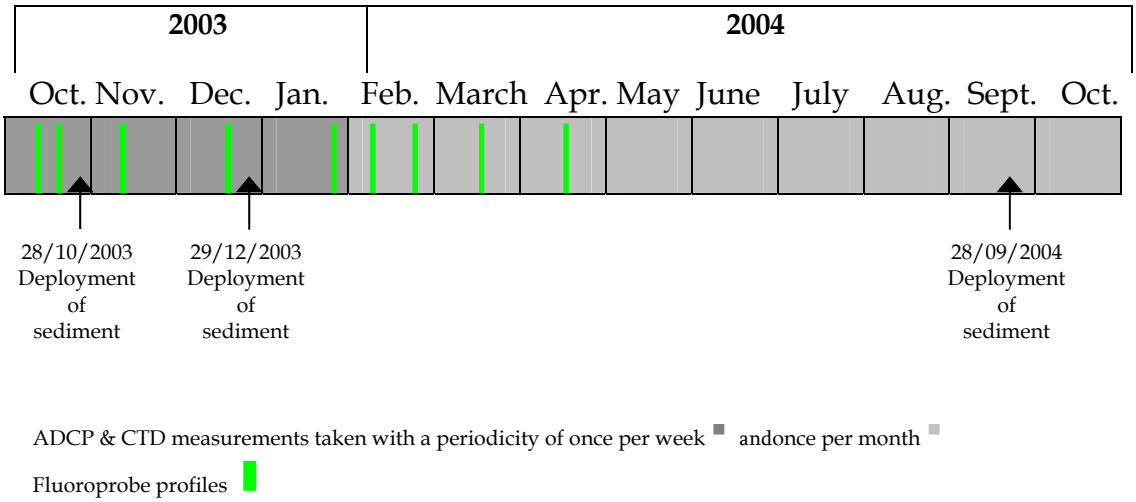

Each day of the intensive campaign had the following procedure:

First of all it was taken a transect with the ADCP along the south lobe of the lake crossing over the centre of basin B1 and B2 (see blue line in Figure 3.3). After that, CTD and Fluoroprobe profiles of the whole water column were undertaken at four different stations: the centre of B1, the plain, the centre of B2 and the sill (ST4, ST3, ST2 and ST1 respectively in Figure 3.3).

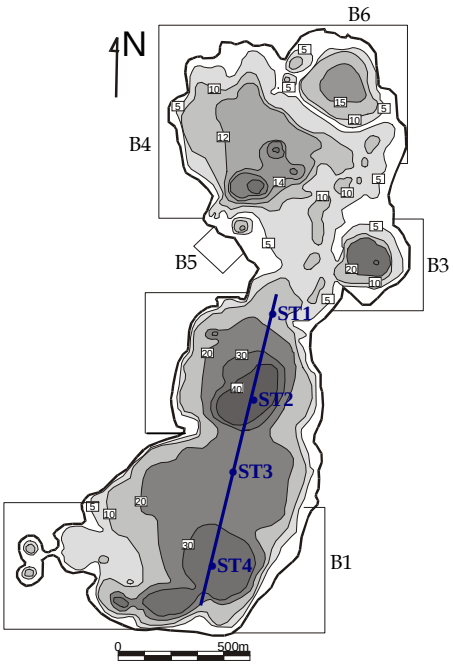

Figure 3.3
Bathymetric map of Lake Banyoles constructed from echo-sounding profiles (Moreno-Amich & Garcia-Berthou, 1989). The lake is divided into six basins. Also in the plot the blue line shows the north- south transect with the location of the four stations (ST1- ST4).

3.3.1 Instruments

3.3.1.1 ADCP

An Acoustic Doppler Currentmeter Profiler, based on the Doppler theory (**ADCP, RDI 600 kHz Workhorse Sentinel**) was used to measure the three dimension velocity (u, east-west, v, north-south and w vertical) in the whole water column of a transect along the main axis of the lake in the southern lobe, having also a pressure sensor from which the depth could be known.

The ADCP can take data at real time or in a continuous way, moored, and it consists of a 4-radar beams that fire at moving targets (particles in the water) with a 600 kHz frequency (see Figure 3.4), it covers a range depth of 1 to 150m. The velocity range, at which it works, covers from ±5 m/s (default) to ±20 m/s (maximum), and it has a resolution of 1 mm/s. The 4-beams design improves data reliability by providing redundant data in the case of a blocked or damaged beam and by delivering an independent measurement of error.

Figure 3.4
Acoustic Doppler Currentmeter Profiler (Workhorse Sentinel ADCP).

The ADCP was deployed on the water surface with the beams facing downwards. Data from the ADCP was received from 45 depth bins, each 1 m high, with the first bin at 2 m depth. The sampling rate was set at 1 Hz with the raw data processed to obtain 7.5 min averaged data, with a standard deviation of 0.1 cm s^{-1}.

3.3.1.2 CTD

A Conductivity-Temperature-Depth Profiler (**CTD SBE 19plus SEACAT, Sea Bird Instruments**) was used for accurate measurements of temperature (Figure 3.5). Measurements were undertaken systematically in 4 stations along the main axis of the lake (see Figure 3.3).

The 19*plus* samples at 4 Hz, and permits data output in ASCII engineering units. It profiles conductivity with a range from 0 to 9 S/m, an initial accuracy of 0.0005 S/m and a resolution of 0.00001 S/m; temperature with a range from -5 ºC to 35 ºC, an initial accuracy of 0.005 ºC and a resolution of 0.0001 ºC; depth (Strain-Gauge Pressure) with a range from 0 to 1000 m, an initial accuracy of 0.1% of full scale range and a resolution of 0.002 % of full scale range. It has auxiliary sensors for dissolved oxygen, fluorescence and turbidity,

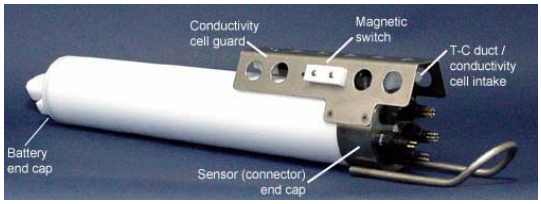

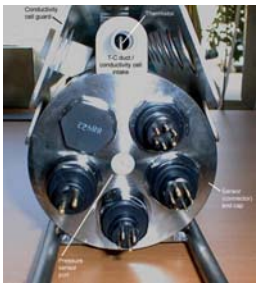

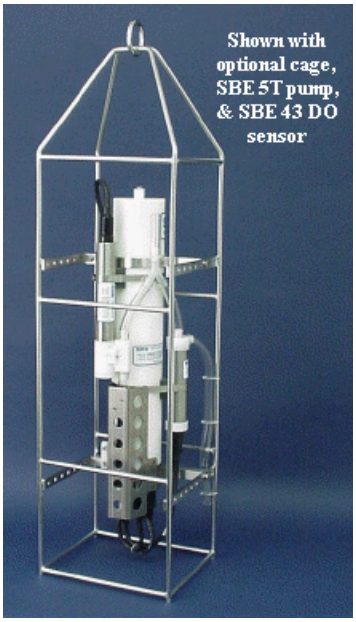

Figure 3.5
Several photos where can be observed the different CTD parts and sensors (top and bottom) as well as the protection cage (right).

which has a linearity with less than 2% of deviation from 0 to 750 FTU, and a sensitivity of 200 mV/FTU and a range of 25 FTU.

3.3.1.3 LISST

A laser *in situ* scattering and transmissometry probe based on the diffraction theory (**Lisst-100, Sequoia Scientific, Inc.**) was used to measure the particle size distribution. Lisst-100 consists of a laser beam, an array of ring detectors to analyse the light received, a data storage unity and a battery

system, and is controlled by a computer aboard a ship. Lisst-100, see Figure 3.6, covers a measurable size range from 1.2 to 200 μm and it also measures the depth by means of a pressure sensor, with a resolution of 5 cm. Previous works (Traykovsky et al., 1999; Serra et al., 2001) demonstrate that Lisst-100 is an appropriate instrument for estimating the concentration of suspended particles in a water body. Particle size distribution profiles were performed with a spatial resolution of 0.25 m.

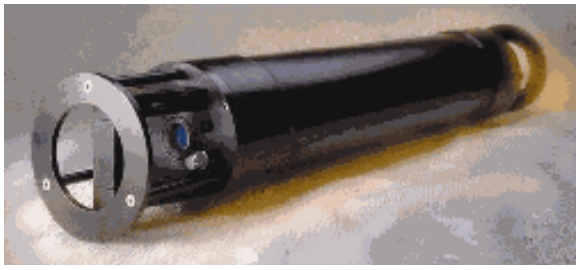

Figure 3.6
Laser in situ Scattering and Transmissometry probe (Lisst 100).

The LISST-100 determines the size distribution of an ensemble of particles from their characteristic multi-angle forward scattering. The multi-angle measurements are at small forward angles, from 0.051 to 51. At these small angles, the particle scattering is independent of both the particle refractive index and the composition of the particles and depends only on the particle size. The instrument emits a collimated laser beam that produces the scattering of the particles. The scattered light is focussed by means of a lens in a ''ring detector'' placed in the focal plane of the lens. All rays originating at a particular angle to the optical axis arrive at the detector at a point in the focal plane that lies at the same angle from the lens axis. The detector is formed by 32 concentric rings of silicon and each ring responds to the scattering integrated over a narrow range of angles.

The measured diffracted energy in the rings is related to the area distribution of the particles by means of a kernel matrix that has to be inverted in order to obtain the area distribution of the particles. The volume distribution is then

computed from the area distribution by multiplication of the area in each size bin with its mean diameter.

We only used the LISST-100 to measure the particle distribution in the water column the first two days of campaign. Measurements were made at depth-intervals of 0.5–1 m from the surface of the lake to the bottom. To avoid possible vertical displacements due to the boat movements, five consecutive measurements were made at each depth, and averaged.

3.3.1.4 Fluoroprobe

A chlorophyll measuring device with integrated spectral algae class analysis probe (**Fluoroprobe, BBE, Inc.**) was used for ultrasensitive measurement of phytoplankton.

The bbe- FluoroProbe uses a fluorometric method for the differentiation of algal populations *in vivo*. This instrument measures the chlorophyll content *in situ* from the surface down to depths of 100 m using prompt fluorescence response. Its measuring range is from 0 to 200 µg chl-a/L with an extended resolution of 0.015 µg chl-a/L. The light sources are LEDs with selected wavelengths (see Figure 3.7). The fingerprints of four algae classes and the yellow substances are already stored in the FluoroProbe. The LEDs emit pulsed light at selected wavelengths: 450 nm, 525 nm, 570 nm, 590 nm and 610 nm. Fluorometric Emission is measured at 680 nm by photomultiplier at an angle of 90 degrees to the exciting light source.

Figure 3.7
(Left) Chlorophyll measuring device (Fluoroprobe, BBE, Inc.) (Right) Fluoroprobe 's light sources emitting at selected wavelengths.

The bbe Fluoroprobe also measures the depth by means of a pressure sensor, the water temperature and transmission which automatically take place during each analysis to compensate the influence of substances that cause turbidity.

3.3.2. Methods

3.3.2.1 Sediment tramps

Three field surveys were undertaken between October 2003 and October 2004 along the main axis of the lake. Measurements were taken at four stations (ST1 –ST4, Figure 3.8 -left-). In these surveys water samples were taken from the surface to the bottom with sedimentation tramps. Sediment tramp arrays (Figure 3.9) were deployed along transect (blue line in Figure 3.3) in the southern lobe of the lake and replaced after 5 days. Each sediment trap array (Figure 3.8) consisted of two to four traps located at depths of 10 and 14 m in ST1; 10, 20 and 30 m in ST2 ; 10 and 20 m in ST3, and 10, 20 and 24 m in ST4.

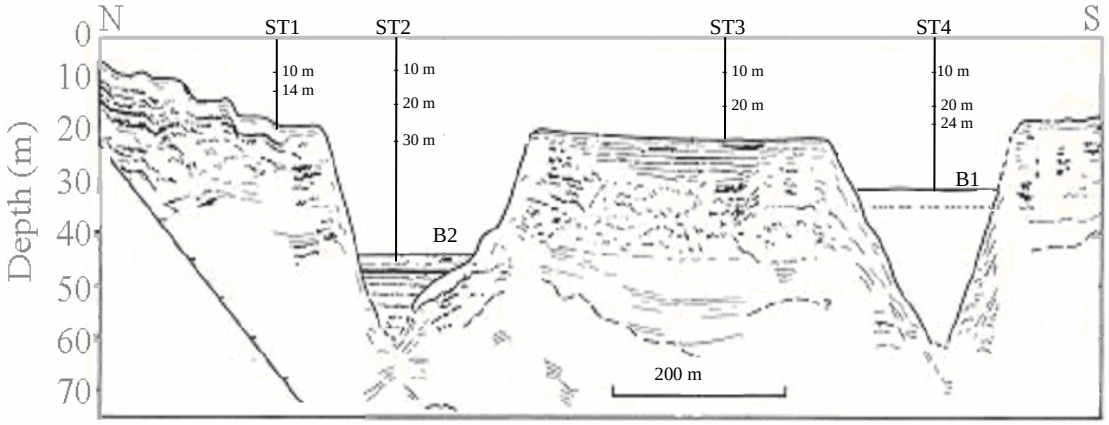

Figure 3.8
Schematic interpretation of the section from B2 to B1 from a North- South seismic transect (Canals et al. 1990) where different depths, where the sediment tramps are deployed, are shown.

In order to determine the nature of the particles (organic or inorganic) these samples were analysed in laboratory afterwards. Samples of 20 ml of water with sediment were filtered in glass-fibre filters, dried and later heated with a muffle furnace at 500 ^{o}C (following the procedure detailed by Kristensen & Andersen, 1987; UNE 77034). From the difference between the mass of the

samples before and after being heated, the amount of organic matter could be quantified.

Figure 3.9
Sediment tramps arrays. It has place for 6 bottles although they are only three used in the photo.

3.3.2.2. Calibration ADCP- Backscatter

All the particle studies done till now in Lake Banyoles have been done with data taken with LISST-100, which covers a measurable particle size diameter range from 1.2 to 230 μm. During the 2003 October campaign, some profiles with both instruments (LISST-100 and ADCP) were taken in order to correlate the particle concentration with the backscattering signal. Unfortunately, this was not possible because they work in a different diameter range. The ADCP frequency is 600 kHz, thus the particle size at which this instrument is sensible is of the order of millimetres, and therefore the ADCP backscattering signal will be related to particle sizes of the order of millimetres. This pattern might change if the amount of small particles is large, as happens in the region with the hydrothermal plume. This can be seen in Figure 3.10, although small particles (20 μm diameter) dominate, the ADCP backscattering gives a larger signal in the region where we find particles larger than 50 μm diameter. From the particle concentration profile we can differentiate two layers. The upper layer, from 0 to 15 m depth, with a low particle concentration

and the layer bellow with large values of particles concentration due to the presence of the hydrothermal plume.

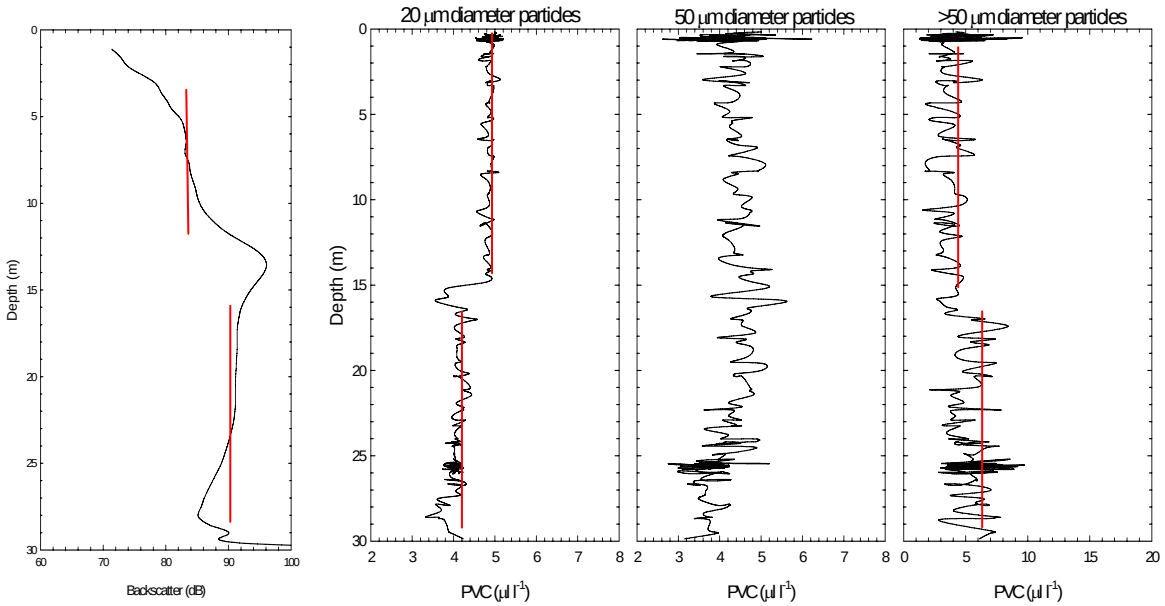

Figure 3.10
ADCP backscatter profile and PVC of different diameter particles obtained with LISST-100 in basin B1 the 10/22/2003.

The aim of this study was to acquire a better understanding in the dynamics of the chronic hydrothermal plume in B1 and the eventual hydrothermal plume in B2 for determining their horizontal and vertical evolution. The ADCP gave us the opportunity to have an image of the particle distribution in the water column of the lake. It was then necessary to identify the ADCP backscattering signal in dB with a physical parameter with the purpose of quantifying the particle distribution in the lake. The ADCP backscattering signal was then correlated with the signal from a turbidimeter (Figure 3.11), resulting an equation for the regression line: *Turbidity* (FTU) = 0.2242 *backscatter* (dB) - 16.348, with a R^2 value of 0.6989.

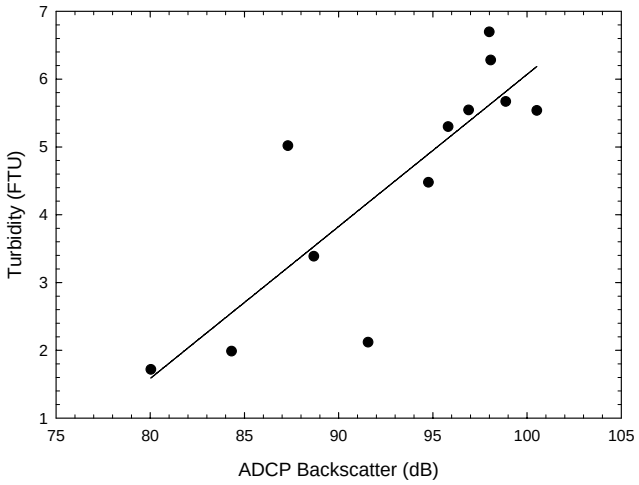

Figure 3.11
Regression line correlating ADCP Backscatter to Turbidity

3.4 Water temperature evolution

Temporal and spatial development of density gradients, due to changes in vertical temperatures in the water column, result in vertical and longitudinal zonation in aquatic systems.

A monomictic lake is one which mixes once a year (in winter in Lake Banyoles). From spring to autumn there is thermal stratification, and therefore no mixing occurs. In the spring the upper layers start to be heated by the sun and become less dense, floating on the denser layers below them. As the temperatures fall in the autumn, the surface waters become cooler and denser than the bottom waters and sink until a uniform temperature and density is shared by the entire lake. The layer of high stability, where a large temperature gradient in the depth can be found is called the *metalimnion*.

Lake Banyoles is a monomictic lake. Temperature evolution in basins B1 (Figure 3.12) and B2 (see Figure 3.13) and in the intermediate zone (see Figure 3.14), hereafter known as the plain (see Figure 3.8), shows that the thermocline starts to develop in March and deepens as surface water is warmed by solar irradiation (Colomer et al., 1996). In winter this stratification disappears and the entire water column can be mixed.

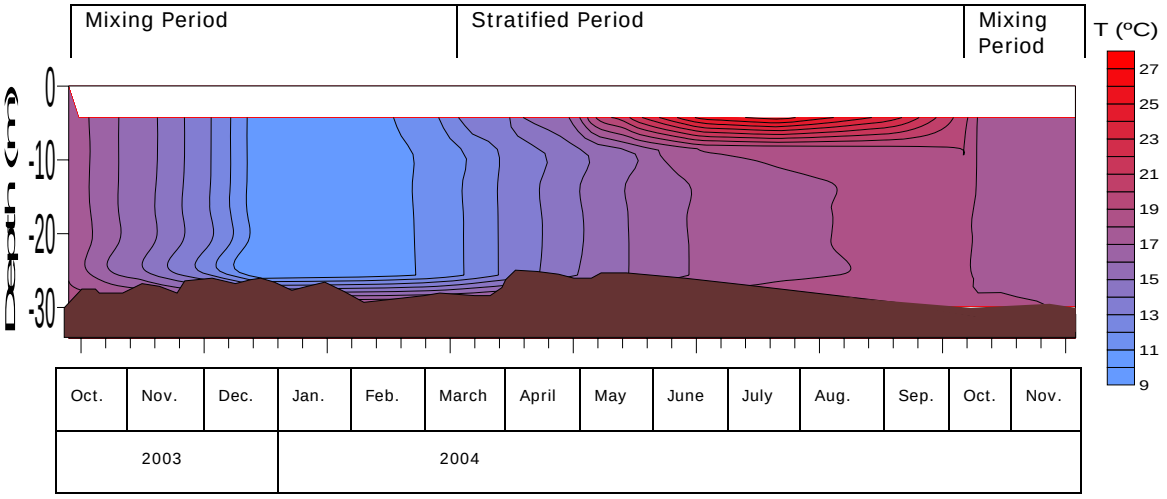

Figure 3.12
Temperature evolution in basin B1 from October 2003 to November 2004. The brown area in the figure represents the vertical and time evolution of the lutocline level (Z_L) during this period.

On the other hand, throughout the year, the warm water can easily be seen entering through the spring at the bottom of B1, with an increase in temperature up to 19 ºC at the lutocline level. This water is afterwards transported upward by the chronic hydrothermal plume in B1 (Colomer et al., 2001). Although this can also be seen in basin B2, the hydrothermal plume there is not chronic and can only be seen during the fluidization periods (Colomer et al., 2003), that is, when sediment resuspends and migrates upward. In the last twenty one years (1986–2006), while the sediments in B1 were found to be in suspension, the sediments in B2 usually remained compacted at the bottom of the basin, except for periods of high precipitation when monthly rainfall was ~ 2.7 times greater than mean monthly rainfall, as has been explained in Chapter 2, that corresponds to Soler et al. (2007). These fluidization events (F1, F2, etc.) were detected while measuring the depth of the lutocline (Z_L) in B2 (Figure 3.13), that is the depth where an abrupt increase in temperature can be found, indicating the presence of sediment and warm water.

As the surface area of B1 is larger than that of B2 (5.6 hm^3 and 4.6 hm^3, respectively) it has more inertia and heats and cools more slowly than B2. This can be seen in Figures 3.12 and 3.13. B1 is cooler at the beginning of summer but

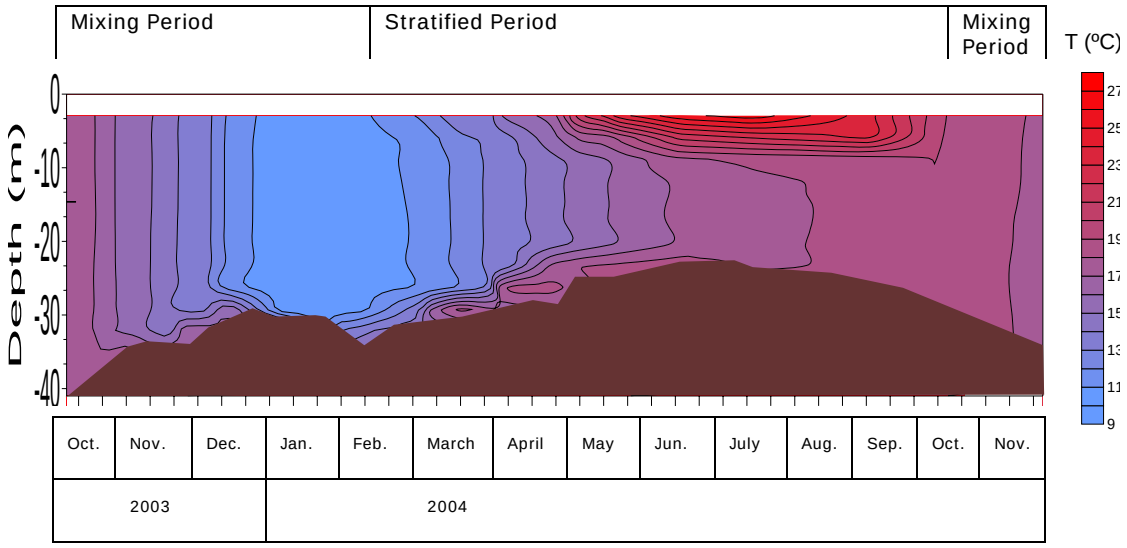

Figure 3.13
Temperature evolution in basin B2 from October 2003 to November 2004. The brown area in the figure represents the vertical and time evolution of the lutocline level (Z_L) during this period.

when the autumn starts the water temperature in B1 is higher than it is in B2. This behavior is also affected by the fact that the water entering through the spring in basin B1 is warm, at ~19ºC.

From the temperature evolution in the plain shown in Figure 3.14, a delay can be seen in the development of the thermocline in spring and, as expected, the mixing comes after the autumn arrives. There is also a slight increase in temperature at the bottom caused by lateral intrusion from basin B1.

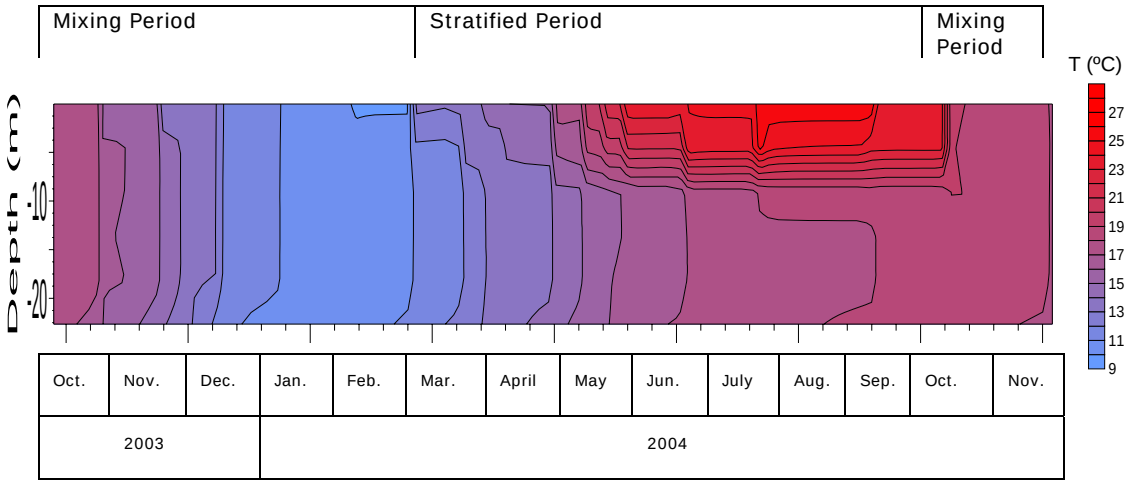

Figure 3.14
Temperature evolution in basin B1 from October 2003 to November 2004. The brown area represents the bottom.

3.5 Fluidization events and their consequences

As has been seen in Chapter 4, anomalous rainfall periods lead to the vertical displacement of the lutocline. During the tenth and eleventh fluidization (see F10 and F11 in Figure 3.15) intensive temperature and Z_L measurements were done in basins B1 and B2.

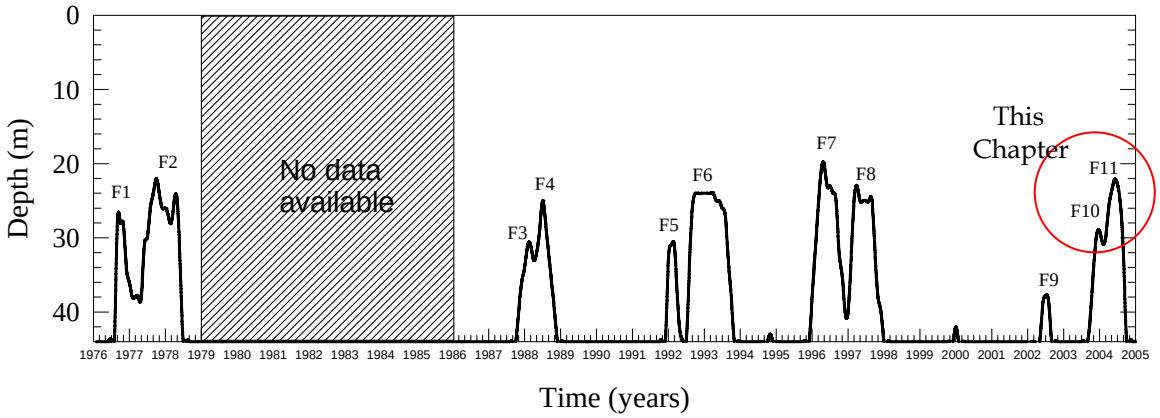

Figure 3.15
Lutocline depth at B2 during the period 1976-2004, where fluidization events are identified (from F1 to F11). The sampling frequency of the lutocline depth for F1 to F4 was 15 days while for F5 to F11 it was a week.

The zone of sediments in suspension in B1 has a vertical thickness of 45 m, a mean sediment mass concentration from 100 to 130 g/l, and a temperature of 19.1ºC, with only small deviations measured throughout the year (Casamitjana & Roget, 1993; Colomer et al., 2002). In B2 the sediment concentration mass varies from 280 g/l at the beginning of the fluidization events to 180 g/l when sediments remain in suspension.

Although the lutocline in B2 has an important vertical displacement with a maximum of 23 m in June 2004, being the lutocline therefore situated at 22 m depth, the maximum displacement is less in B1 reaching a depth of 27 m and thus migrating 4 m from its deepest position at 31m (see Figure 3.15 and 3.16).

This important difference between both basins is due to the chronic fluidization character of B1 and the episodic character of B2.

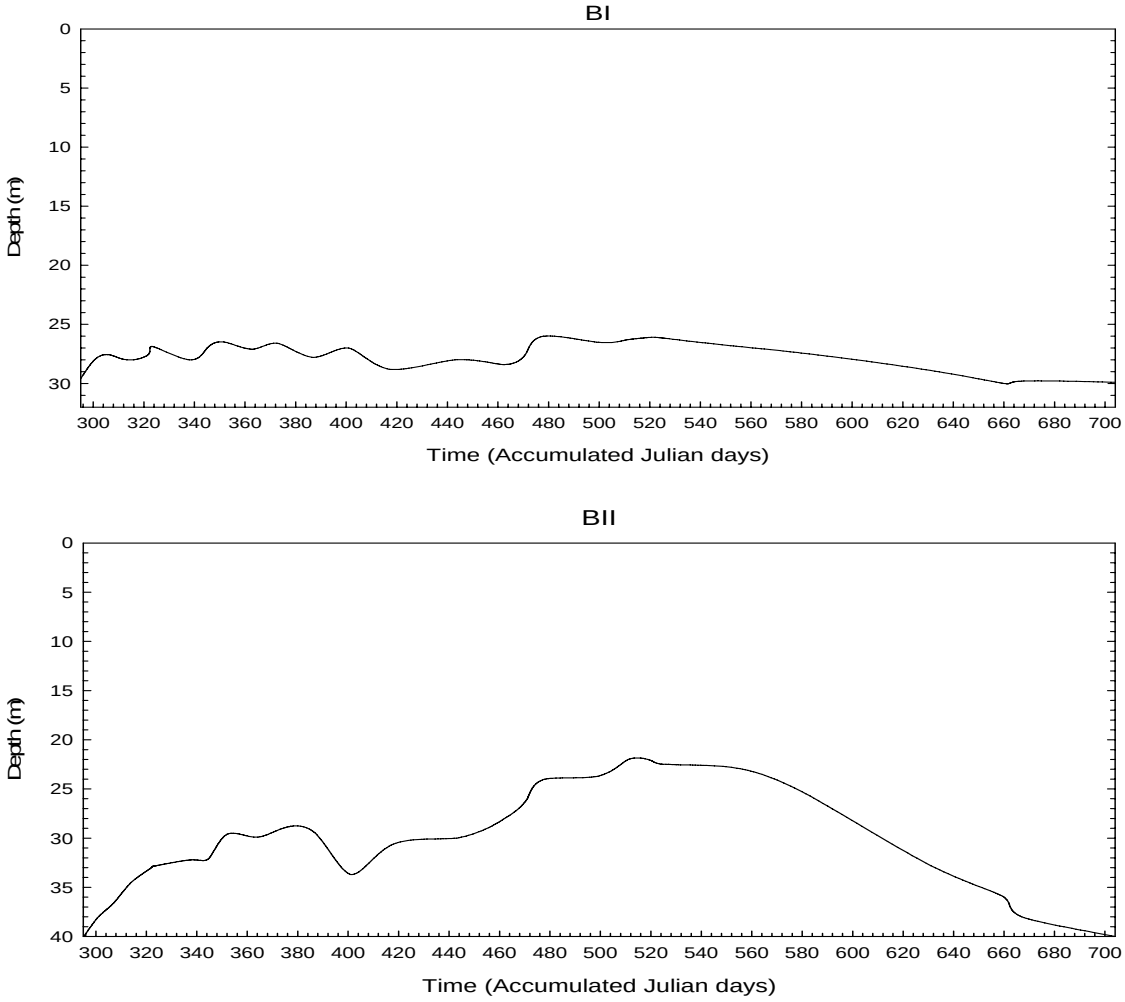

Figure 3.16
Lutocline depth temporal evolution in B1 (a) and B2 (b), from October 2003 to November 2004.

3.6 Sediment distribution

Depending on the nature of the source, plumes can also transport particles (then termed turbid plumes) and increase the turbidity of the water body where they develop, which might in turn produce important ecological, biological and physical implications in the water system. Turbidity, usually measured as a result of particle suspension, plays an important role in light extinction, nutrient supply, fish limiting-respiration and reduction of the effectiveness of visual piscivorous predators (Serra et al., 2002a).

As hydrothermal plumes in Lake Banyoles develop from the lutocline, which we must remember is an interface rich in sediments, they are turbid plumes, i.e.

sediment particles are transported from the lutocline level through the lake hypolimnion (Serra et al., 2002b).

The particle size distribution (PSD) obtained up and down the water column (see Figure 3.17) presents a trimodal shape, with peaks centered at 8 μm, 50 μm and 200 μm. The two smaller peaks are characteristic of the hydrothermal plume (Serra et al., 2002b) and the larger one correponds to a few dead phytoplankton cells that have settled throughout the water column.

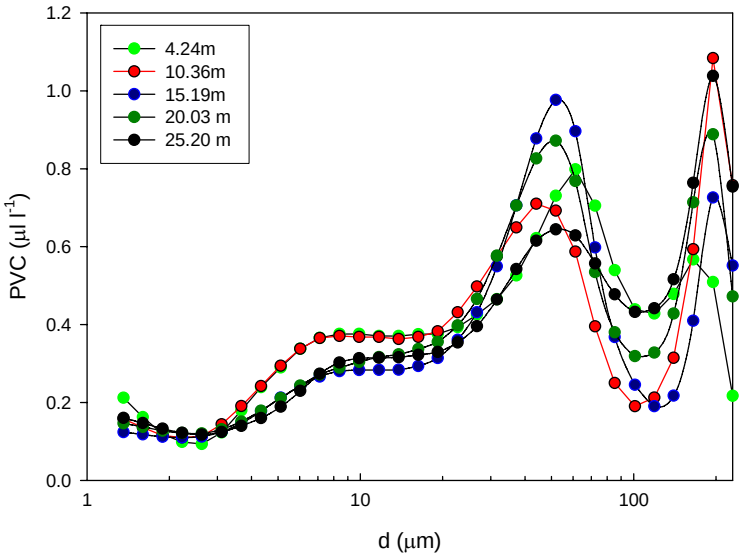

Figure 3.17
PSD of particles obtained at different depths of the water column in B1 on 10/22/2003. The PSD has been measured with the LISST-100.

The laboratory analyses of the sediment collected during the field campaigns show a high percent of inorganic matter up and down the water column (Figure 3.18). When comparing the first and the third field campaigns, however, the percent of organic matter increases in September 2003, in accordance with the fact that it is easier to find the rest of the organic matter (detritus) in the water column in September than in October. This organic matter comes from the algae that develop when the springs starts and live in the epilimnion through the summer.

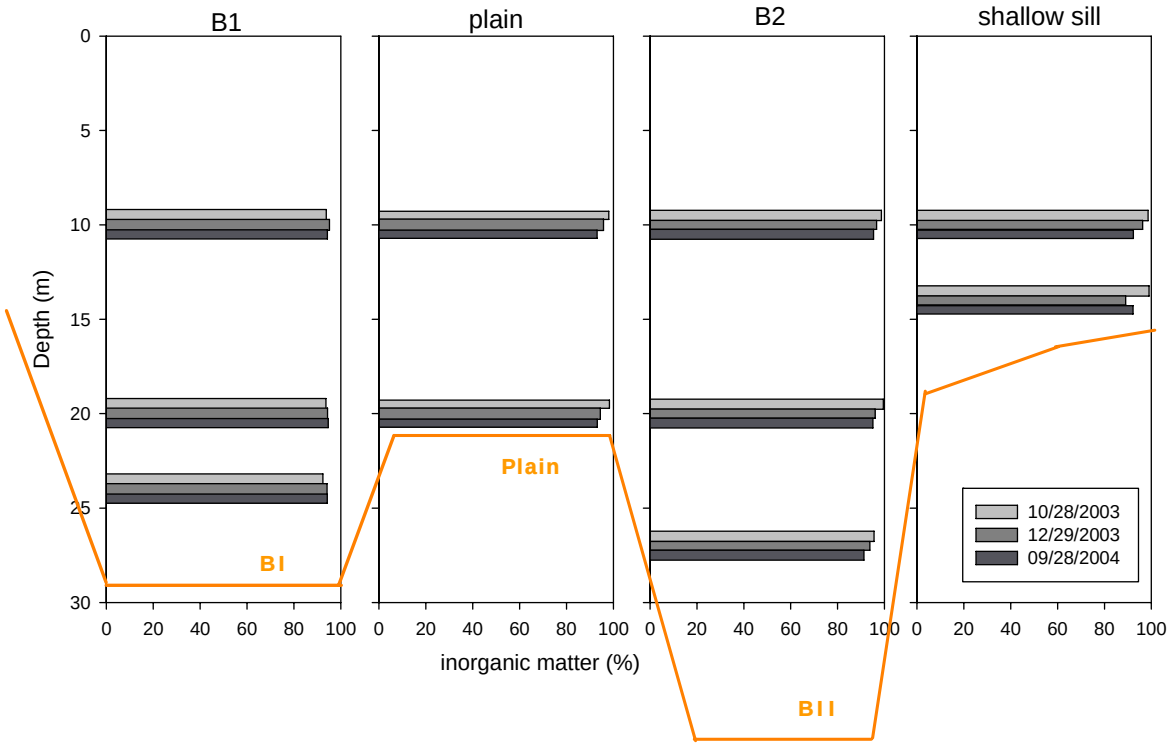

Figure 3.18
Values of the percent of inorganic matter from the sediment traps obtained at different depths of the water column at B1, B2, the plain and the shallow sill that divides the lake in two lobes, for the days 10/28/2003, 12/29/2003 and 09/28/2004.

3.7 Temporal evolution of basins B1 and B2

Thanks to their turbid character, the sediments that hydrothermal plumes carry upward are perfect tracers and reveal their vertical and horizontal distribution. Some studies have been done to correlate the particle concentration with the ADCP (Bunt et al., 1999, Buckner, 2001).

As the dynamics of hydrothermal plumes is affected by lake stratification, all the ADCP backscatter images taken during the period from October 2003 to November 2004 will be classified depending on whether the column is stratified or not. Temperature profiles in basins B1, B2, and the plain will be included beside the ADCP images. All these data (ADCP data describing the vertical and horizontal distribution, and T giving the lake mixing) will help to explain the evolution of the hydrothermal plume development during a whole year.

3.7.1 Mixing Period: the end of summer

22OCT03 (Figure 3.19, top)

At the end of October the lake starts to mix, and this can be seen in the temperature profiles. In basin B1 the temperature has a nearly constant value of 17.9 ºC, although a slow increase with depth can be seen. At 29.5 m, when the profiler reaches the lutocline, the temperature increases suddenly to 18.6 ºC. In the plain the temperature can be also considered constant with a small increase at 13 m. Basin B2 also has this slight temperature variation at 13 m, and from 20 to 22m it has a thermocline. This thermocline can be found at the entrance of the cone-like depression; it is caused by the accumulation, at the interior of the V-shaped bathymetry, of water that remains nearly isolated from the hypolimnetic waters of the lake. This second thermocline can be found during the end of the stratified period in cases where the source on the bottom is not active. Basin B1 has a mean temperature 0.2 ºC higher than B2; this is caused by the difference between the volume capacities of the two basins (as has been explained in Section 3.4).

The ADCP backscattering signal shows the chronic hydrothermal plume in basin B1, with a maximum height that reaches the water surface. There is a lateral intrusion at 15 m depth that can be seen in the plain, as well as in B2, where the sediments still remain consolidated at the bottom. In basin B2 an accumulation of particles at 20 m depth can also be seen, which might be due to particles coming from the plain bottom accumulating, settling from the B1 lateral intrusion and finding in the thermocline a barrier to their vertical settling.

3NOV03 (Figure 3.19, center)

Temperature profiles show that the water column is entirely mixed in B1 and the plain. In B2 the temperature increases from the bottom to 20 m depth, which shows us the existence of a convective process at the bottom of the basin. The hydrothermal plume in B2 can also be seen in the ADCP backscattering image, as well as in the upward velocity component of the ADCP data (see figures in

Annex A). The hydrothermal plume develops from the bottom to the surface, breaking the particle layer found at 20 m depth, the thermocline. At the north of the basin an important quantity of particles can be seen coming from the north of basin B2. These particles are transported by a gravity current driven by the differential heating of the two lobes of the lake (north and south) caused by differences in their morphometry and in underground incoming heat. This gravity current appears during the mixing period (Roget et al., 1993; Roget and Colomer, 1996).

In basin B1, the hydrothermal plume is very active: ADCP gives a large backscatter signal indicating the plume source occupying almost the entire basin. There is a discontinuity in the backscattering signal at the subsurface layer of the lake, which gives the idea of a chimney with several plumes developing in its interior (this will be discussed in Section 3.8).

The fluidization event in B2 began, after a very rainy second fortnight of October, with a mean monthly rainfall of 257.2 mm measured by the weather station situated in Olot, close to the recharge area of the lake. The preceding ten months before the beginning of the fluidization event were very dry, so it took a long time for the water to arrive from the recharge area to the subterranean springs at the bottom of the lake.

10NOV03 (Figure 3.19, bottom)

At this time the water column was completely mixed, as can be seen in the temperature profiles. Besides this, at the bottom of the temperature profile of basin B2 a positive inflection can be observed, showing the initiation of the convective process (Levy and Fernando, 2002). The convection in B1 can be also seen in the temperature profile with an increase in temperature from 22 m depth to the lutocline.

The backscattering signal in basin B2 is very similar to that for 3 November; the only difference is the accumulation of particles around the single plume. When the plume appeared, it broke through the layer of settled particles at 20 m depth and transported them vertically. After that, they settled again around the plume

contributing to the increase in the concentration of particles at 10 m depth together with the particles coming from the north of the basin through the gravity current, and, by a lateral intrusion, from the plain and the hydrothermal plume in basin B1, at the southern part of the basin. This settling process is also seen in the plain. While on 3 November the entire water column could be found full of particles (green at the top and yellow and red at the bottom), a quite clear water column (blue at the top and green at the bottom) can now be seen all over the zone.

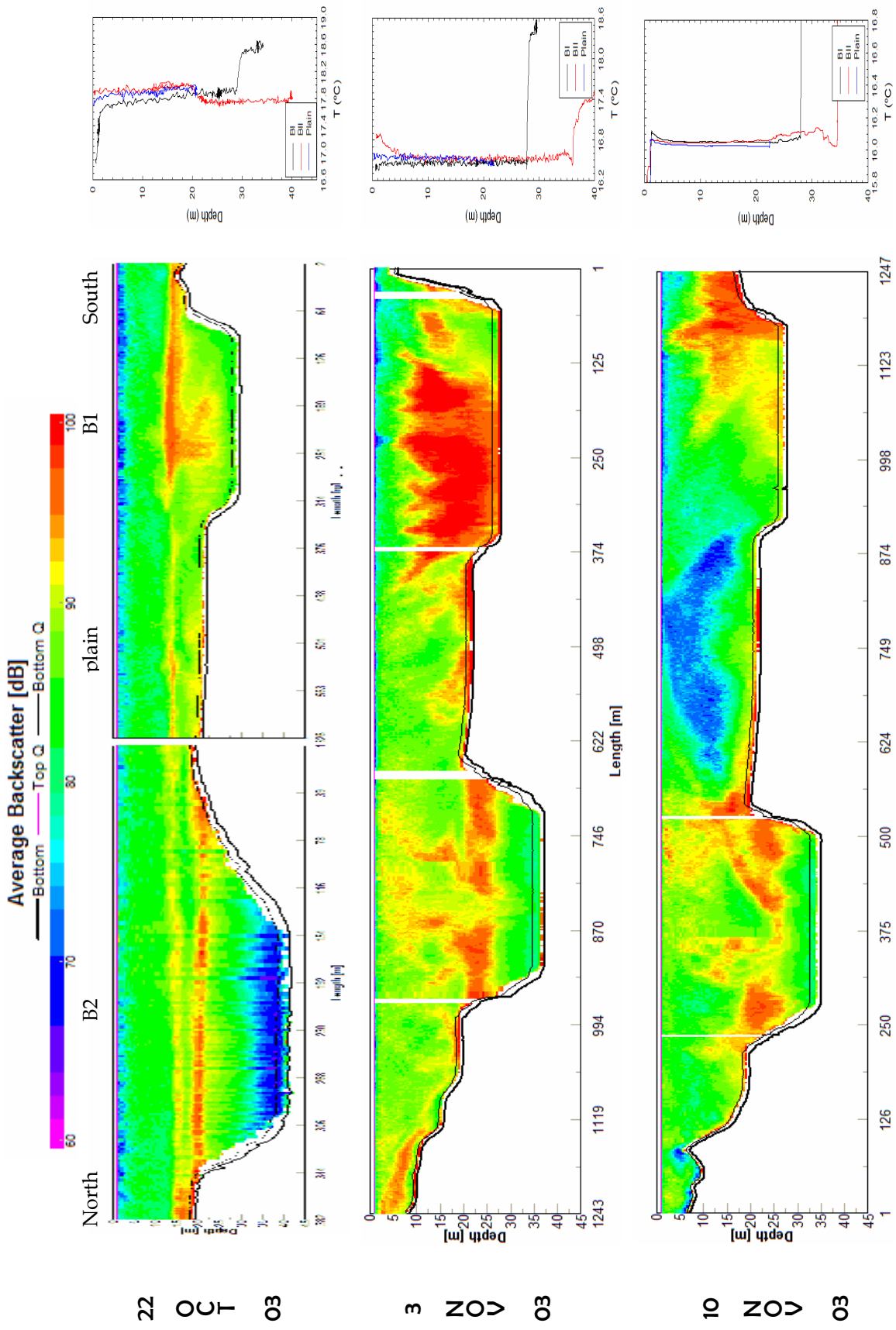

Figure 3.19
ADCP Backscatter transect along the southern lobe of Lake Banyoles (left) and Temperature profile in both basins: B1 and B2, and the Plain.

18NOV03 (Figure 3.20, top)

There was no temperature data available.

The ADCP backscatter in basin B1 shows the hydrothermal plume developed in the southern part of the basin. Sediments reach the water surface and at 13 m depth they spread laterally towards the north of the lake. In basin B2, the single plume, still developed, has mixed all the particles that had settled at 20 m depth.

20NOV03 (Figure 3.20, center)

The hydrothermal plume is fully developed at the southern part of basin B1, arriving to the surface because the water column is mixed and there is no thermocline to limit it. As can be observed from the backscattering signal, the plain is quite clear of particles. In basin B2 particles remain at 20 m depth. At this time this particle layer is not broken although the single plume is still developed, as can be observed from the temperature profile, where there is still the positive inflection near the bottom, and also in the upward velocity of the ADCP data (figures found in Annex A).

4DEC03 (Figure 3.20, bottom)

The hydrothermal plume remains developed in basin B1, as can be seen from the temperature profile, and it arrives at the surface. The plain is full of particles, which come by lateral intrusion from basin B1. The particle layer at ~22 m depth in B2 is broken again by the plume that is still developed there, as can be seen in the positive inflection in the temperature profile. At the beginning of December it rained in the recharge area, with quantities between 47.6 mm in Olot and 68.2 mm in Agullana, in the first three days. Together with a wet recharge area, this made the water arrive quickly to the springs, keeping the hydrothermal plumes active.

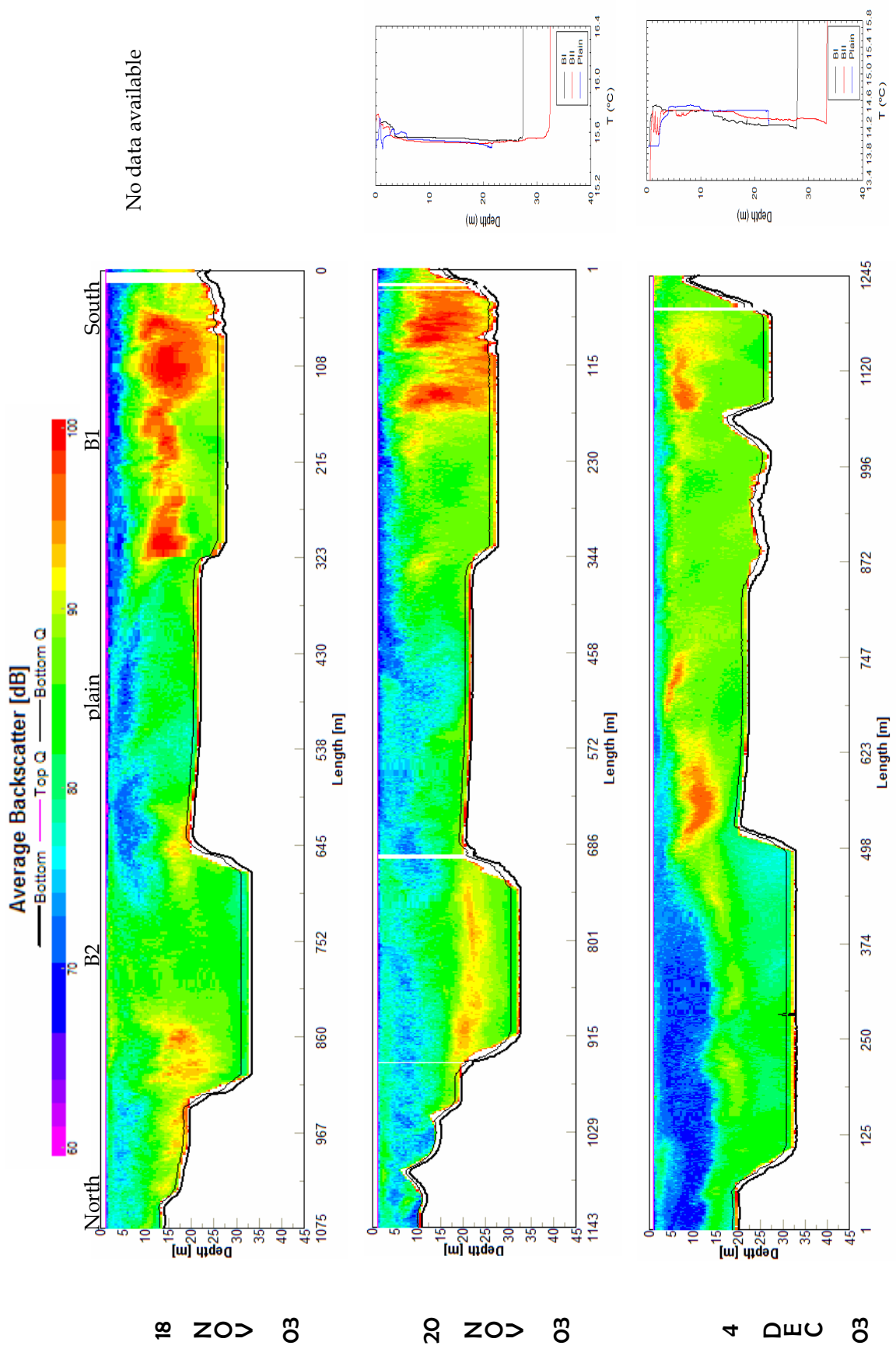

Figure 3.20
ADCP Backscatter transect along the southern lobe of Lake Banyoles (left) and Temperature profile in both basins: B1 and B2, and the Plain.

11DEC03 (Figure 3.21, top)

The temperature profile shows that the plume developed in basin B2 is more active than the one in basin B1: the positive inflection near the bottom of basin B2 still can be seen and it is greater than the inflection in the temperature profile of basin B1. The break of the sediment layer at 20 m depth and an accumulation of particles near the plain bottom can be seen in the ADCP backscatter image. As the temperature profile in the plain shows an increase of temperature near the bottom, it could be then said that particles come from lateral entrainment from basin B2 towards the plain.

18DEC03 (Figure 3.21, center)

Unfortunately we do not have temperature data for this survey.

ADCP backscatter shows nearly the entire lake without particles (blue color) except for the water column above basin B1 where the hydrothermal arrives to the surface. In basin B2, the sediment layer break cannot be seen. Hereafter this change might be attributed to a change in the behavior of the plume development of B2 corresponding to the transition from a single plume to a chronic one (see Chapter 4).

29DEC03 (Figure 3.21, bottom)

After the transition period the plume in basin B2 starts to behave like the chronic plume of B1. This change is easily seen in the ADCP backscatter image where the accumulation of particles (in yellow) is on the bottom of the basin. From temperature profiles it can be seen that the water column is mixed, and therefore, without any barrier of thermal stratification, the plume can develop completely to the surface. Using Equation 3.8, and the values $B_o = 1.124 \cdot 10^{-7}$ m^2s^{-3} and $N = 0.0034$ s^{-1}, estimated from temperature data, the value of h_{max} has been calculated to be larger than the lake depth (h_{max}= 36,4 m); this indicates that the plume collapses at the lake surface. In basin B2, the smaller buoyancy, $B_o = 4.615 \cdot 10^{-8}$ m^2s^{-3} causes the maximum height to be of 25.5 m. This does not match with the ADCP backscatter figure where a value of

h_{max} ~ 20 m can be found in basin B2. It is probably caused by a slight deviation from the center of the plume during the transect for data acquisition.

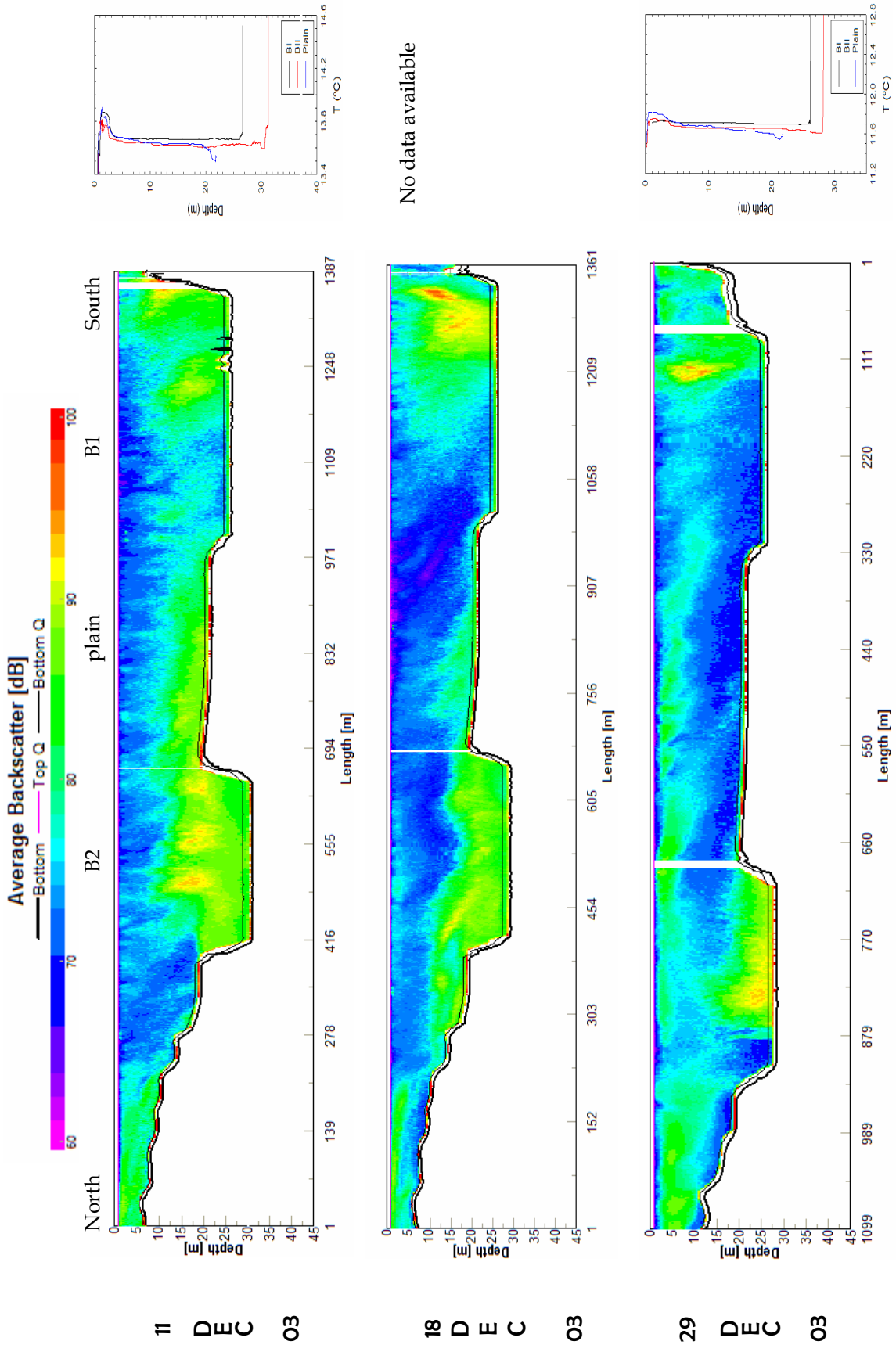

Figure 3.21
ADCP Backscatter transect along the southern lobe of Lake Banyoles (left) and Temperature profile in both basins: B1 and B2, and the Plain.

8JAN04 & 22JAN04 (Figure 3.22, top and center, respectively)

Temperature profiles for both days show the water column mixed in the whole lake; only a small diurnal thermocline can be seen near the surface. The hydrothermal plume in B1 migrates up to the lake surface on both days, 8 January and 22 January. In basin B2, it can be seen on both days that the hydrothermal plume develops to ~15 m. On 8 January, the ADCP backscatter shows particles at the north of basin B2; these particles are found afterwards in the southern part of the lake on 22 January. This displacement of particles can be related to the gravity from the northern lobe that can be found during this period of the year (Roget and Colomer, 1996).

5FEB04 (Figure 3.22, bottom)

The hydrothermal plume in basin B1 looks more active according to the red color that indicates a higher quantity of particles transported upward from the lutocline. Although a clear positive inflection cannot be seen in any of the temperature profiles, it transports a high quantity of sediment, reaching the lake surface. In B2, convection can be seen all along the basin bottom, in contrast to the beginning of the fluidization event and related to the chronic behavior of this plume in this period. Its shape is similar to the one in basin B1 on 3 November, with a chimney formed by several plumes. (In this case they are two different plumes, one in the northern part of the basin bottom and the other in the southern part, as can be observed from the ADCP data signal.) The estimated maximum height of the plume is ~ 17 m, in accordance with the ADCP backscatter data where the h_{max} is ~15 m. Lateral intrusion from the northern lobe of the lake can also be seen.

21FEB04 (Figure 3.23)

The hydrothermal plume in basin B1 collapses at the lake surface. In B2, convection can be seen all along the basin bottom, with the presence of several plumes that reach the lake surface like in B1. The maximum heights of these plumes found with the ADCP backscattering signal is in accordance with the estimated maximum height of ~53.37 m in B2 and of ~76.32 m in B1. Particles

from the lutocline migrate to the surface where they spread laterally. Lateral intrusion by the northern density current can still be seen.

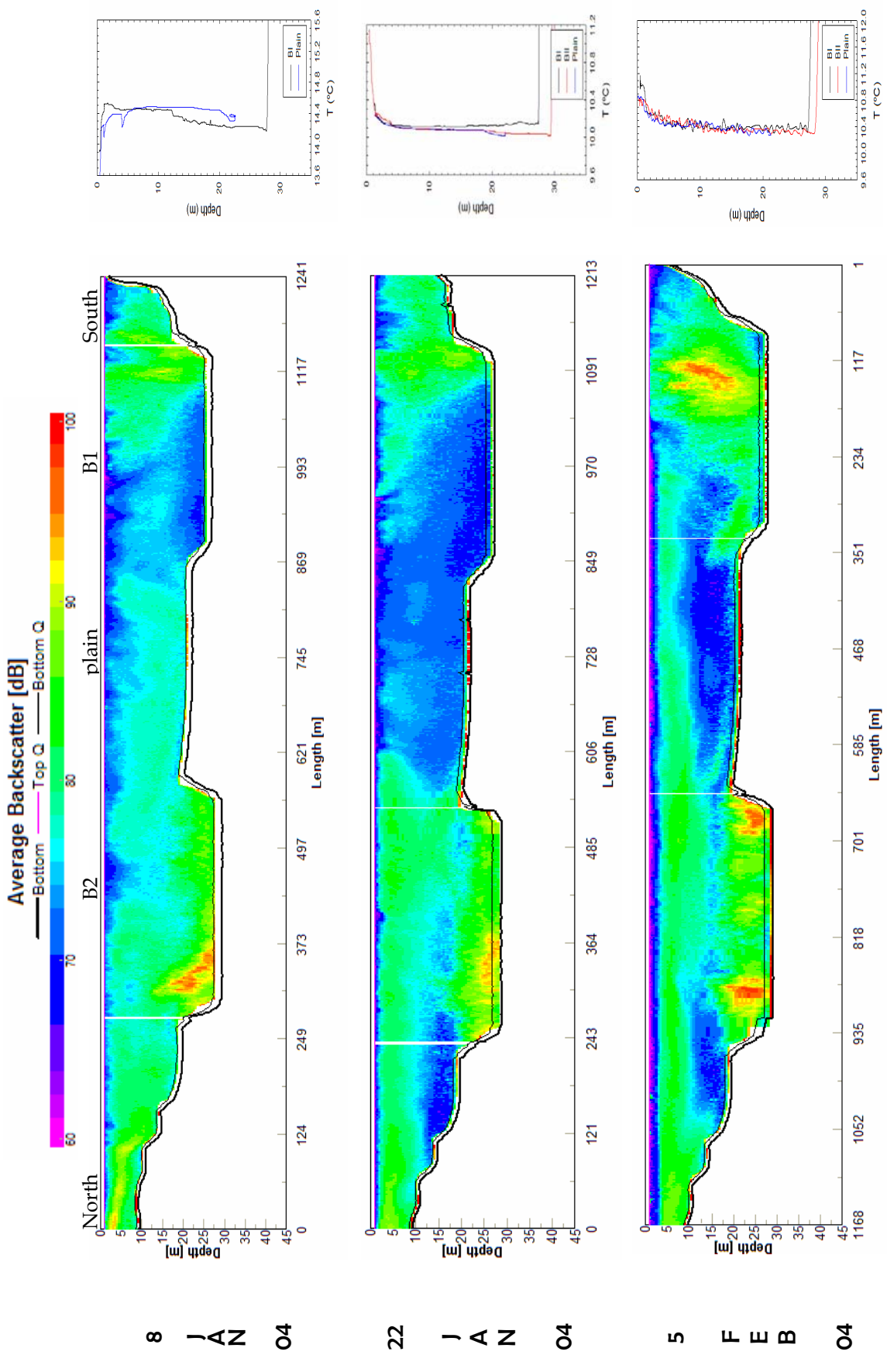

Figure 3.22
ADCP Backscatter transect along the southern lobe of Lake Banyoles (left) and Temperature profile in both basins: B1 and B2, and the Plain.

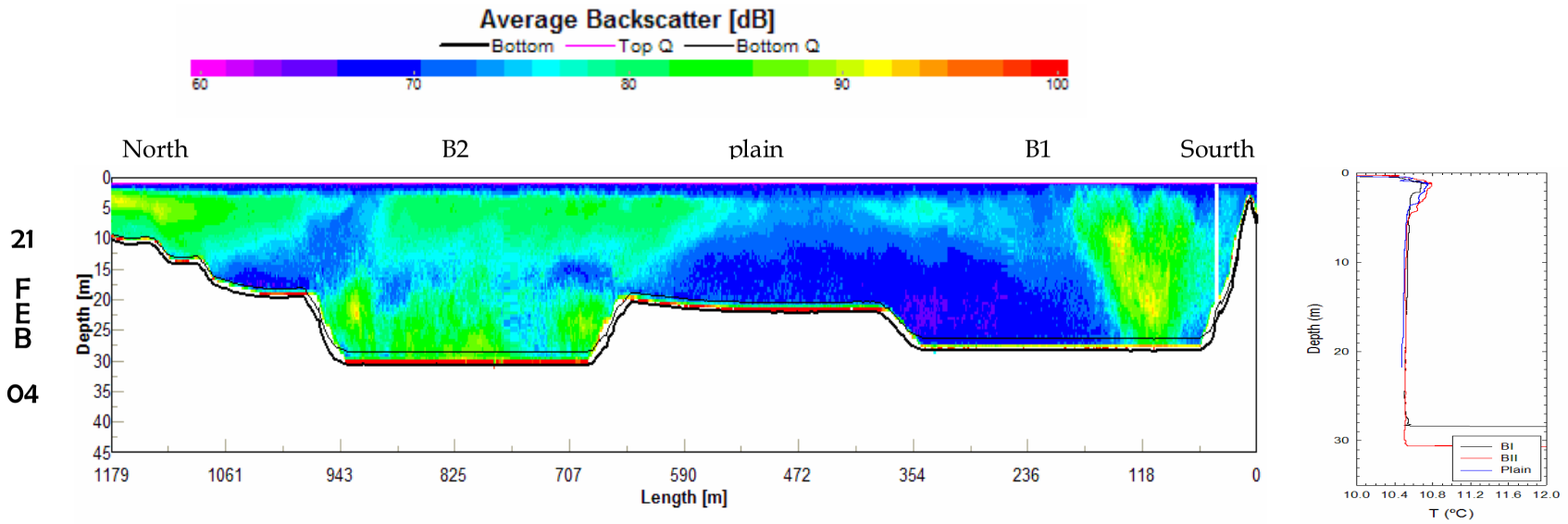

Figure 3.23
ADCP Backscatter transect along the southern lobe of Lake Banyoles (left) and Temperature profile in both basins: B1 and B2, and the Plain.

3.7.2 Beginning of the stratified period

6APRO4 (Figure 3.24, top)

The entire water column in the lake is stratified. The epilimnion thickness depends on the lake zone, being ~3.5 m in the plain and in B2, and ~5 m in B1. Two thermoclines can be found in the lake. In basin B1 the first thermocline is found at ~5 m depth (with a thickness of ~0.1 m) and the second at ~7.5 m (with a thickness of ~0.5 m). In basin B2 the first thermocline is found at ~3 m depth (with a thickness of ~0.1 m) and the second at ~6 m (with a thickness of ~2 m). In the plain the first thermocline is found at ~3.5 m depth (with a thickness of ~1.5 m) and the second at ~6 m (with a thickness of ~2 m). The ADCP backscatter signal shows that although both hydrothermal plumes in B1 and B2 are still active, they transport a small quantity of sediment (blue) upward. The central part of the water column is very clean throughout the lake (pink); particles can only be found from the lake surface to the thermocline, which acts as a barrier to their settling.

22APRO4 (Figure 3.24, center)

Temperature profiles are much the same as at the beginning of the month. Both the plain and the B2 temperature profiles have become more similar and the second thermocline in B1, which was at ~8 m depth, is still there. In fact, it acts as a barrier to the vertical development of a hydrothermal plume. The maximum height in basin B2 is ~12 m, although with the values of B_o and N, and using Equation 5.8, a value of ~27 m has been found, but as the thermocline starts at ~7 m and the Richardson number is bigger than 11 (=Ri_c), the hydrothermal plume should collapse at the thermocline, which means at ~7 m instead of ~12 m.

For the first time the depth at which the lutocline in B2 can be found is shallower than the depth of the lutocline in B1. The sediments, transported upward from the bottom of B2 by convection, have overflowed the V-shape basin and settled on the plain, which corroborates the results of previous studies (Serra et al, 2005).

13MAY04 (Figure 3.24, bottom)

Temperature profiles help to understand the abrupt distribution of particles in the water column. The thermocline acts as a barrier to the vertical transport of sediments. In the ADCP backscatter, the particle layer (green color) developed from lake surface to the thermocline can be seen, and its thickness changes at the same time that the thickness of the epilimnion does.

3.7.3 Stratified Period

3JUN04 & 5JUL04 (Figure 3.25, top and center)

A summer stratified water column with a well-developed epilimnion (from the surface down to 5 m) and the thermocline below it (with a thickness of ~5 m) can be seen throughout the lake.

ADCP backscatter signal shows the plumes in basins B1 and B2 to be quite inactive during both days. There is a particle layer just on the thermocline throughout the lake, where the ADCP backscattering signal detects both organic and inorganic suspended particles. This layer, which can be seen from now until the mixed period (starting at the end of September), is related to an algal population. This is in accordance with an increase in Chl a at this depth (see Annex B) and also an increase in the oxygen concentration (see Annex B).

5AUG04 (Figure 3.25, bottom)

As explained previously, the particle layer, just on the thermocline, can be seen throughout the lake. Large backscattering signals can be also seen on the bottom, showing the hydrothermal plume activity in both basins. In basin B1 the convection is situated at the north of the basin, and in B2 it is located in the middle of it, with the extremes of the source more active than the center. In both cases the vertical development is limited by the thermocline.

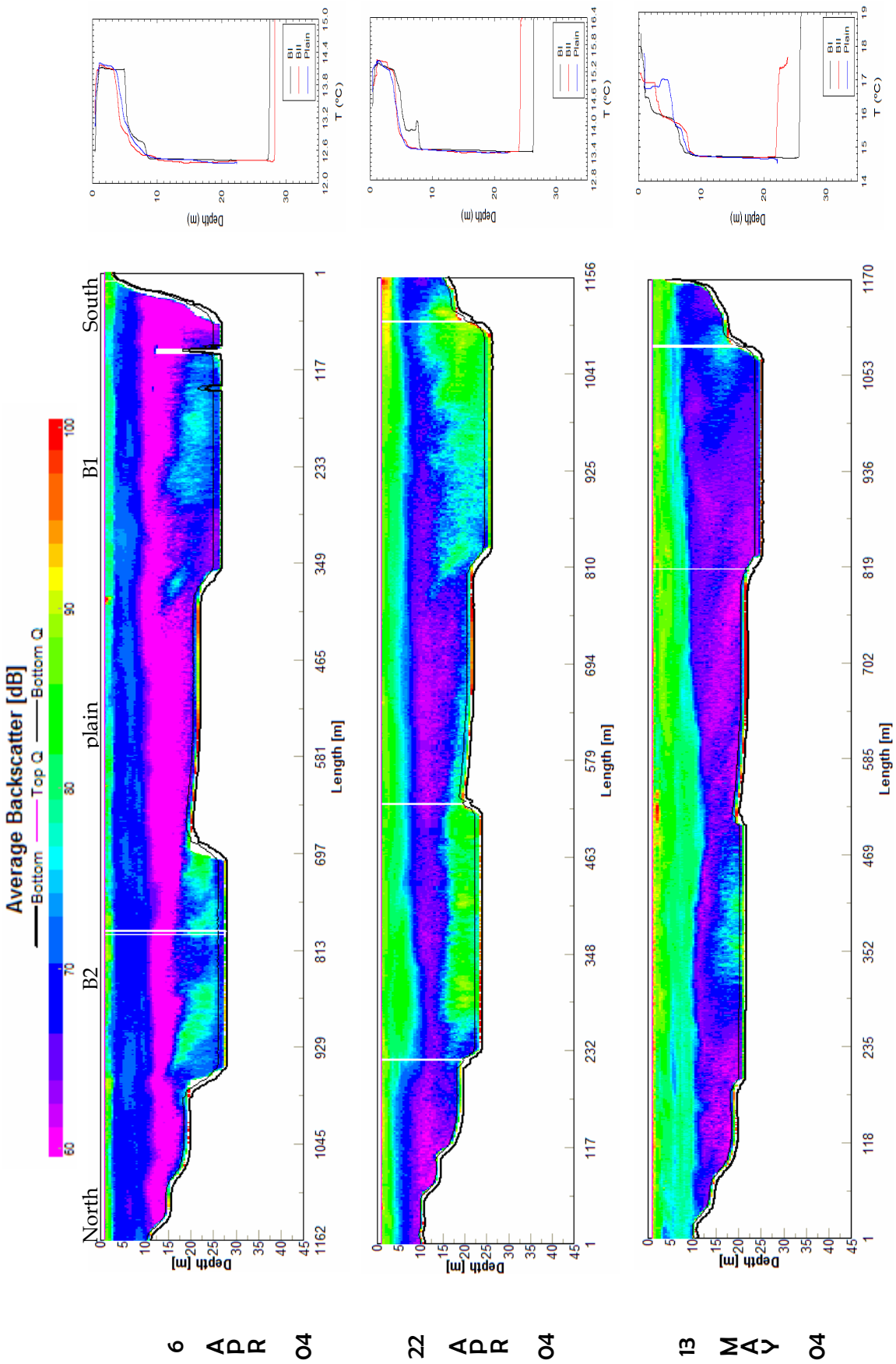

Figure 3.24
ADCP Backscatter transect along the southern lobe of Lake Banyoles (left) and Temperature profile in both basins: B1 and B2, and the Plain.

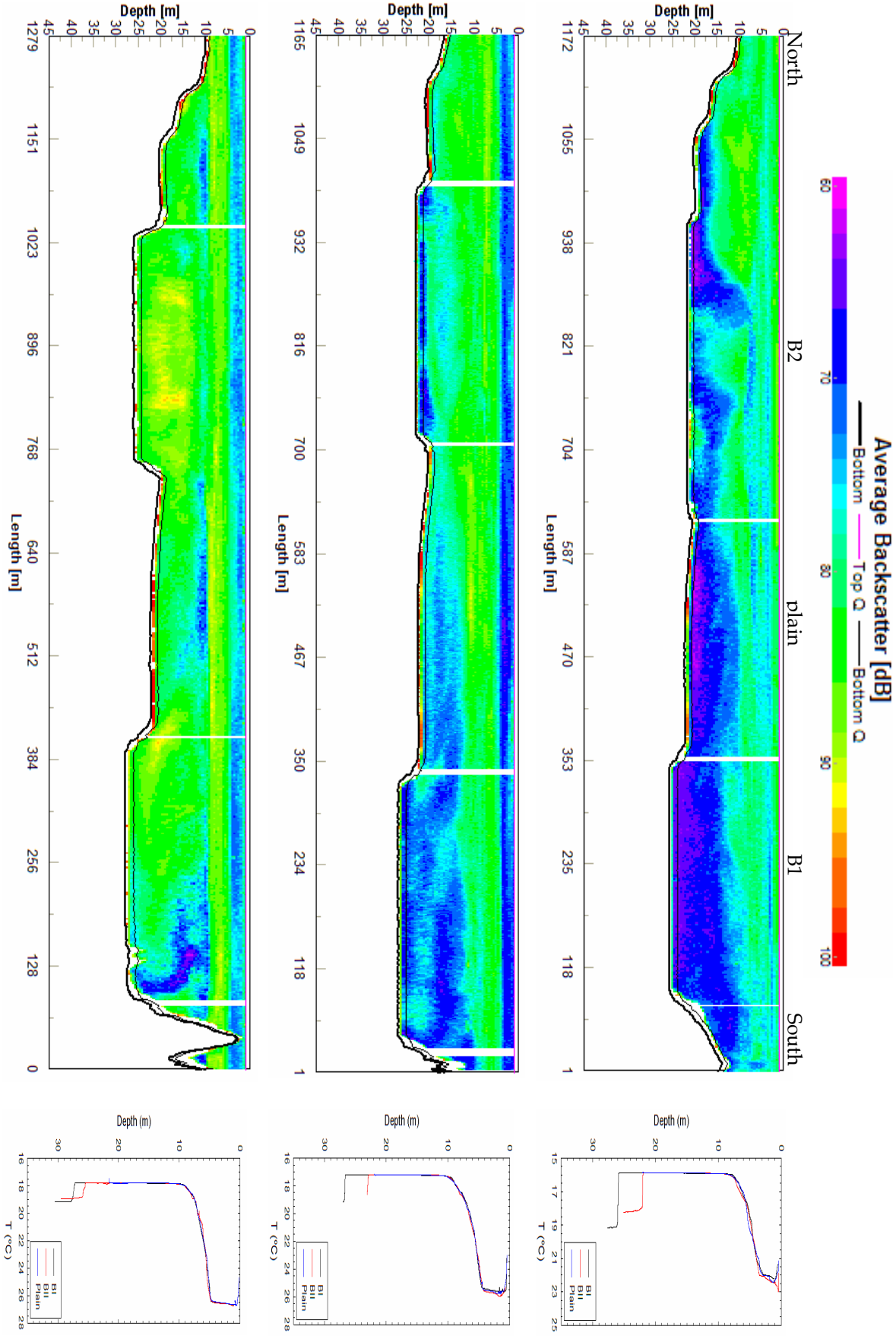

Figure 3.25
ADCP Backscatter transect along the southern lobe of Lake Banyoles (left) and Temperature profile in both basins: B1 and B2, and the Plain.

3.7.4 Beginning of the Mixing Period

22SEP04 (Figure 3.26 top)

The water column is still stratified, as temperature profiles show. As on previous days, the particle layer can be seen just on the thermocline (from 5 to 10 m depth). The hydrothermal plume is still active in basin B1, while all the water above the lutocline in basin B2 has a low backscattering signal, indicating that the convective activity in B2 is finished. Although it cannot be seen in the B2 temperature profile because the graphic values range is too large, there is a particle layer at 20 m depth, coinciding with the second thermocline.

21OCT04 (Figure 3.26, center)

A particle layer between 10 and 14 m depth (red) can be seen in basin B1. It is formed by particles that have settled, and sediment that comes from the lutocline, transported by the hydrothermal plume, which at this time has developed in the middle of the basin. Particles from above and from below are trapped by the thermal distribution of the water column. The thermocline is sinking and it can now be found at 14 m depth, but there is a thin thermocline at 5 m too, caused by an unusually warm October. The accumulation of particles can also be seen in basin B2, where particles settled till now at the first thermocline (from 5 to 10 m) and particles that were trapped in the second thermocline (z= 20 m) have formed a wide particle layer of 15 m width.

28OCT04 (Figure 3.26, bottom)

The particle layer in basin B2 has compressed itself, becoming thinner and having a higher concentration of particles (strong red). This is caused by the settling of the particles in its interior. The hydrothermal plume has developed in the center of basin B1. The thermocline in B1 has weakened and the plume can cross it.

3.7.5 Mixing Period

4NOV04 (Figure 3.27)

As can be seen from the temperature profiles, in November the water column of the lake is mixed. In basin B1 the temperature has an almost constant value of 17.8 ^{o}C with depth except for the first 4 m, which are more sensitive to diurnal temperature variation. At 30.5 m, when the profiler reaches the lutocline, the temperature increases markedly. In the plain the temperature can also be considered constant with depth except for the first meters. Basin B2 has this slight temperature variation at the surface too. Temperature values are similar to the other two temperature profiles (in B1 and the plain) but at 19 m this similarity starts to change: a secondary thermocline caused by the cold water accumulation at the bottom due to the V-shaped bathymetry appears.

From the ADCP backscatter signal it can be seen in basin B1 and the plain that almost the whole water column is full of particles. Therefore, in contrast to the stratified period, in the mixing period particles from the plume reach the surface of the lake.

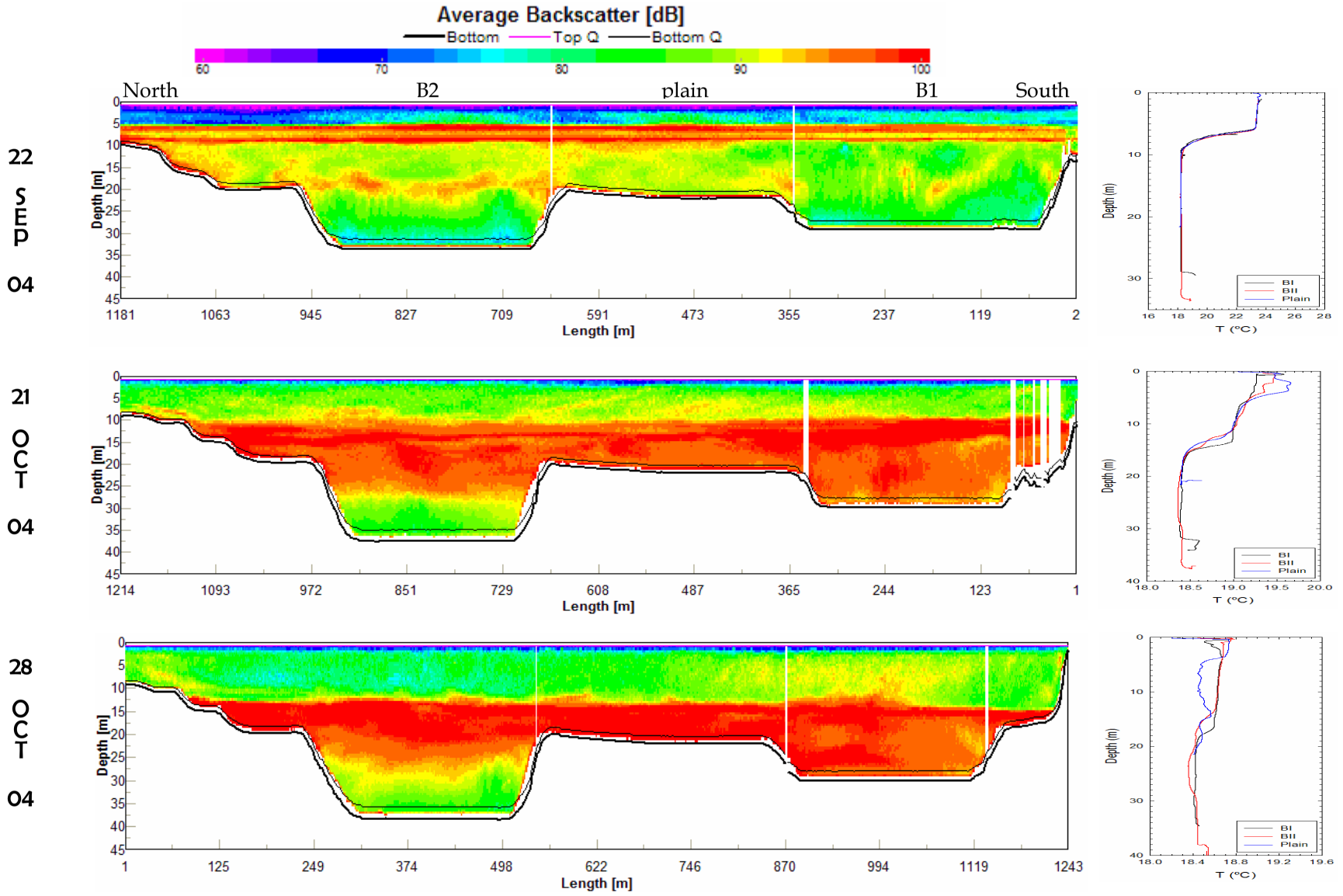

Figure 3.26

ADCP Backscatter transect along the southern lobe of Lake Banyoles (left) and Temperature profile in both basins: B1 and B2, and the Plain.

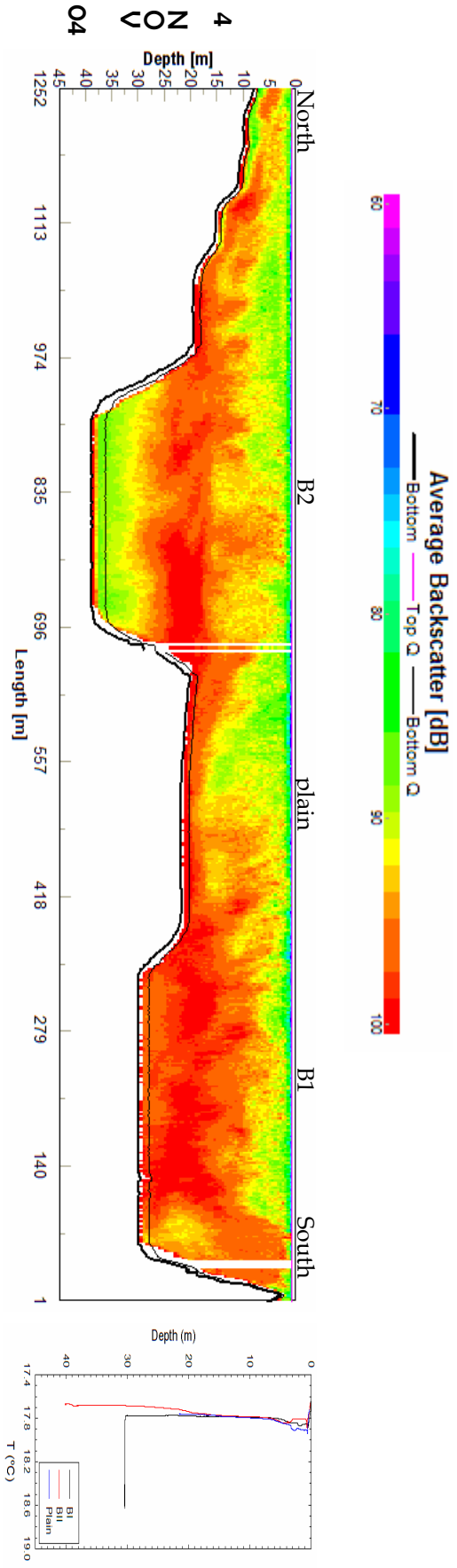

Figure 3.27
ADCP Backscatter transect along the southern lobe of Lake Banyoles (left) and Temperature profile in both basins: B1 and B2, and the Plain.

3.8 Summary and Discussion

3.8.2 Basin B1

Figure 3.28 shows the concordance between the theoretical values of plume maximum height (black dots) resulting from Equation 3.8 and the experimental values (green crosses) measured by the ADCP backscatter signal seen in Section 3.7. As has been explained in Section 3.2, convective flows do not penetrate through density interfaces but propagate radially along the base of the mixed layer when their Richardson number (Eq. 3.5) is larger than the critical value: Ri_c ~11 (Narimousa, 1996). For that reason, the values of h_{max} from the model situated above the thermocline depth (taken as the base of the metalimnion) are not allowed when the Richardson number is larger than the critical value, Ri_c. In Lake Banyoles the Richardson number values found are always above the critical number, falling between 26 and 812. Therefore, any slight stratification of the water column represents a physical barrier for the vertical development of the plume.

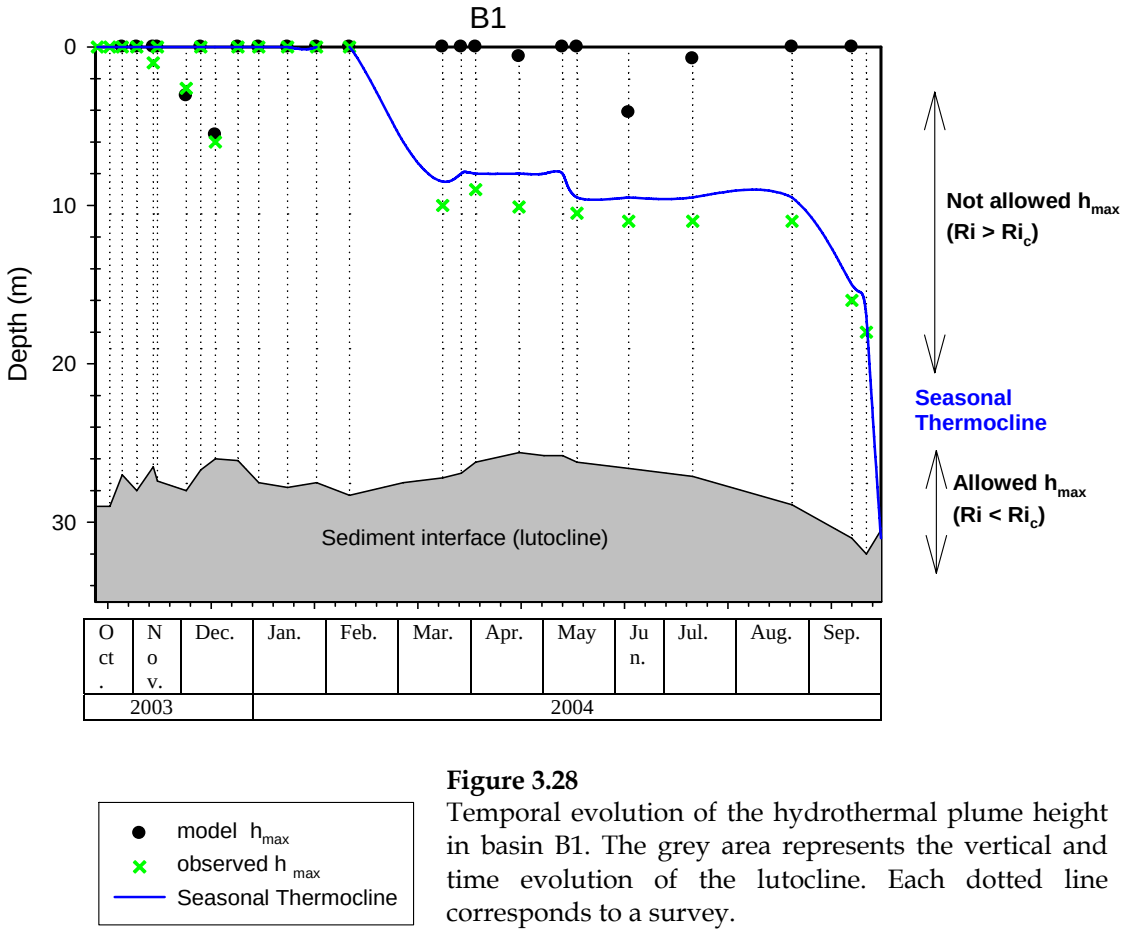

Figure 3.28
Temporal evolution of the hydrothermal plume height in basin B1. The grey area represents the vertical and time evolution of the lutocline. Each dotted line corresponds to a survey.

During the stratified period, the maximum height of the plume obtained by the backscattering signal of the ADCP (green crosses) coincides with the height of the seasonal thermocline. Therefore the thermocline acts as a barrier to the penetration of the plume to the upper layers of the lake.

During the mixing period, when stratification has disappeared, the plume can freely develop within the whole column. Maximum height values of the plume found by open convection models give values larger than the lake depth, indicating that the plume collapses at the lake surface in accordance with experimental data. Sometimes buoyancy is not strong enough and the plume does not arrive to the surface. This can be seen in the surveys carried out on 4 December and 18 December.

On the other hand, the spatial inhomogeneity found in the chronic plume in B1 is very interesting. After the exhaustive, year-long campaign, it can be seen from the ADCP backscatter signal that the hydrothermal plume in B1 develops at different zones of the lutocline, showing also a temporal variation throughout the entire study period. Sometimes the hydrothermal plume develops in the northern part of the basin (Figure 3.19, center; Figure 3.30, bottom), sometimes in the southern part (Figure 3.19, bottom; Figure 3.20, center; Figure 3.21, center; Figure 3.22, bottom; and so on) and sometimes in the center (Figure 3.26, center and bottom). It can also be found that it is not only an isolated plume, but a chimney with several plumes (Figures 3.19 and 3.20, center). This variability of the hydrothermal plume development with time is produced by the inhomogeneity in the lutocline temperature. These differences in temperature could be explained by two hypotheses.

Hypothesis #1. Although it was thought that lutocline temperature in B1 was quite constant throughout the year, it can be seen that there is a variation, which can be temporal (see Figure 3.29) and spatial (see Figure 3.30 that corresponds to temperature profiles in basin B1, measured at the same time but at different places).

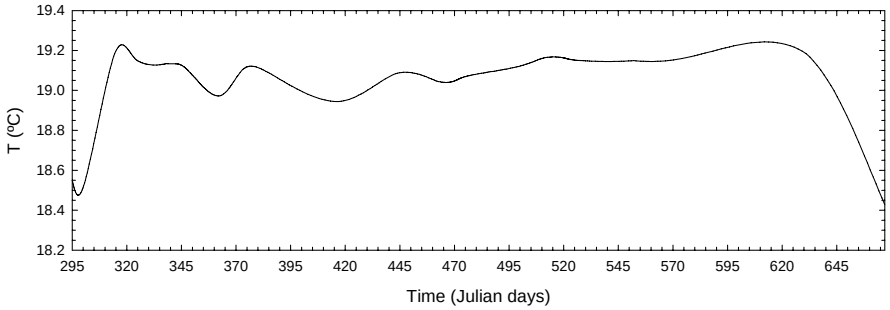

Figure 3.29
Lutocline temperature evolution in BI, from 10/22/2003 to 11/04/2004.

This variation in the temperature of the lutocline can produce a significant difference in the maximum height reached by the plume. In fact, a difference of 0.5 ºC can produce a variation between 6% and 57% of the buoyancy flux per unit area of the plume, and between 2% and 16% of the maximum height of the plume, depending on the environment, that is to say on different water stratification conditions.

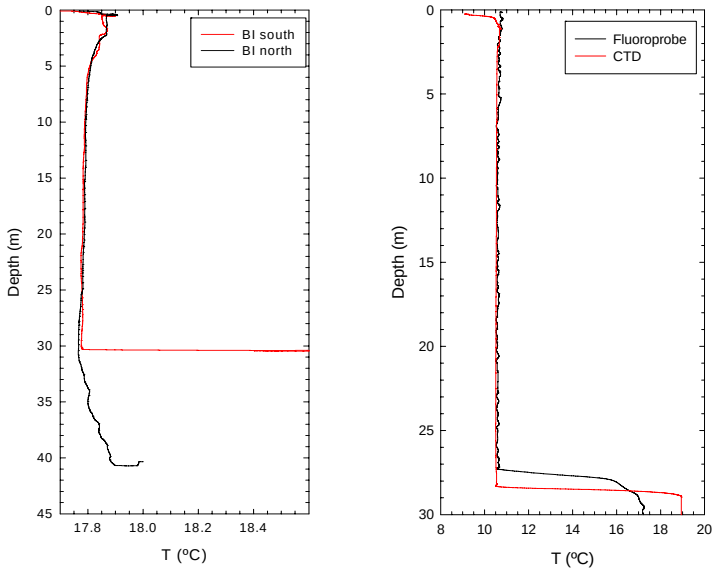

Figure 3.30
Temperature profiles in B1 measured at separate points on the dates 11/04/2003 (left) and 02/21/2004 (right).

Hypothesis #2. Lateral entrainment of colder water above the lutocline can generate an increase of the density anomaly. This increment produces an increase of the buoyancy (by the increase of the difference of temperature), which in turn produces more lateral entrainment (see Figure 3.31). This could produce the difference in buoyancy values which in turn produces different maximum heights of the hydrothermal plume. This changes in density values can produce localized convective holes as has been seen in laboratory experiments (Narimousa, 1996).

To understand better which of both causes provokes the inhomogeneity or if both do, it would be necessary to perform more field campaigns with the

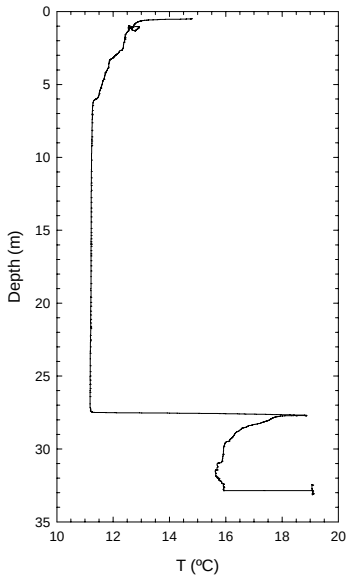

Figure 3.31
Temperature profile in B1 measured on 18/03/2004.

purpose of determining the spatial structure of the plume, as well a to know if there is also temporal inhomogeneity.

3.8.2 Basin B2

As can be seen in ADCP backscatter graphics (Section 3.7), the fluidization in basin B2 can be divided into two periods.

Period 1: At the beginning of the fluidization, a single plume can be found, caused by the fact that the lutocline is still consolidated and the water from the springs flows through preferential paths in the sediment. Therefore not

all the source will be equally active in the hydrothermal process. This regime, called "single-plume convection", develops in a baroclinically stable regime (R_{oR}>0.2, where $R_{oR}=(B_o/(f^3\ R^2))^{1/4}$) when the ratio between the radius of the source and its height (R/H) is < 0.7 (Okada et al., 2005). This new regime, in which multiple convective plumes do not fully develop, has only been described in numerical experiments (Okada et al., 2005), and has not been described previously in the field. Here we present a detailed description of the development of a single plume in the field (Chapter 4).

Period 2: When subterranean springs in B2 have resuspended and fluidized the confined and consolidated sediment at the bottom, its behavior is like the chronic plume in B1. Instead of entering through constrained paths, the entire lutocline, in suspension, is warmer than the water above it and generates a hydrothermal plume, and the whole source is active.

This change in B2 dynamics generates an important variation in the upward velocity. When water enters through preferential paths, the water pressure through small diameter sources causes a high mean upward velocity, w=0.05 m/s, as can be clearly seen at the top of Figure 5.23. After this, there is a transition period, when, as the incoming water resuspends the confined sediment, there is more than one preferential path, which causes the water pressure to decrease and the upward velocity to also start to decrease (Figure 5.23, center). Finally, when the sediments are totally fluidized, as can be found in basin B1, where the chronic hydrothermal plume develops, the preferential paths disappear, and B2 behaves like the plume in B1. In the fluidized period, the upward velocity equals the particle settling velocity (as was first described by Roget, 1987 and Colomer et al., 1998). This velocity is of the order of $0.512 \cdot 10^{-5}$ m/s which is too small to be detected by the ADCP, which only detects velocities down to values of 0.001 m/s.

In order to determine the settling velocity of sediments in B1 and B2, sediment samples below the lutocline in both basins have been taken with Ruttner

bottles. Sediments have then been freely settled and the depth of the interface has been recorded at different times, from which we could estimate its settling

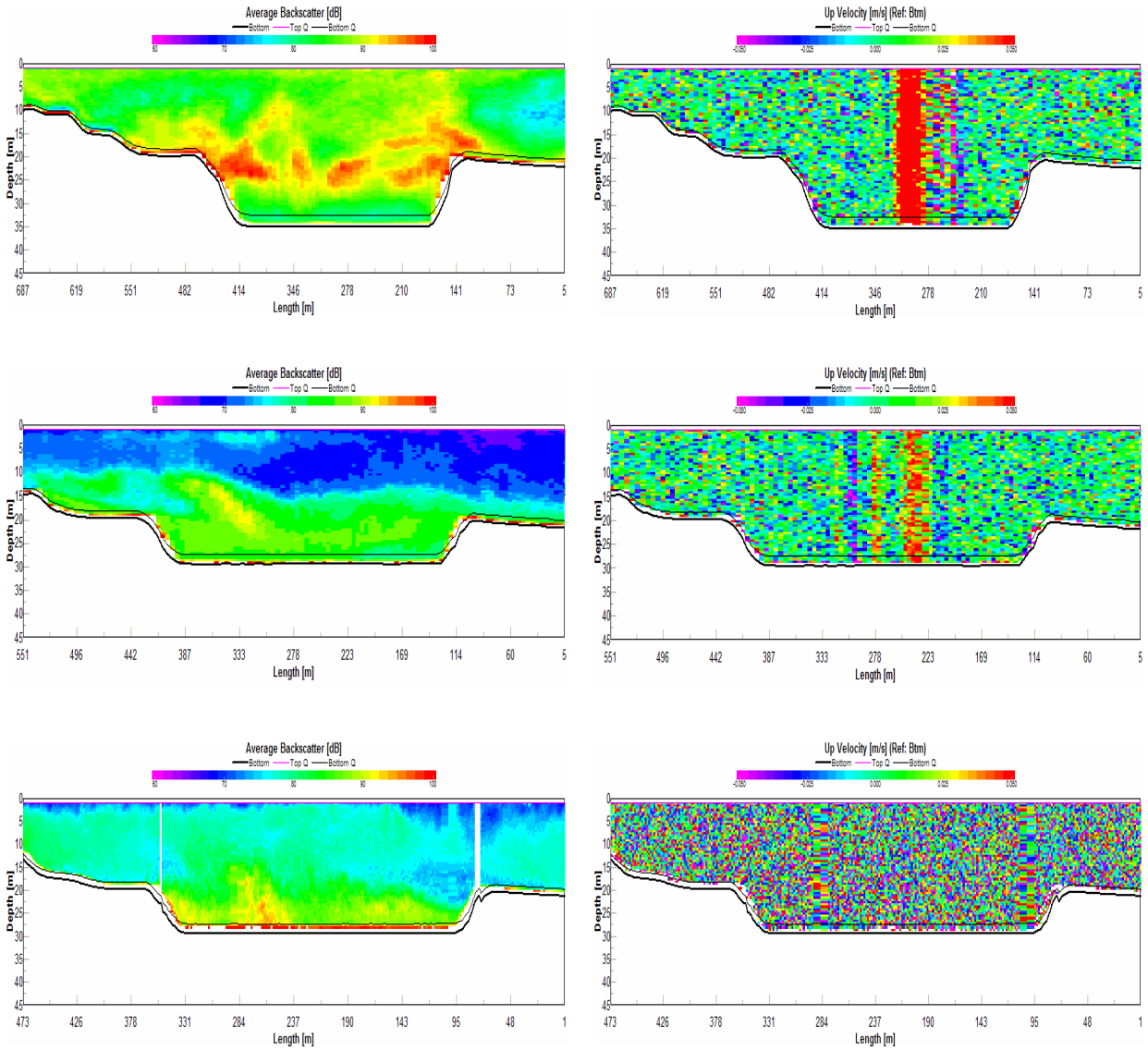

Figure 3.32
ADCP backscatter (left) and upward velocity (right) transects in B2 at different fluidization states: single plume convection, in 11/10/2003 (top); transition period, in 12/18/2003 (center); and 02/05/2004 (bottom).

velocity. A settling velocity of $v = (0.52 \pm 0.025) \cdot 10^{-5}\, m/s$ has been found for B2 and one of $v = (1.10 \pm 0.02) \cdot 10^{-5}\, m/s$ for B1. Experimental data with its regression line can be seen in Figure 3.33.

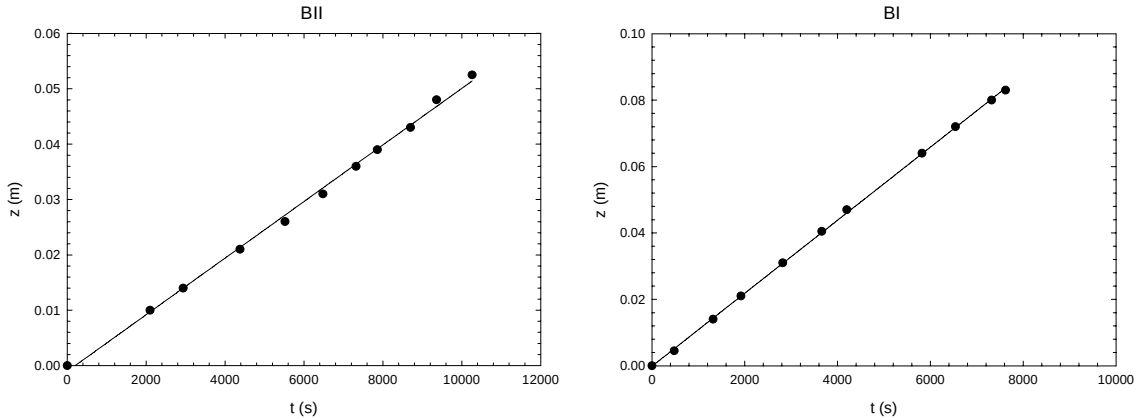

Figure 3.33
Correlation between settled space and time of sediment in basins B1 (right) and B2 (left) to find the settling velocity in each.

The two different behaviors in basin B2 can be well differentiated from the buoyancy values of B1 and B2 for the entire study period (Figure 3.34) and also from the values of R/H (Figure 3.35). The most important difference between B1 and B2 when they behave as a single plume can be attributed to the fact that upward velocity in

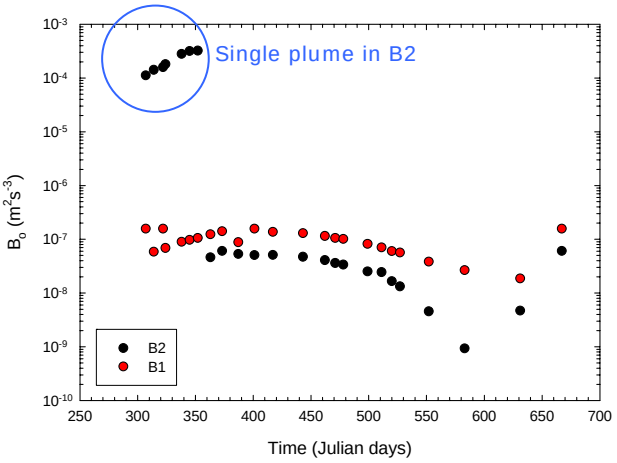

Figure 3.34
Buoyancy flux value evolution in basins B1 and B2, from October 2003 to November 2004.

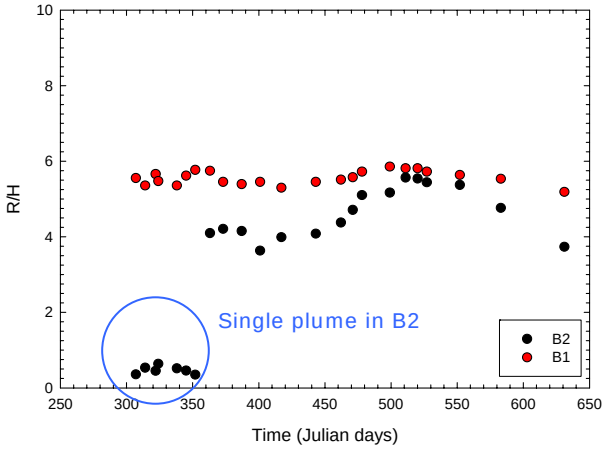

Figure 3.35
Time evolution of the ratio R/H in basins B1 and B2, from October 2003 to November 2004.

B2 is ~5 orders of magnitude larger than that in B1, and the radius of the source is ~5 times smaller.

For the period when the hydrothermal plume in basin B2 behaves like the hydrothermal plume in basin B1, we can compare the experimental values of h_{max} (measured by the ADCP backscatter images, green crosses) with h_{max} values determined for the conceptual model from Equations 3.8 and 3.9 (black dots). During the stratified period, we would expect the plume height experimental values to collapse with the thermocline, but as can be seen in Figure 3.36 this does not occur. Plume maximum heights found in basin B2 are limited, not by the thermocline but by any level of thermal stratification at which Ri=11. Accordingly, the height at which the Richardson number reaches its critical value has been calculated (grey line in Figure 3.36) and coincides in each survey with the experimental value (green cross).

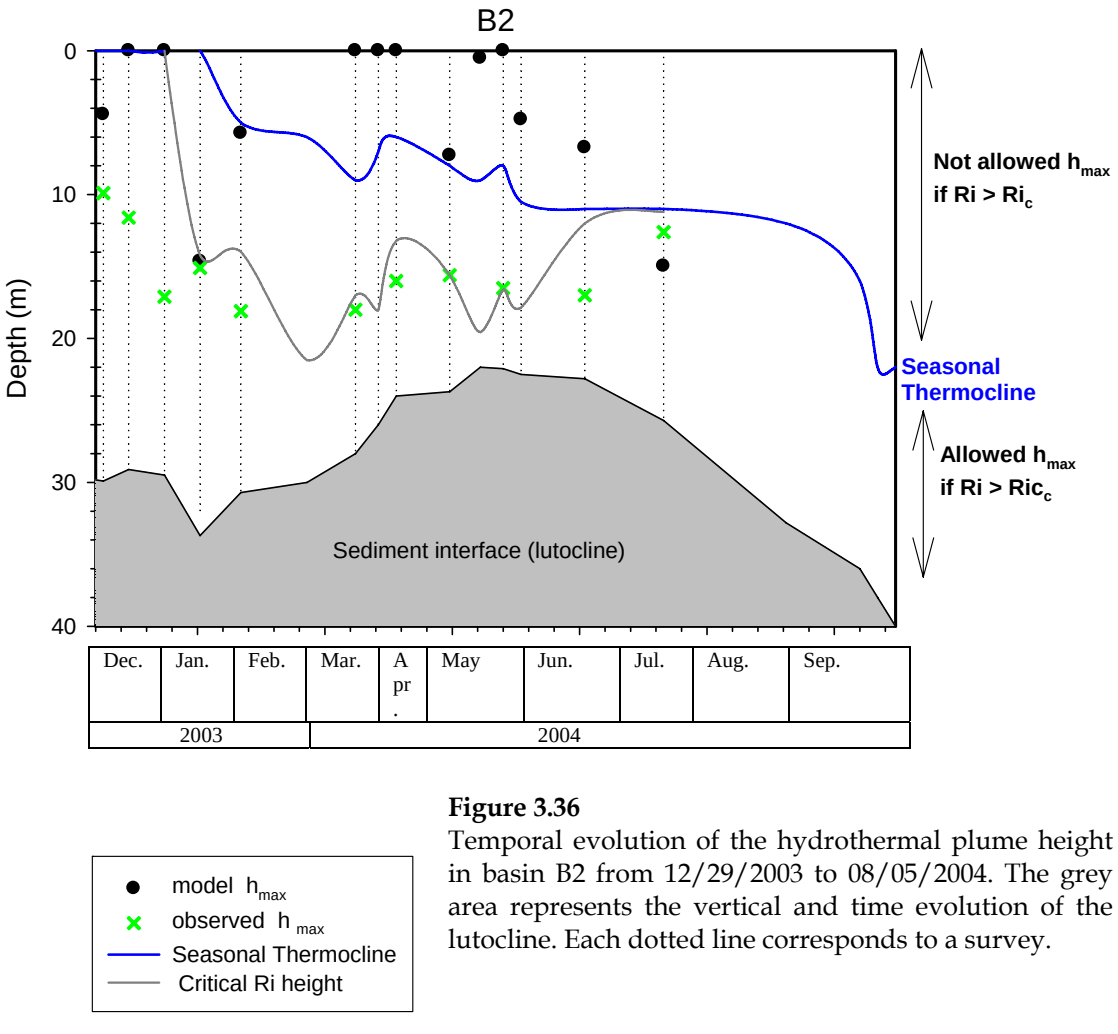

Figure 3.36
Temporal evolution of the hydrothermal plume height in basin B2 from 12/29/2003 to 08/05/2004. The grey area represents the vertical and time evolution of the lutocline. Each dotted line corresponds to a survey.

Reference List

Abella, C.A., 1980. Comparative population dynamics of planktonic phototrophic bacteria, PhD Dissertation, UAB, Bellaterra, Spain, 1980.

Asociación Española de Normalización y certificación (AENOR), 2002. Calidad del agua. Determinación de los sólidos en suspensión fijos y volátiles, UNE77034.

Buckner, E., 2001. A comparison of the sediment flux in the channel and shoals of the estuarine turbidity maximum region of the Chesapeake Bay. *VIMS 2001 Governor's School Final Report*, 24 p.

Bunt, J.A.C., P. Larcombe, and C.F. Jago, 1999. Quantifying the response of optical backscatter devices and transmissometers to variations in suspended particulate matter, *Continental Shelf Research*, 19, 1199-1220.

Canals, M., H. Got, R. Julia and J. Serra, 1990. Solution-collapse depressions and suspensates in the limnocrenic lake of Banyoles (NE Spain). *Earth Surf. Proc. Land.,* 15, 243-254. Bunt, J.A.C., P. Larcombe, and C.F. Jago, 1999.

Casamitjana, X. and E. Roget, 1993. Resuspension of sediment by focused groundwater in Lake Banyoles, *Limnology and Oceanography*, 38(3), 643-656.

Chen, C.T. and F.J. Millero, 1986. Precise thermodynamic properties for natural waters covering only the limnological range, *Limnol. Oceanogr.*, 31(3), 657-662.

Colomer, J., E. Roget, and X. Casamitjana, 1996. Daytime heat balance for estimating non-radiative fluxes of Lake Banyoles, *Hydrological Processes*, 10, 721-726.

Colomer, J., J.A. Ross, and X. Casamitjana, 1998. Sediment entrainment in kart basins, *Aquat. Sci.*, 60, 338-358.

Colomer, J., T. Serra, J. Piera, E. Roget and X. Casamitjana, 2001. Observations of a hydrothermal plume in a karstic lake, *Limnology and Oceanograph,* 46**,** 197-203.

Colomer, J., T. Serra, M. Soler and X. Casamitjana, 2002. Sediment fluidization events in a lake caused by large monthly rainfalls, *Geophys. Res. Lett., 29*(21), doi:10.1029/2001GL014299.

Colomer, J., T. Serra, M. Soler and X. Casamitjana, 2003. Hydrothermal plumes trapped by thermal stratification, *Geophys. Res. Lett. 30*(21), 2092, doi:10.1029/2003GL018131.

Fischer, H.B., E. J. List, R.C.Y. Koh, J. Imberger, and N.H. Brooks, 1979. Mixing in Inland and Coastal Waters, *Academic Press*, London, UK.

Kristensen, E. and F. Andersen, 1987. Determination of organic carbon in marine sediments: a comparison of two CHN- analyser methods, *J. Exp. Mar. Biol. Ecol., 109*, 15-23.

Kundu, P.K., 1999. Fluid Mechanics, Academic Press, Inc., USA

Levy, M.A., and H.J.S. Fernando, 2002. Turbulent thermal convection in a rotating stratified fluid, *Journal of Fluid Mechanics*, 467, 19-40.

Lu, J., S.P. Ayra, W.H. Snyder, and R.E. Lawson, Jr., 1997. A laboratory study of the urban heat island in a calm and stably stratified environment. Part I: Temperature field, *J. Appl. Meteorol*., 36, 1377-1391.

Moreno-Amich and Garcia-Berthou, 1989. A new bathymetric map based on echo-sounding and morphometrical characterization on the lake Banyoles (NE-Spain), *Hidrobiología*, 185, 83-90.

Narimousa, S., 1996. Penetrative turbulent convection into a rotating two-layer fluid. *Journal of Fluid Mechanics*, 321, 299-313.

Roget, E., 1987. Estudi dels cabals sorgents per les cubetes de Banyoles. *Minor Thesis*. Universitat Autònoma de Barcelona.

Roget, E., J. Colomer, X. Casamitjana, and J.E. Llebot, 1993. Bottom currents induced by baroclinic forcing in Lake Banyoles (Spain), Aquatic Sciences 55(3), 206-227.

Roget, E. and J. Colomer, 1996. Flow characteristics of a gravity current induced by differential cooling in a small lake, Aquatic Science, 58(4), 367-377.

Serra, T., J. Colomer, X. P. Cristina, X. Vila, J. B. Arellano and X. Casamitjana, 2001. Evaluation of a laser 'in situ' scattering system for

measuring the concentration of phytoplankton, purple sulphur bacteria and suspended inorganic sediments in lakes. *Journal of Environmental Engineering, 11*(127), 123-130.

Serra, T., J. Colomer, Ll. Zamora, R. Moreno-Amich and X. Casamitjana, 2002a. Seasonal development of a turbid hydrothermal plume in a lake, *Water Research, 36*(11), 2 753-2 760.

Serra, T., J. Colomer, E. Gacia, M. Soler and X. Casamitjana, 2002b. Effects of a hydrothermal plume on the sedimentation rates in a karstic lake. *Geophysical Research Letters.* 10.1029/2002GL015368. 29 (21): 25-28. ISSN: 0094-8276.

Serra, T., J. Colomer, R. Julià, M. Soler and X. Casamitjana, 2005. Behaviour and dynamics of a hydrothermal plume in Lake Banyoles, Catalonia, *Sedimentology 52*(4), 795-805.

Traykovski, P., R. J. Latter and J. D. Irish, 1999. A laboratory evaluation of the laser in situ scattering and transmissometry instrument using natural sediments. *Marine Geology*. *159*, 355-367.

Visbeck, M., J. Marshall, and H. Jones, 1996. Dynamics of isolated convective regions in the ocean, *J. Geophys. Res*., 26, 1721-1731.

Whitehead, J.A., J. Marshall and G.E. Hufford, 1996. Localized convection in rotating stratified fluid, *Journal of Geophysycal Research, 101* (C10), 25 705- 25 721.

Effects of a turbid hydrothermal plume on the sedimentation rates in a karstic lake

T. Serra,[1,2] J. Colomer,[1,2] E. Gacia,[3] M. Soler,[1] and X. Casamitjana[1]

Received 23 April 2002; revised 24 May 2002; accepted 4 June 2002; published XX Month 2002.

[1] The formation of a hydrothermal plume has been recently found in the main basin of a karstic lake. The hydrothermal plume carries a concentration of particles in suspension that are transported up to an equilibrium depth. At the equilibrium level, particles are transported horizontally as a turbidity current. The particle volume concentration in the hypolimnion, where the turbidity current occurs, has been found to be homogeneous for points close to the source of the plume. However, there is a decrease in the particle concentration points from close to the source of the plume to the points far from the source, which indicates that the sedimentation of particles from the turbidity current occurs. This sedimentation process has been attributed mainly to double diffusive sedimentation rather than to single particle sedimentation. Here we demonstrate the effect of this turbidity current on the zonal sedimentation rates at the southern lobe of the lake. *INDEX TERMS:* 4239 Oceanography: General: Limnology; 4558 Oceanography: Physical: Sediment transport; 4832 Oceanography: Biological and Chemical: Hydrothermal systems. **Citation:** Serra, T., J. Colomer, E. Gacia, M. Soler, and X. Casamitjana, Effects of a turbid hydrothermal plume on the sedimentation rates in a karstic lake, *Geophys. Res. Lett.*, *29*(0), XXXX, doi:10.1029/2002GL015368, 2002.

[2] A chronic hydrothermal turbid plume has been found to develop in the karstic lake Banyoles, situated in Catalonia, north-eastern Spain (Figure 1) [*Serra et al.*, 2002]. The hydrothermal plume was located in the main basin of the lake, in Basin 1 (B1). The lake is formed by 6 basins (BI-BVI, Figure 1a), with B1 being the largest and deepest (~75 m) from where the water enters and resuspends sediments from the bottom upwards. Sediments are transported up to a sediment interface, the lutocline (at ~30 m depth), which separates the region of clean water above, region A, from the high sediment concentration (100 g l^{-1}) region below, region B (Figure 1b). As a result of the high sediment concentration in region B, the lutocline acts as a false bottom at ~30 m depth as measured by echo-sounding profiles (Figure 1a). The temperature of the water at the lutocline level is warmer (~19°C, constant throughout the year) than the hypolimnetic water immediately above and this difference in temperature generates the convection process that drives the hydrothermal plume [*Colomer et al.*, 2001]. The plume develops upwards carrying a suspension of particles from the lutocline up to an equilibrium depth, i.e. forming a turbid hydrothermal plume. At the equilibrium depth, the water spreads laterally forming a mesopycnal turbidity current, as classified by *Mulder and Alexander* [2001] for a volume sediment concentration <10%. This turbidity current was ~0.02 K warmer than the surrounding water and had a typical thickness of ~1 m [*Colomer et al.*, 2001].

[3] Sedimentation from turbidity currents and density interfaces has been found to be an effective mechanism for the transport of suspended material through the bottom of the water body where it develops. The sedimentation process may occur because of the flocculation of small particles into larger settling aggregates and/or double diffusive sedimentation (DDS). DDS from turbidity currents has been reported in riverine outflows [*Parsons et al.*, 2001; *Koren and Klein*, 2000], volcanic eruptions [*Woods*, 1995] and also in laboratory surface sediment-laden water currents [*Parsons and García*, 2000].

[4] The aim of this study is to demonstrate the effects of the mesopycnal turbidity current in the sedimentation rates of the water column of lake Banyoles. For this purpose, measurements of the particle size distribution (PSD) and particle volume concentration (PVC) were taken with an in situ laser particle size analyser, which measures particles in the size range 1.2–250 μm, at different stations on the lake (SI-SVI, see Figure 1). Three sets of sediment traps consisting of structures containing 5 units of 20 ml glass tubs with an area to volume ratio of 5 [see, details in *Gacia and Duarte*, 2001] were also deployed at three selected stations on the lake (at SIII, SVI and at a point between SIV and SV, see Figure 1a). The sediment trap arrangements (sT1, sT2 and sT3) measured sedimentation rates at four different depths (8, 12, 15 and 19 m deep). Finally, a multiparametric probe (Hydrolab) measured the oxygen concentration at different depths of the water column and it basically performed measurements at the centre of BI (SI).

[5] The field campaign was carried out at the end of July of 2000, when the water column was well stratified. The epilimnion was ~5 m deep at a temperature of ~26°C and the thermocline was ~5 m thick (Figure 2). Below the thermocline, the hypolimnion was completely mixed and remained at a constant temperature of ~16°C, down to a depth of 28.5 m. A phytoplankton population was found within the thermocline layer, together with an increase in the oxygen concentration up to 8 mg l^{-1}, as could also be observed from microscopic observations of the water samples. The PVC at SI was found to be constant at ~4.5 μl l^{-1} from the lutocline level up to a depth of 15 m, and decreased upwards to the base of the thermocline, reaching values of 3.5 μl l^{-1}. The PVC increased again (up to ~4.5 μl l^{-1})

[1]Department of Physics, University of Girona, Montilivi Campus, Girona, Spain.
[2]Centre d'Estudis Comarcals de Banyoles, Banyoles, Spain.
[3]Centre d'Estudis Avançats de Blanes, Blanes, Spain.

0094-8276/02/2002GL015368$05.00

Sediment fluidization events in a lake caused by large monthly rainfalls

Jordi Colomer, Teresa Serra, Marianna Soler, and Xavier Casamitjana
Department of Physics, University of Girona, Girona, Spain

Received 25 October 2001; revised 30 October 2001; accepted 12 November 2001; published XX Month 2002.

[1] In the last fourteen years (1986–1999), fluidizations of confined bed–sediments due to underground springs in basin BII of lake Banyoles (Spain) have been detected. As a result of periods of high precipitation, sediment confined at the bottom of karstic basins migrates from 45 m depth to approximately 25 m depth. Fluidization processes are associated to monthly rainfall 1.5 to 4.5 times larger than the long-term mean (1970–1999). As a result of a fluidization event, the water column of the lake maintains the particle volume concentrations of suspended sediment (pVC) as high as 44 μl/l, which is ∼8–29 times larger than the usual values of pVC. *INDEX TERMS:* 3309 Meteorology and Atmospheric Dynamics: Climatology (1620); 4239 Oceanography: General: Limnology; 4558 Oceanography: Physical: Sediment transport

1. Fluidization Processes in the Main Basins of Lake Banyoles

[2] Lake Banyoles (42°07′N, 2°45′E) is situated in the northeast of Spain, in the Catalan prePyrenees, and 30 km west from the Mediterranean coast (Figure 1a). It is a small multibasin lake (surface area of 1.12 km^2) of mixed tectonic-karstic origin, composed of several basins. The main supply of water to the lake is through subterranean springs located at the bottom of the basins of the lake [*Abella*, 1980; *Casamitjana and Roget*, 1993; *Colomer et al.*, 1998]. An underlying fault (at the East of the lake), which acts as a barrier to ground water movement in a complex series of confined aquifers, forces the vertical discharge of the ground water flow through the bottom of the basins (Figures 1a and 1b). The aquifers are supplied by the percolation of precipitation in two watersheds located 20 km to the northwest of Banyoles (Alta Garrotxa, Figure 1b). The main basins of the lake, BI and BII (see Figure 2) have a maximum depth of 75 and 77 m, respectively [*Canals et al.*, 1990]. As a result of cumulative episodes of land subsidence, the basins have cone-shape structures as can be seen, for example, in the seismic profile at BI (Figure 2).

[3] Sediments in BI (Figure 2) are normally found in suspension (is a case of sustained hydrologic pressure, as also seen exceptionally in a karst pond in the Florida aquifer system, page 57 in the vol. 195 (March) of National Geographic, *Ringle and Skiles*, [1999]). In contrast, sediments in BII normally remain at the bottom of the basin forming a dense sediment bed, at 45 m depth. However, an increase in the amount of precipitation in the recharge area produces an increase of groundwater discharge that eventually resuspends the sediments (Figure 2 top right). The mean mass concentration of the fluidized sediment bed in BI ranges from 100 to 130 g/l meanwhile the sediment concentration in BII varies from 280 g/l at the beginning of a fluidization event to 180 g/l when sediments remain in suspension. During a fluidization process, the sediment resuspension is characterized by the formation of a dense sediment interface (see the flat signal in the echosounding and seismic profiles in BI and BII in Figure 2) that advances upwards from 45 m depth to ∼25 m depth; the time evolution of the position of the sediment interface is shown in Figure 3 (bottom panel). The momentum of the underground spring and the characteristics of the sediment (mainly the particle size diameter) determine the maximum height that the sediment interface can rise to [*Casamitjana et al.*, 1996; *Colomer et al.*, 1998]. Also, the temperature at the sediment interface increases from 17.5°C at the beginning of the event to 19.4°C in the suspension state, which is caused by the enhanced circulation of incoming warm water within the fluidized bed.

[4] Since 1986 monthly temperature measurements were carried out at a station located at the center of BII, at intervals of 1 m depth. Moreover, since 1998 monthly measurements of pVC at the same depth intervals were done (data that will be discussed later on in the text). In this study the depth of the sediment interface identifying the top of the fluidized bed was found to be the depth of maximum inverse vertical temperature gradient (between 8°C/m and 2°C/m), i.e., warmer temperature below

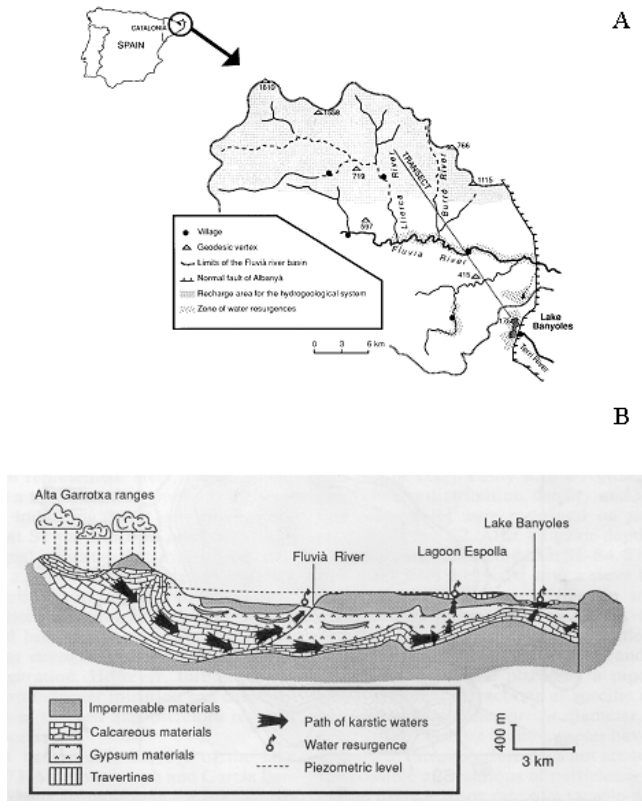

Figure 1. (a) General location map of Lake Banyoles and schematic representation for the hydrological system in the Lake Banyoles region. (b) Path of karstic water, along the transect marked in panel A [adapted from *Brusi et al.*, 1990].

0094-8276/02/2001GL014299$05.00

Hydrothermal plumes trapped by thermal stratification

Jordi Colomer, Teresa Serra, Marianna Soler, and Xavier Casamitjana
Department of Physics, University of Girona, Campus de Montilivi, Girona, Spain

Received 9 July 2003; revised 16 September 2003; accepted 1 October 2003; published 5 November 2003.

[1] Hydrothermal plume penetration through density interfaces has been widely studied in laboratory experiments. It has been found that competition between plume buoyancy and background stratification (parameterised as the Richardson number) is crucial in determining whether or not the plume will penetrate through a density interface. In this paper, we present the analysis of field data concerning two hydrothermal sediment-laden plumes in a stratified lake. Measurements of the particle concentration within these plumes have been used to determine their vertical, spatial and temporal development in the water column. The results show that neither of the plumes penetrate the lake thermoclines for large Richardson numbers, which is in accordance with the results found in laboratory experiments. *INDEX TERMS:* 1719 History of Geophysics: Hydrology; 1845 Hydrology: Limnology; 1854 Hydrology: Precipitation (3354); 1884 Hydrology: Water supply; 4558 Oceanography: Physical: Sediment transport; *KEYWORDS:* plume, stratification, sediment, karst basin, Richardson number.
Citation: Colomer, J., T. Serra, M. Soler, and X. Casamitjana, Hydrothermal plumes trapped by thermal stratification, *Geophys. Res. Lett.*, *30*(21), 2092, doi:10.1029/2003GL018131, 2003.

1. Introduction

[2] Lake Banyoles (42°07′N, 2°45′E), in the eastern Catalan pre-Pyrenees, is a small multibasin lake (surface area of 1.12 km^2) of mixed tectonic-karstic origin, composed of six main basins (B1–B6, see Figure 1). B1 is the largest basin and supplies around 85% of the total incoming water and the rest is supplied by river inflows. Eventually, B2 supplies water to the lake at a rate comparable to B1. An underlying fault (to the east of the lake), which acts as a barrier to ground water movement in a complex series of confined aquifers, forces the vertical discharge of the ground water flow through the bottom of the basins. The subterranean springs mix the sediments above up to a fairly sharp interface known hereafter as the lutocline. The difference in temperature between the suspension zone below the lutocline and the water above induces the development of a hydrothermal plume, in the same way that convective plumes develop from localized sources [*Maxworthy*, 1997] in oceanic and atmospheric deep convection [*Schott et al.*, 1993; *Schott et al.*, 1996; *Fernando and Smith*, 2001], microbursts [*Lundgren et al.*, 1992], urban heat islands [*Lu et al.*, 1997] and polynyas [*Chapman and Gawarkiewicz*, 1997]. The lutocline is well detected by seismic profiling and is located at a depth Z_L from surface (Figure 2a). In the last seventeen years (1986–2002), while the sediments in B1 were found to be in suspension, the sediments in B2 usually remained compacted at the bottom of the basin (Figure 2a), except for periods of high precipitation (Figure 2b), when sediment resuspended and migrated upward, producing the fluidization of the sediment. These fluidization events (F1, F2, etc.) were detected when measuring the depth of the lutocline (Z_L) in B2 (Figure 2c). The shallower depth of the lutocline in B2 was found to be at about 24 m during the F7 event in 1996 (Figure 2b). The last fluidization event, F9, was detected between May and September 2002 (Figure 2c) with the lutocline undergoing a vertical displacement of around 8 m.

[3] We chose to examine the dynamics of the hydrothermal plumes in Lake Banyoles for three main reasons. First, the history of sediment fluidizations in basins B1 and B2 has been studied over the past 17 years. These studies [*Casamitjana and Roget*, 1993; *Colomer et al.*, 2001; *Colomer et al.*, 2002] reveal that the plume developing in B1 is permanent (chronic plume) and that the plume in B2 develops episodically (episodic plume). The plume in B1 was reported for the first time in 1998 whereas this paper is the first to describe the plume in B2. Second, these hydrothermal plumes carry particles in suspension (turbid plumes), which affect both fish distribution [*Serra et al.*, 2002a] and sedimentary records between basins B1 and B2 [*Serra et al.*, 2002b]. Third, the development of localized convection in rotating stratified fluids have been largely studied using both laboratory and field oceanic experiments, especially for the case of deep and intermediate water masses of the world's oceans [*Schott et al.*, 1993; *Maxworthy*, 1997], but it has not yet been described in a lake.

[4] The sampling was conducted over a period of 109 days from May 18th to September 3rd, 2002, in the small lake of Banyoles (Figure 1). Fourteen surveys were made during this period. The stations along each transect were separated from each other by ~150 m, between B1 and B2 (Figure 2a). At each station, conductivity, temperature and depth were measured with a CTD profiler (Seabird SBE19, Seacat). Particle size distribution and concentration were also measured with an *in situ* laser particle size analyser (Lisst100, Sequoia Instruments), which measures particles in the size range 1.2–250 μm.

[5] Hydrothermal plumes are best thought of as efficient mixing agents, responsible solely for 'churning' the column where they develop [*Visbeck et al.*, 1996]. Assuming that the input of unstable buoyancy flux at a surface of radius R is balanced by the lateral removal of flux by eddies ejected out of the convective region, *Whitehead et al.* [1996] and *Visbeck et al.* [1996] were able to determine the depth of the convection. Similar results were found by *Colomer et al.* [1998] when considering that the depth of convection is determined by the inhibition of vertical growth due to the stratification of the water column. For both hypotheses, the maximum height to which a plume migrates has been found

0094-8276/03/2003GL018131$05.00

Teresa Serra, Marianna Soler, Ramon Julià, Xavier Casamitjana and Jordi Colomer. “Behaviour and dynamics of a hydrothermal plume in Lake Banyoles, Catalonia, NE Spain”, Sedimentology. Vol. 52, issue 4 (July 2005) : p. 795-808

http://dox.doi.org/10.1111/j.1365-3091.2005.00611.x

Manuscript received 5 June 2002; revision accepted 16 February 2005

Abstract

A hydrothermal plume forms in Lake Banyoles, NE Spain, as a result of convection above a springwater-fed suspension cloud ponded on the lake floor. The plume propagates upwards reaching a level of neutral buoyancy from where a turbidity current spreads out laterally. Two-dimensional temperature and particle concentration measurements show the fate of the hydrothermal plume and its associated turbidity current and reveal its seasonal development. Silt particles transported by the plume have been used as tracers to determine the maximum and equilibrium heights of the plume. When the lake is stratified, the vertical transport of sediment is confined to the lake hypolimnion, as the thermocline limits the vertical propagation of the plume. In contrast, when the lake water column is mixed, the plume reaches the surface of the lake. The field measurements have been compared with models for thermal convection from finite isolated sources. Measurements of the flow velocity at the source of the hydrothermal plume (i.e. the rim current velocity) indicate that cold hypolimnetic water is entrained by the plume. Sedimentation rates measured from sediment traps at the zone where the turbidity current develops vary between 10 and 25 g m^{-2} day^{-1}, and result from continuous silt particle sedimentation from the turbidity current. Sedimentation rates in traps are higher for stations situated close to the source than those further away (<5 g m^{-2} day^{-1}). Moreover, the results demonstrate that double diffusive sedimentation from the turbidity current was dominant over grain-by-grain settling, causing a mixed distribution of sediments in the region where the turbidity current spreads. The deposition of silt particles could explain the occurrence of silt layers interbedded with biocalcarenites in the littoral zones of the lake and the stratigraphy identified by seismic profiles and cores taken from the lake floor.

Keywords: Double diffuse sedimentation • plume • sediment cores • thermal convection • turbidity current
.

4 Single-plume convection in Lake Banyoles

Known that anomalous rainfall events develop the fluidization of the lutocline in basin B2 (seen in Chapter 4), which cause the development of a hydrothermal plume, and already seen how this affects the general dynamics in Lake Banyoles (seen in Chapter 5), it would be interesting to study this isolated convection phenomena in detail.

While the hydrothermal plume in B2 was studied in detail for the first time in 2002 (Colomer et al., 2003), its vertical development was restricted to the first meters from the lutocline source due to the strong thermal stratification of the water column and therefore its behavior and effect on the lake was completely different than that studied in 2003. In the present field work, the fluidization in autumn 2003 (F10), produced during the mixed period of the lake allowed the hydrothermal plume to develop all along the water column, and consequently we could study it in detail. As mentioned in methods section (Chapter 3),

intensive field work was carried out weekly in order to have a detailed evolution of the vertical fluidization and the vertical development of the plume. Results can be found in the paper here below, from the *Journal of Geophysical Research -Oceans*, (in press).

Soler, M., T. Serra, and J. Colomer (2008). "Scaling analysis of single-plume convection from a hydrothermal source". *Journal of geophysical research-oceans*. vol. 113, C05012,

http://dx.doi.org/10.1029/2006JC004073

Group of Environmental Physics, Physics Department, University of Girona, 17071 Girona, Spain

Abstract

The characteristics of a convective single plume developing from a hydrothermal lake source of radius R have been investigated. The study was motivated by the aim to estimate velocity and buoyancy scaling laws obtained from numerical models of convection from isolated sources of finite extent. This has been done for the case $R/H < 0.7$, where H is the water column depth, and for the case of baroclinically stable convection. The single plume described hereafter presents the following characteristics: $0.35 < R/H < 0.64$, $RD/R > 25.8$, where RD is the Rossby radius of deformation. From the results, the density anomaly scales with the buoyancy flux Bo applied over the source and the depth according to $g' = (3.81 \pm 0.06)\, Bo^{2/3}/ H^{1/3}$, and a single vortex ismaintained around the forcing disk with a mean radial velocity scaling according to $Ur = (1.57 \pm 0.43)\, Bo^{1/3} R/H^{2/3}$. The experimental results described here will be compared to the results found for the numerical model by Okada et al. (2004).

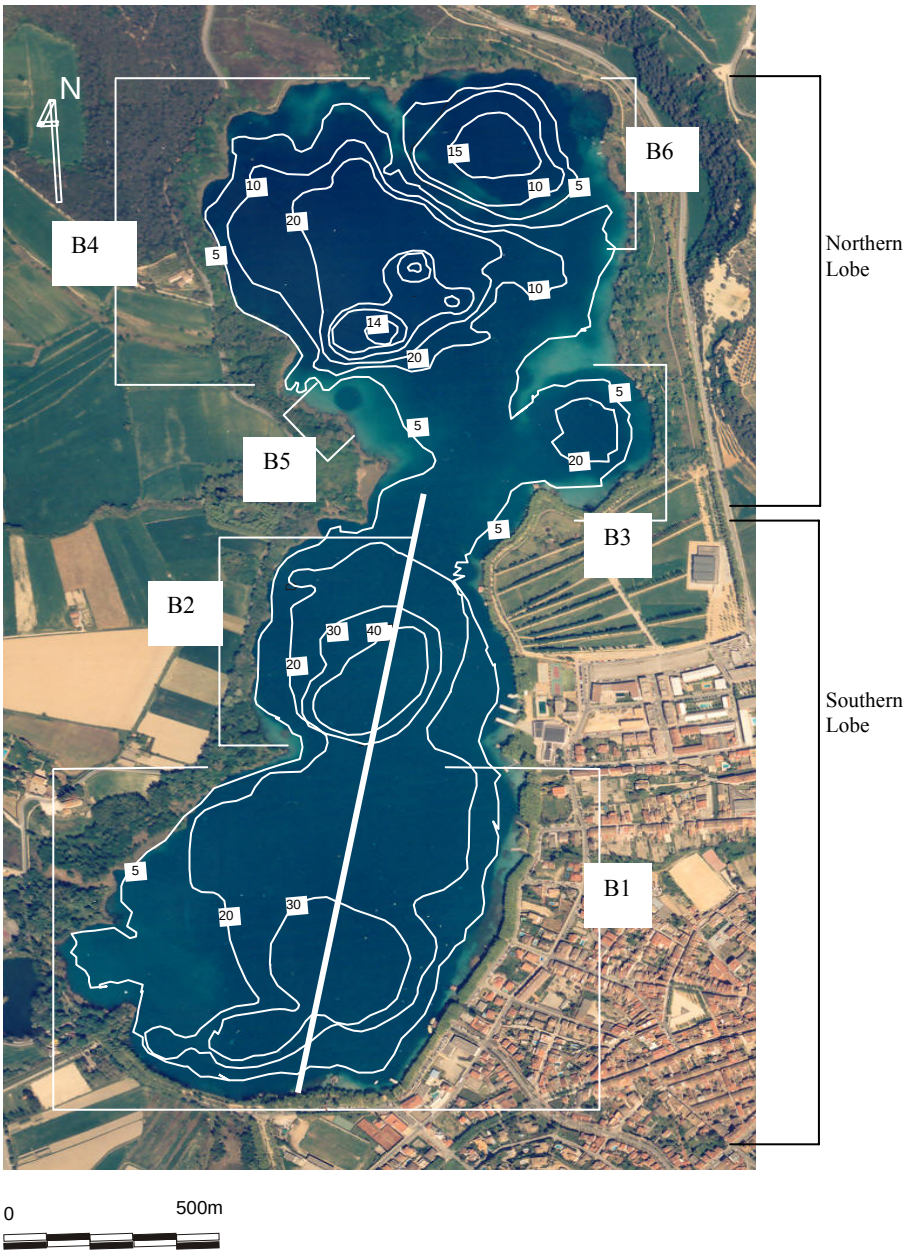

Figure 1

Aerial photograph of Lake Banyoles. The lake is divided into six basins, some of them clearly seen in the photograph (kindly provided by the Cartography Institute of Catalonia, ICC). Basin B1 and B2 are located in the southern lobe, and B3, B4, B5 and B6 are in the northern lobe. Also in the plot, contour depths (with characteristic values in meters) and the line between B2 and B1 indicating the field transect of experimental values, are shown.

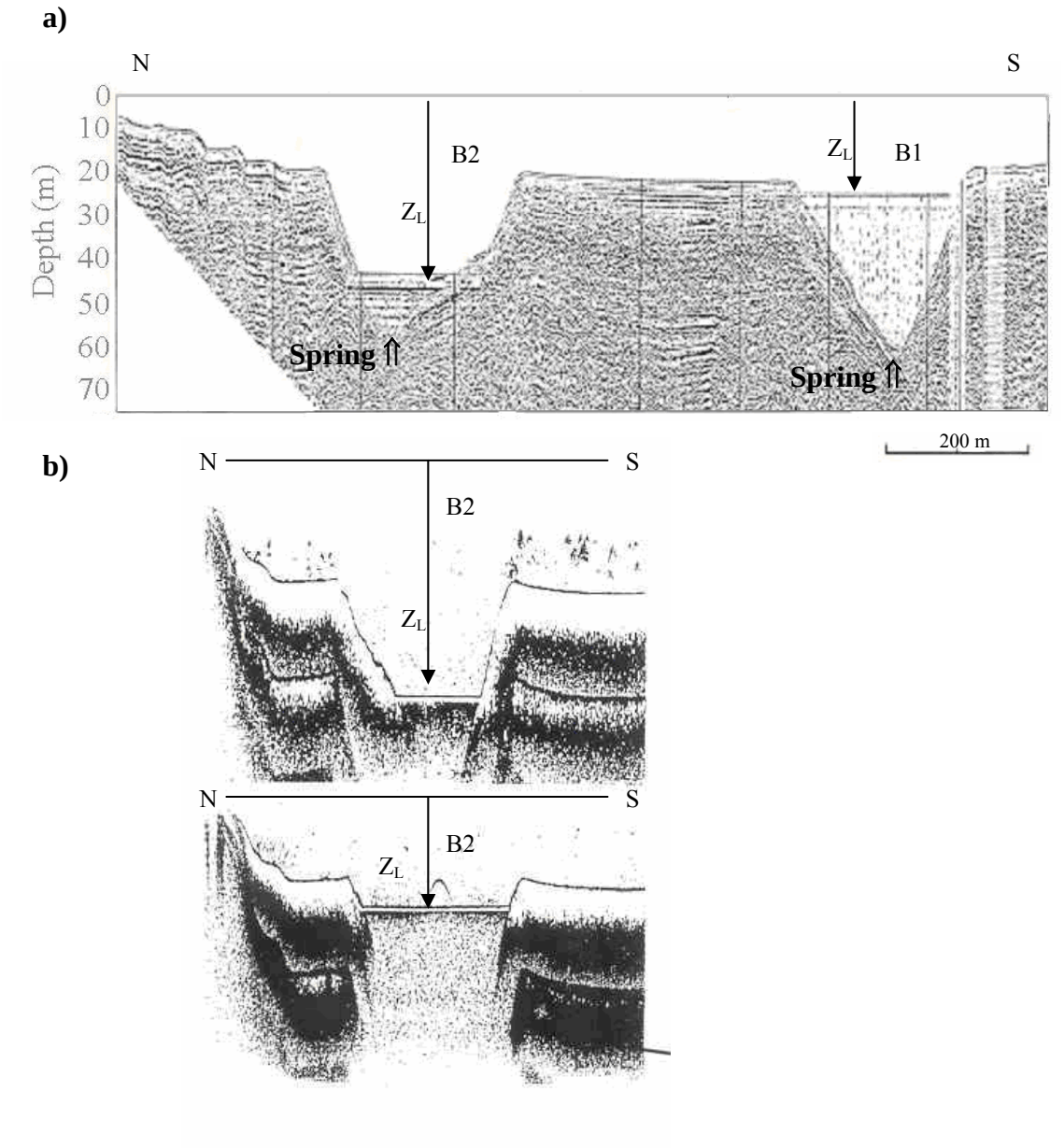

Figure 2

(a) North-South seismic transect (Canals et al. 1990); in the southern lobe the lutocline is well detected by the flat horizontal signal, at depths Z_L (b) Echo sounding transect in B2 showing the two states of the sediment bed: non-fluidized (top) and fluidized (bottom).

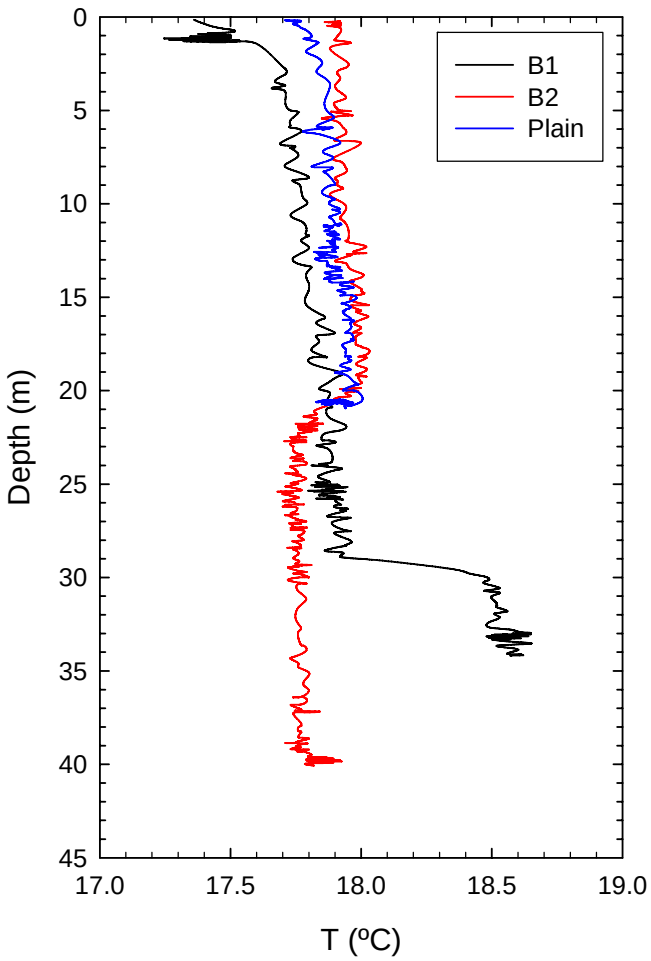

Figure 3

Temperature profiles in B1, B2 and the plain before the fluidization in basin B2 measured on 22 October 2003.

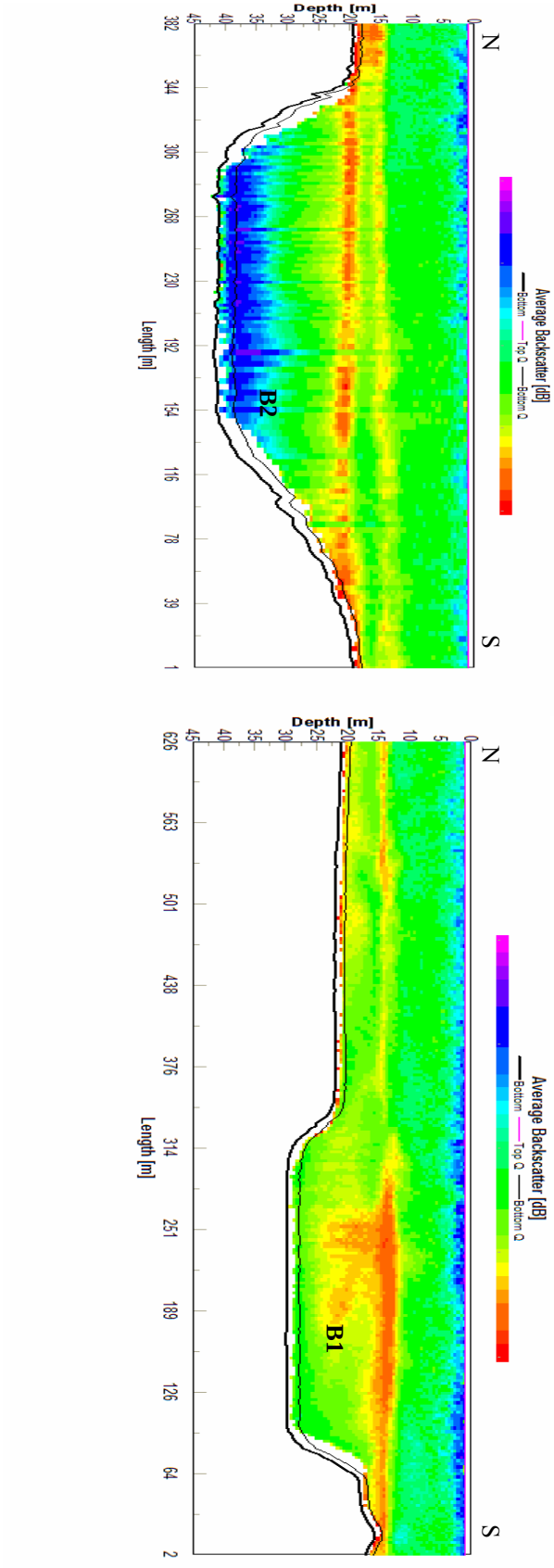

Figure 4

North-South ADCP backscatter transect from basin B2 to B1 measured on 28 October 2003.

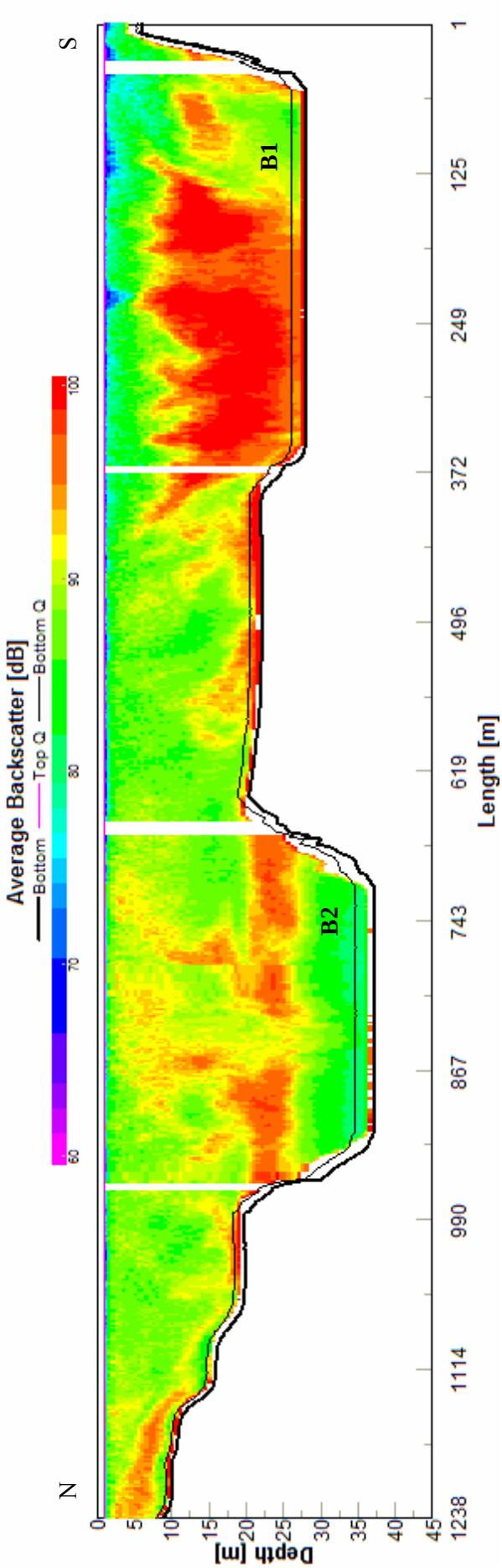

Figure 5

North-South ADCP backscatter transect in basins B2 and B1 on 3 November 2003

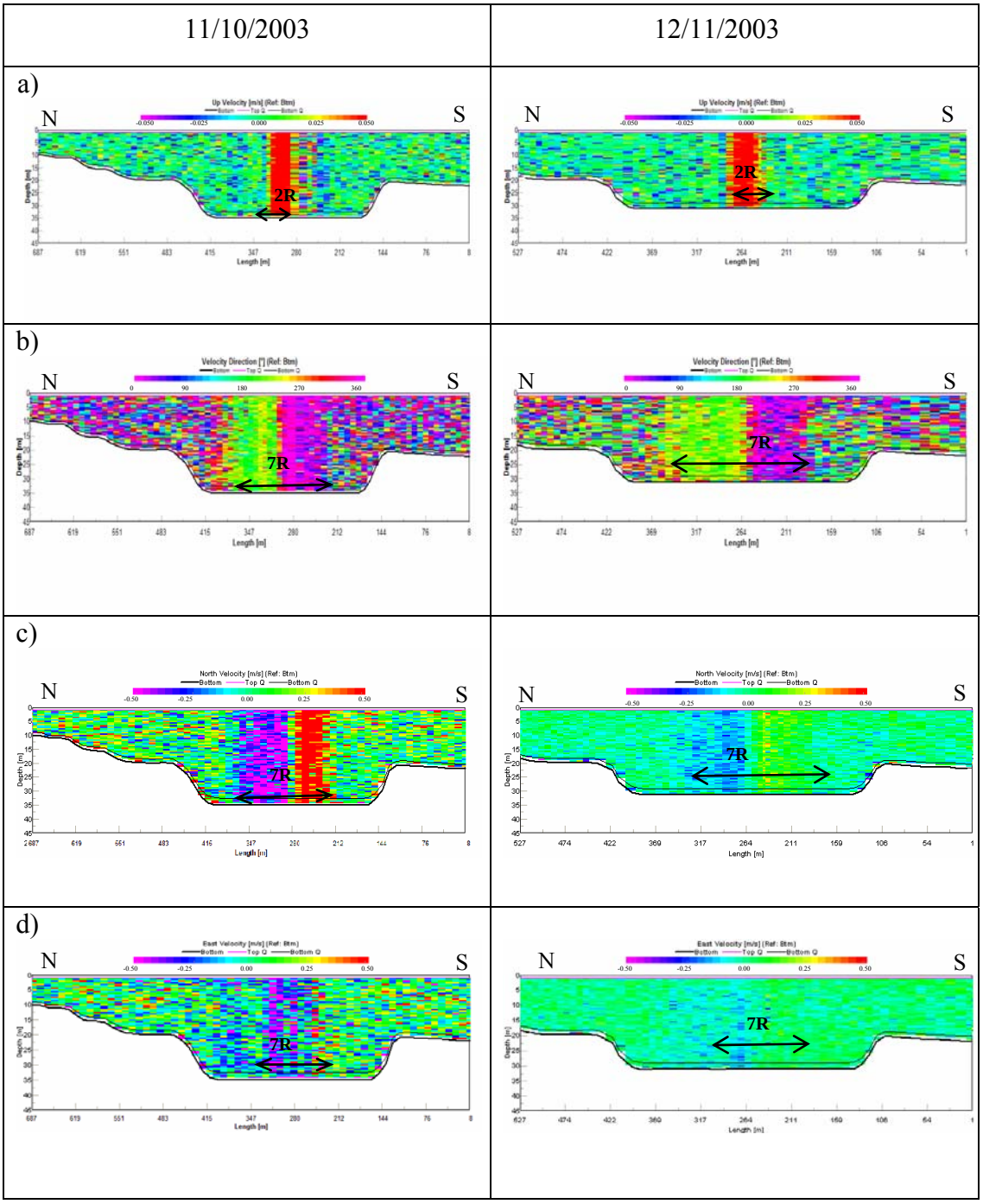

Figure 6

Transects of ADCP Up velocity (a), velocity direction (b), north velocity (c) and east velocity (d) measured on: November, 10 th 2003 (left), and December, 11 th 2003 (right).

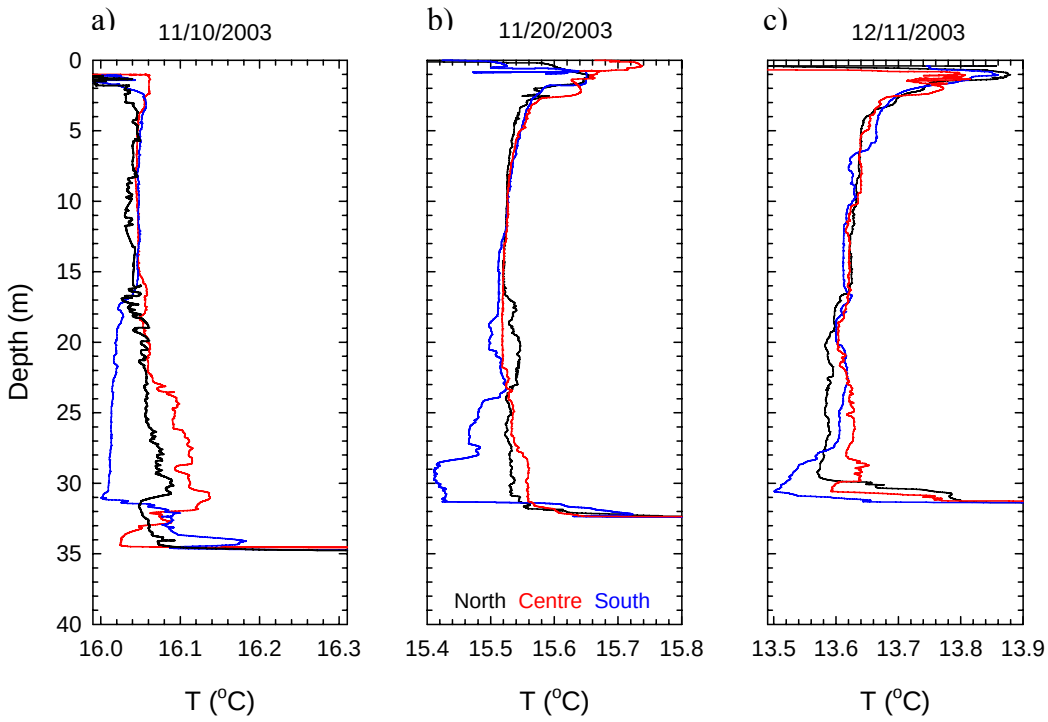

Figure 7

CTD Temperature profiles measured at the north, center and south of the single-plume source at different dates: (a) 10 November 2003 (b) 20 November 2003 and (c) 11 December 2003.

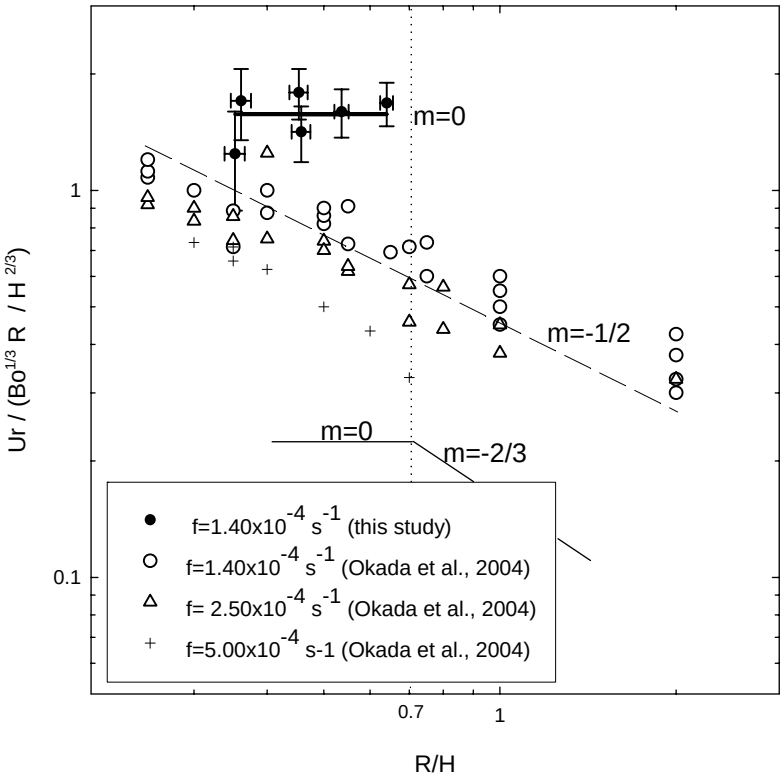

Figure 8

Radial velocity at a circle 2R around the center of the plume non-dimensionalized by $Bo^{1/3} R H^{-2/3}$, as a function of the aspect ratio R/H with numerical results data from Okada et al., 2004. Solid lines indicate the predicted slope values for R/H < 0.7 and R/H > 0.7, dashed line shows the slope obtained with numerical experiment data (Okada et al., 2004) for R/H < 0.7 and R/H > 0.7.

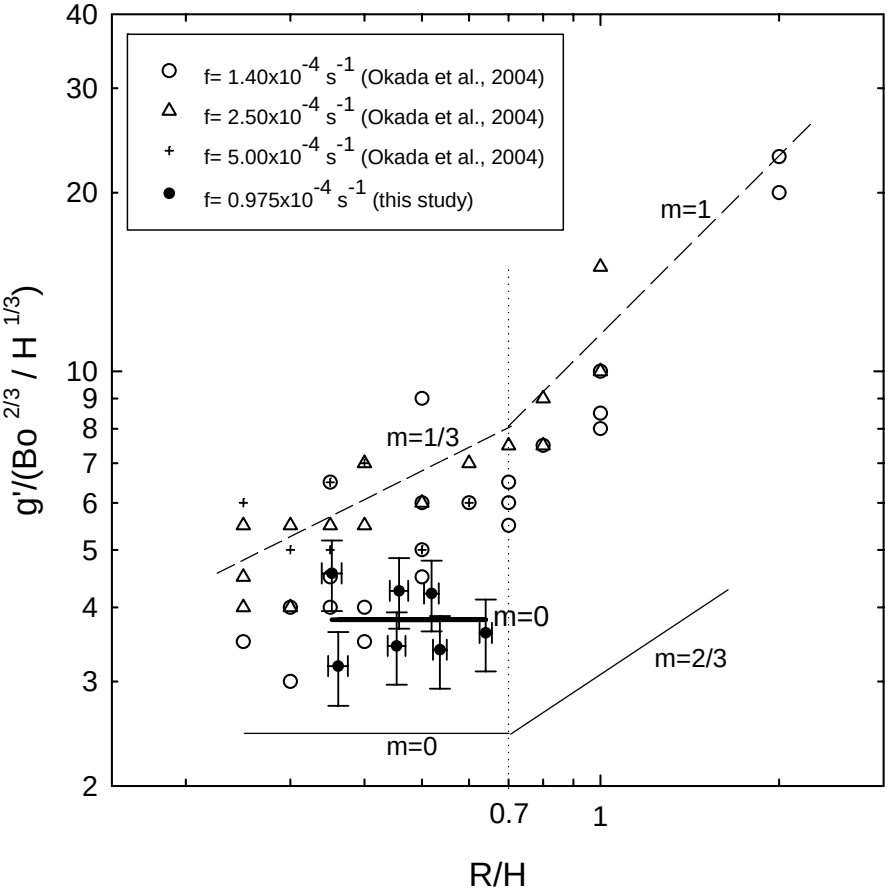

Figure 9

Density difference non-dimensionalized by $Bo^{2/3}\ H^{-1/3}$, as a function of the aspect ratio R/H. Present data with error bars, solid lines indicate the predicted slope values for $R/H < 0.7$ and $R/H > 0.7$, dashed lines shows the slopes obtained with numerical experiments data (Okada et al., 2004) and bold solid line indicates the slope found with experimental data.

5 Application of the MITgcm model. Localized convection source

Experimental data is the better way to asses if theoretical models explain natural processes (Speer and Marshall, 1995; Legg, et al., 1996; Legg et al., 2001; Pham et al., 2006) but they have some limits that models do not, such as the irreproducibility of the phenomena, the impossibility of studying the process in a three dimensional way and the impossibility of seeing how it could develop in a different environment which, in turn, would reveal what natural processes were like in the past or what they will be like in the future.

Hydrothermal plumes in Lake Banyoles, the chronic plume in B1 and the episodic plume in B2, have had an important role in the hydrodynamics and biology of the lake. The vertical transport of sediment particles (clay, silt and

mud) from the lake bottom is due to both hydrothermal plumes and their subsequent dispersion all over the lake area associated with density currents at the neutral floatability zone of the plumes (Serra et al., 2005). These influences on the lake dynamics originated a long time ago, as shown in the stratigraphy identified by seismic profiles and cores taken from the lake floor (Serra et al., 2006). It would be interesting to study the development of the hydrothermal plumes in the past and calibrate the model with experimental data. It would also be interesting to study the vertical development of the plumes, the equilibrium and maximum height of hydrothermal plumes under different conditions of stratification and buoyancy, so that we could predict future scenarios under which water quality would not be acceptable. This analysis could be of special interest for the water management of the lake.

Moreover, it has to be taken into account that although we have a large amount of experimental data and can see a clear evolution of stational variations, the experimental data obtained from longitudinal transects along the lake during field campaigns have a two-dimensional spatial scale. Three-dimensional variations are not known, so it is very difficult to separate the physical mechanisms that can determine particle concentration variations in a single point.

To define the most important mechanisms that determine the fate of transported particles through the lake, a high resolution numerical model, **MITgcm** (**MIT G**eneral **C**irculation **M**odel, designed for the study of the atmosphere, ocean, and climate) has been modified to study all the temporal and spatial scales associated with convective processes. This was made possible through a three month stay in the Geophysical Fluid Dynamic Laboratory, Princeton University, N.J., USA, working with an expert in numerical models, Dr. Sonya Legg (grant: 2004BE00073).

5.1 The Model

The model is designed to study transport into convective plumes using a technique where all the fluid parcels are conditioned to the evolving parcels

which allows us to know the development of a unique parcel into the general evolution. This global model can determine the plume properties in function of non-dimensional numbers like the Rossby number, the Rayleigh number and the Prandtl number, which let us evaluate the effects of rotation, floatability and diffusivity of the hydrothermal plume.

The **MITgcm** is a numerical model with a non-hydrostatic formulation to simulate fluid phenomena over a wide range of scales. Its adjoint capability enables it to be applied to parameter and state estimation problems. By employing fluid isomorphisms, one hydrodynamical kernel can be used to simulate flow in both the atmosphere and the ocean.

5.1.1 Non-hydrostatic ocean modelling

MITgcm supports hydrostatic, quasi-hydrostatic and non-hydrostatic algorithms. This means the model can be used to study both large-scale/global studies and small-scale processes (see Figure 5.1).

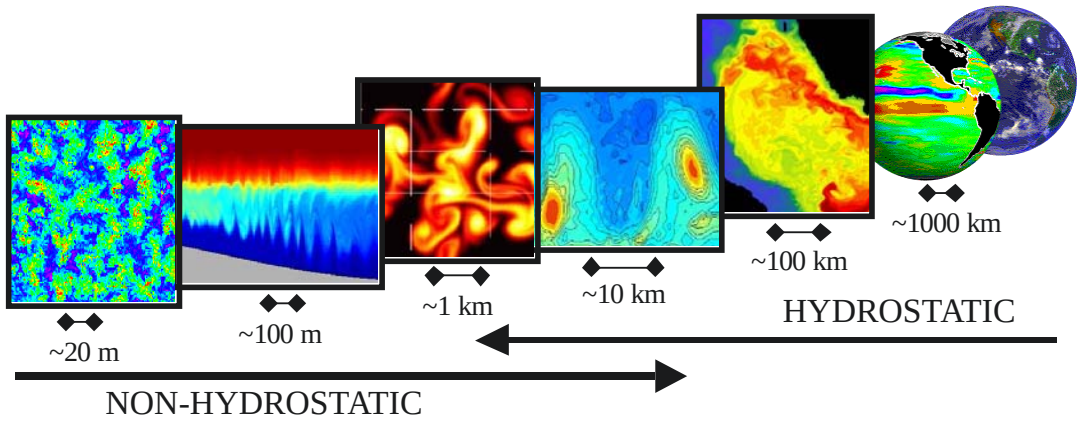

Figure 5.1
Schematic of scales indicating where hydrostatic dynamics give way to non-hydrostatic dynamics. (Figure from Adcroft et al., 2005)

The quasi-hydrostatic and non-hydrostatic sets are more accurate than the widely used hydrostatic primitive equations. Quasi-hydrostatic models relax the precise balance between gravity and pressure gradient forces by including in a consistent manner cosine-of-latitude Coriolis terms which are neglected in

primitive equation models. Non-hydrostatic models employ the full incompressible Navier Stokes equations, required in the study of small-scale ocean phenomena which are not in hydrostatic balance (Marshall et al., 1997). Inclusion of the non-hydrostatic terms means that MITgcm can properly represent processes that involve overturning of fluid parcels leading to static instability. Examples of such processes include deep convection and Kelvin-Helmholtz instability processes.

5.1.2 Finite-volume methods and the representation of topography

MITgcm is discretized by carving up the fluid domain into "finite volumes" with six sides. In the interior of the fluid this creates a grid of box shaped elements. The topography (solid bottom) intersects the grid, so the volume is shaped to fit the topography. This can be done in varying degrees of approximation, such as piecewise constant or discontinuous partial steps ("lopping"), piecewise linear or even higher order.

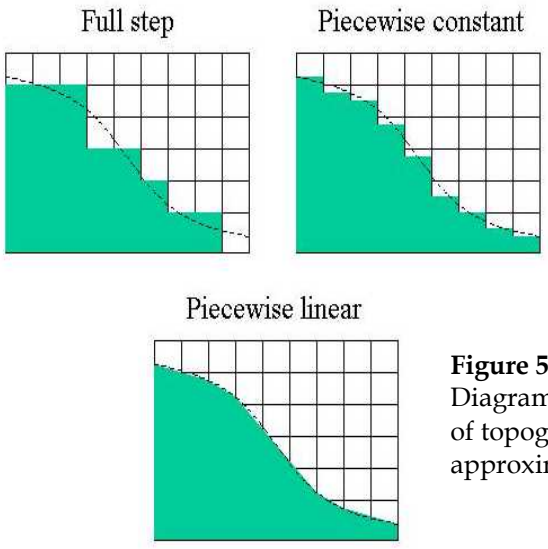

Figure 5.2
Diagram of different degrees of topography approximation.

In contrast, the finite difference method used in ocean models until recently would fit the topography to the grid; there is clearly a large representation error.

5.1.3 High order, non-linear (scalar) advection schemes

Accurate numerical representation of advection has always been a major research area in computational fluid dynamics. In addition to conventional schemes (linear 2nd, 3rd and 4th order), MITgcm has developed some higher order non-linear methods in the class of flux-limited methods. Flux-limited methods are highly non-linear and can be constructed to guarantee monotonicity and to optimize shape preserving properties. In multiple dimensions the MITgcm model uses a technique that retains these qualities for three dimensional flows.

An example of how the advection scheme can impact the solution is shown in Figure 5.4. A gravity plume, forced by deep water formation on the shelf (left), flows and accelerates down the slope. The shear between the plume and ambient fluid leads to Kelvin-Helmholtz billows which lead in turn to detrainment and entrainment of the plume fluid.

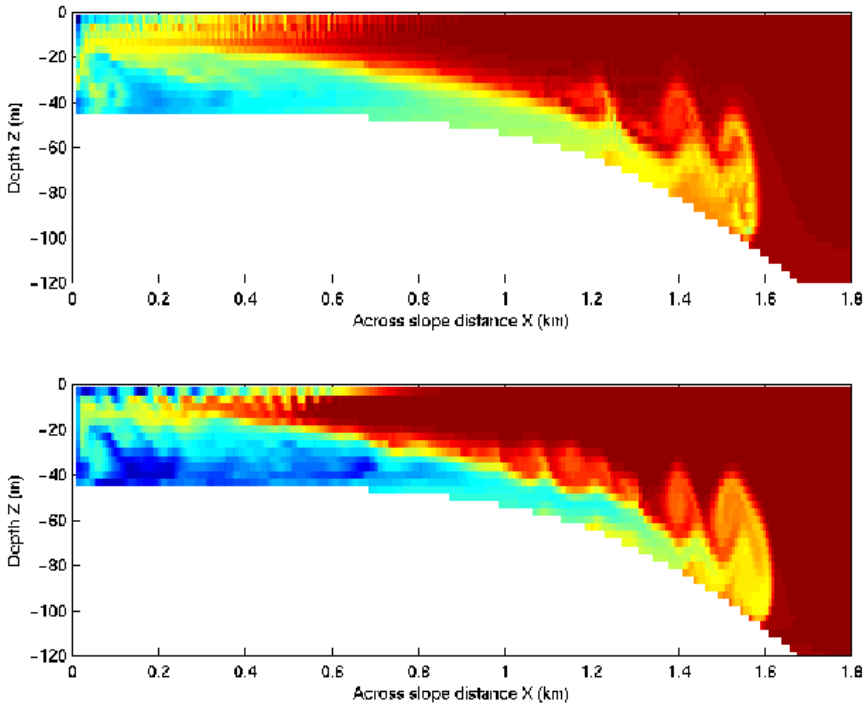

Figure 5.4
Advection schemes showing a gravity plume. The upper panel was calculated using conventional centred second order methods while the lower panel used third order interpolation with a Sweby flux-limiter. The latter has denser water in the plume and stronger contrasts in the billows, all indicative of lower levels of numerical diffusion.

5.1.4 Model equations

The state of the fluid at any time is characterized by the distribution of velocity $\vec{v}$, active tracers θ and S, a 'geopotential' ϕ and density $\rho = \rho(\phi, S, p)$ which may depend on θ, S, and p. The equations that govern the evolution of these fields, obtained by applying the laws of classical mechanics and thermodynamics to a Boussinesq, Navier-Stokes fluid, are written in terms of a generic vertical coordinate, r, so that the appropriate kinematic boundary conditions can be applied isomorphically.

$$\frac{D\vec{v}_h}{Dt} + (2\vec{\Omega} \times \vec{v})_h + \nabla_h \phi = F_{\vec{v}_h} \quad \text{horizontal mtm}$$

$$\frac{D\dot{r}}{Dt} + \hat{\kappa} \cdot (2\vec{\Omega} \times \vec{v}) + \frac{\partial \phi}{\partial r} + b = F_{\dot{r}} \quad \text{vertical mtm}$$

$$\nabla_h \cdot \vec{v}_h + \frac{\partial \dot{r}}{\partial r} = 0 \quad \text{continuity}$$

$$b = b(\theta, S, r) \quad \text{equation of state}$$

$$\frac{D\theta}{Dt} = Q_\theta \quad \text{potential temperature}$$

$$\frac{DS}{Dt} = Q_S \quad \text{humidity/salinity}$$

where:

r is the vertical coordinate

$\frac{D}{Dt} = \frac{\partial}{\partial t} + \vec{v} \cdot \nabla$ is the total derivative

$\nabla = \nabla_h + \hat{k}\frac{\partial}{\partial r}$ is the 'grad' operator

t is time

$\vec{v} = (u, v, \dot{r}) = (\vec{v}_h, \dot{r})$ is the velocity

ϕ is the ' pressure'/' geopotential'

$\vec{\Omega}$ is the Earth's rotation

b is the ' buoyancy'

θ is potential temperature

S is specific humidity in the atmosphere; salinity in the ocean

F_v are forcing and dissipation of $\vec{v}$

Q_θ are forcing and dissipation of θ

Q_S are forcing and dissipation of S

5.2 Changes on the model

The MITgcm model can simulate dense plumes generated by localized cooling on the continental shelf of the ocean influenced by rotation when the deformation radius is smaller than the width of the cooling region. The simulation employs the non-hydrostatic capability of MITgcm to trigger convection by surface cooling: the cold, dense water falls down.

To use the model in our convection cases, where convection is generated on the bottom (as the lutocline is warmer than the environment, it acts as a convective source), we have had to change the boundary conditions introducing a different kind of buoyancy source: the BottomHeatFlux.circle is a Matlab subroutine that generates convection from a circular source on the bottom (Figure 5.5) with heating (in W/m^2) given by a buoyancy flux chosen in the initial parameters ($Q_o=(B_o \cdot \rho \cdot C_p)/(g \cdot \alpha)$) plus a random variation. In order to understand the horizontal spatial distribution of heating flux into the source the model has been run taking two different random values (one of the same order and the other two orders of magnitude smaller than Q, which can be plotted to see how this value denotes the inhomogeneity of the heating source, see Figure 5.6). Results (spatial distribution of buoyancy along the temporal evolution) found with a random value of the same order of magnitude are more in accordance

with the experimental data, meaning that the buoyancy flux on the source has a high inhomogeneity. We can then conclude that the hypothesis in Chapter 3 (see section 3.8.1) about horizontal inhomogeneity is correct.

```
%Gaussian bump heating
Q=(Qo/2)*(1.0 + 0.01*rand([nx,ny]));
r=sqrt(X.^2+Y.^2);
bottomQ(find(r>L))=0;
fid=fopen('BottomHeatFlux.circle','w','b'); fwrite(fid, Q,'real*8'); fclose(fid);
```

```
%Gaussian bump heating
Q=(Qo/2)*(1.0 + 1*rand([nx,ny]));
r=sqrt(X.^2+Y.^2);
bottomQ(find(r>L))=0;
fid=fopen('BottomHeatFlux.circle','w','b'); fwrite(fid, Q,'real*8'); fclose(fid);
```

Figure 5.5
Matlab subroutine to generate a circular source of convection on the bottom with a random value of two orders of magnitude lower than Q (top), or a random of the same order of magnitude (bottom).

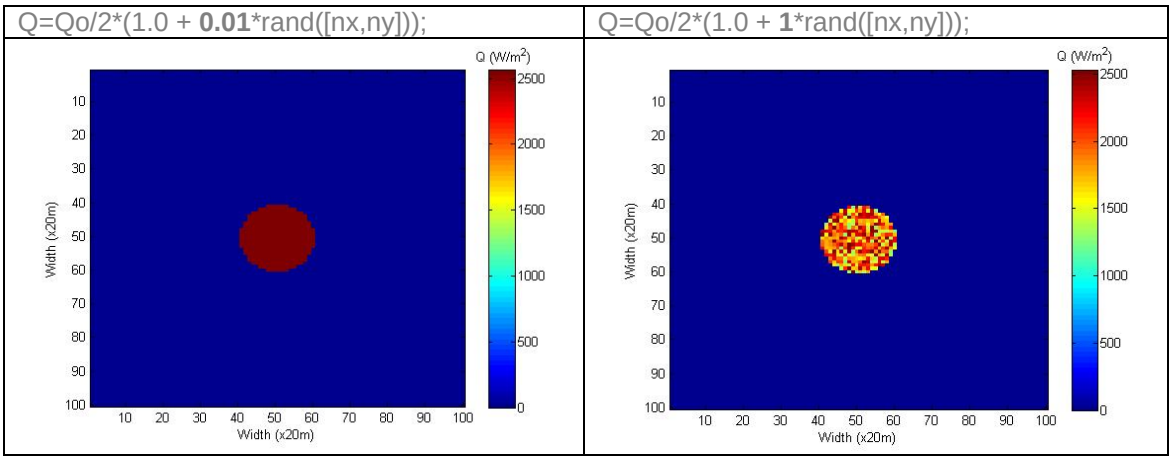

Figure 5.6
Bottom heat, Q, trough a circular source on the bottom generated with a random of two orders of magnitude lower than Q (left), or random of the same order of magnitude (right). These values corresponds to a hydrothermal plume with a Bo=9.34 · 10-7 m^2s^{-3}.

5.3 Running the model

Some parameters have to be chosen before running the simulation as: the Coriolis frequency, f, (which depends on the buoyancy source geography coordinates) and the scale parameters of the plume (as the source diameter) that will affect the buoyancy of the hydrothermal plume and therefore its vertical development.

5.3.1 Lake stratification

In order to account for changes in the lake stratification corresponding to different periods of the year, a new subroutine was written using Matlab. With this subroutine we were able to modify the Brünt-Väisälä frequency in accordance with the stratification pattern of the water column for each scenario. The subroutine is defined below (see Figure 5.7).

a

```
% Temperature profile
Tepilim=10.3;
Thypolim=10.15;
T_down1_thermocline=10.25;
T_down2_thermocline=10.20;
z_up_thermocline= 2.0;
z_down_thermocline= 4.0;
z_down1=5.0;
z_down2=6.0;

for i=1:z_up_thermocline
Tref(i)=Tepilim;
end

for i=(z_up_thermocline+1.0):z_down_thermocline
Tref(i)=Tref(i-1)-(Tepilim-
T_down1_thermocline)/((z_down_thermocline)
(z_up_thermocline));
end

Tref(5)=T_down2_thermocline;

for i=(z_down1+1.0):z_down2
Tref(i)=Tref(i-1)-(T_down2_thermocline-
Thypolim)/((z_down2)-(z_down1));
end

for i=(z_down2+1.0):H
Tref(i)=Thypolim;
end

[sprintf('Tref =') sprintf(' %9.6g,',Tref)]

t=0.0*ones(nx,ny,nz);
for k=1:nz
t(:,:,k) = t(:,:,k) + Tref(k);
end


fid=fopen('T.init','w',ieee); fwrite(fid,t,prec); fclose(fid);
```

B

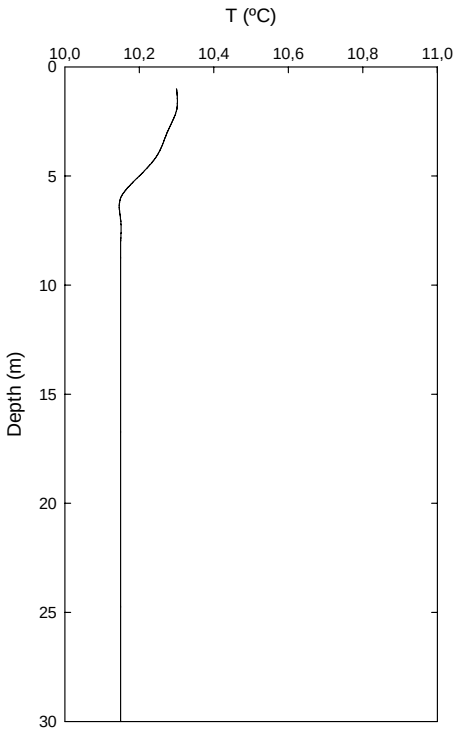

Figure 5.7
a) Matlab subroutine that generates the temperature profile (initial stratification pattern), b) plot of the temperature profile generated.

5.3.2 Grid

A grid of N_x x N_y x N_z = 100x100x30 with a width of $\Delta x = \Delta y$ = 20 m and Δz= 1 m has been used to simulate the hydrothermal plume developed in basin B1. The buoyancy source has been taken as a circle of 400 m diameter (Figure 5.8).

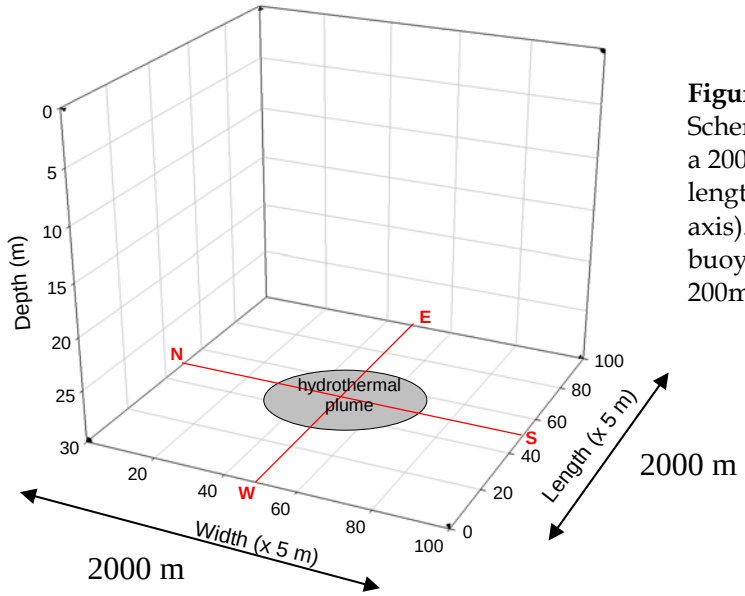

Figure 5.8
Scheme of the grid used for B1. It has a 2000 m width (Y axis), 2000 m length (X axis) and 30 m depth (Z axis). The grey circle represents the buoyancy source with a radius of 200m.

A grid of N_x x N_y x N_z = 100x100x36 with a width of $\Delta x = \Delta y$ = 3 m and Δz= 1 m has been employed to simulate the hydrothermal plume development in basin B2. The buoyancy source has been taken as a circle of 40 m diameter (Figure 5.9).

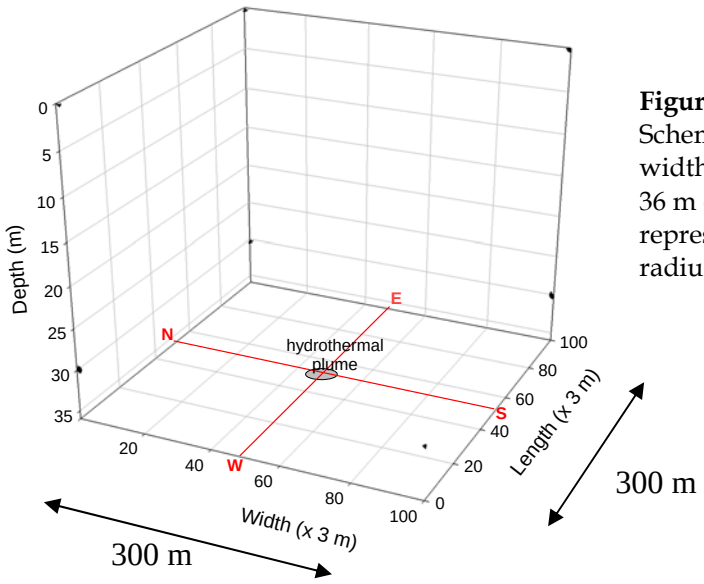

Figure 5.9
Scheme of the grid used. It has a 300 m width (Y axis), 300 length (X axis) and 36 m depth (Z axis). The grey circle represents the buoyancy source with a radius of 20 m.

We have used a domain size one order of magnitude larger than the scale of the forcing disk in order to avoid the influence of grid walls in the hydrothermal plume circulation. This has resulted in a loss in horizontal resolution but the hydrothermal plume dynamics can still be understood.

5.4 Results of the model

Different scenarios have been considered to determine the effect of the source buoyancy and the temperature stratification on the evolution of both hydrothermal plumes that develop in basins B1 and B2. The upward velocity of the WE plane (XZ) (that crosses the source by the middle at y=50, i.e. the red plane in Figure 5.10) has been plotted at different times to view the temporal evolution and the spatial distribution of the hydrothermal plume in each case. The horizontal components, u (east-west) and v (south-north), for the same plane and the horizontal velocity field on the top of the hydrothermal plume (the planes at z=5 m for the mixed period and at z=15 m for the stratified period) and on the bottom of the hydrothermal plume at z=28 m depth (two blue planes and green plane respectively, Figure 5.10) have also been plotted for the last iteration to see the horizontal distribution of the plume.

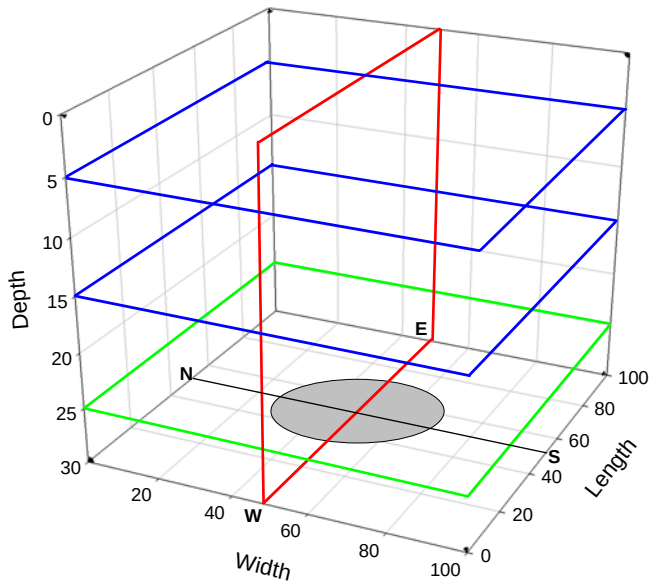

Figure 5.10
Scheme of the grid used with the different planes on which the simulation results have been plotted.

5.4.1 Basin 1 and Basin 2 (behaving as B1)

The different scenarios predicted by the model correspond to changes in the buoyancy flux (B_o) and the initial temperature profile to account for both mixed and stratified situations (through changes in $N^2(z)$). The B_o values used for each scenario are listed in Table 5.1; two of them correspond to scenarios found in the field, and the other two have both been taken changing the B_o by one order of magnitude to see its effect on the dynamics of the hydrothermal plume. When fluidization in B2 is totally developed the hydrothermal plume generated on the bottom of the basin has similar characteristics (B_o and diameter) than those developed in basin B1, therefore both can be simulated with the same scenarios.

	B_o (m^2s^{-3})	**Period**	**Experimental case**	**Figures**
Scenario 1	$8.107 \cdot 10^{-8}$	Stratified	June 2004	7.11, 7.12
Scenario 2	$9.340 \cdot 10^{-7}$	Stratified	-	7.13, 7.14
Scenario 3	$8.107 \cdot 10^{-8}$	Mixed	December 2003	7.15, 7.16
Scenario 4	$9.340 \cdot 10^{-7}$	Mixed	-	7.17, 7.18

Table 5.1
Characteristics from the different scenarios run with the MITgcm to study the hydrothermal plume developed in basin B1.

7.4.1.1 Stratified period

In this period, the water column is completely stratified and divided into three differentiated layers: the epilimnion, the metalimnion and the hypolimnion (see Figure 5.11 top, with epilimnion and hypolimnion separated by a strong stratification between 5 and 10 m). The temperature profile corresponds then to the typical summer stratification. Two cases will be studied depending on the buoyancy flux per unit area value (Table 5.1).

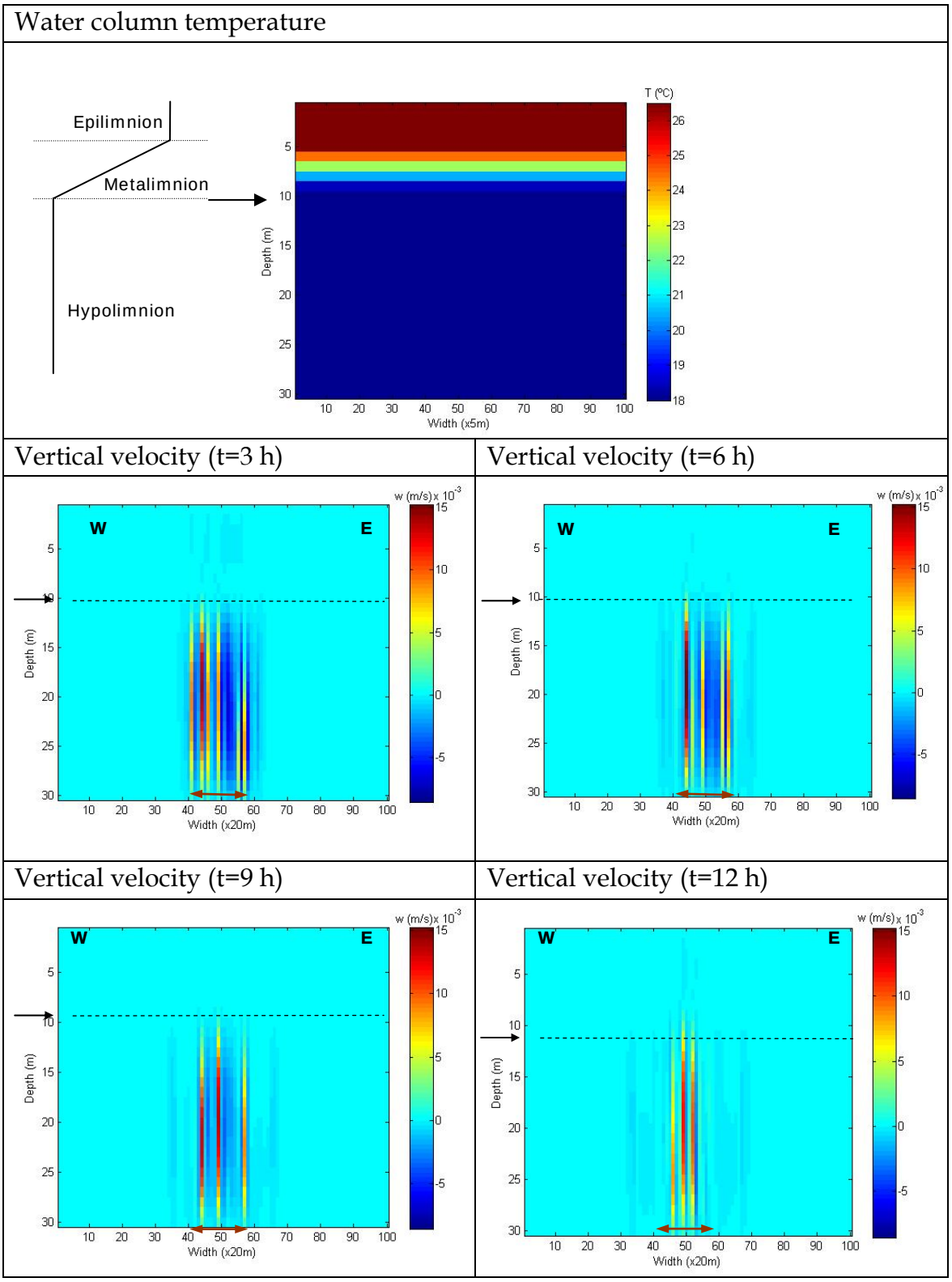

Figure 5.11
Temporal evolution of the vertical velocity for a hydrothermal plume with B_o=8.107·10^{-8} m^2/s^3 in the stratified period. The top panel presents the temperature stratification of the water column. The base of the thermocline (top of the hypolimnion) has been drawn as a dashed line in the rest of the panels. As shown in Figure 5.7, the diameter of the source ranges from 40 (x20m) to 60 (x20m) and is drawn as a double arrow.

As shown in Figures 5.11 and 5.13, the hydrothermal plume is formed by several single plumes with independence of time, this vertical structure is in accordance with experiments done in laboratory tanks (Maxworthy and Narimousa, 1994). The horizontal scale of the single plumes (SP) is of the order of 20 m (downward velocity SP as well as the upward velocity SP), this has been found with a high resolution grid (5 m) (see Figure 5.12), and the vertical scale depends on the stratification. The number of SP change with time, as can be seen in Figure 5.11, and has been found to depend on the scenario considered. Single plumes are in accordance with the hypothesis made in Chapter 5 that allows us to explain the horizontal pattern in the ADCP backscatter images obtained in B1 (see, for example, 3 November 2003 in Figure 3.19) and also obtained in B2 from 29 December 2003 when the plume starts to behave as B1 (see for example 5 February 2004 in Figure 3.22). ADCP backscatter showed a horizontal spatial displacement of the source. This is in agreement with the results from the model (Figures 5.11 and 5.14).

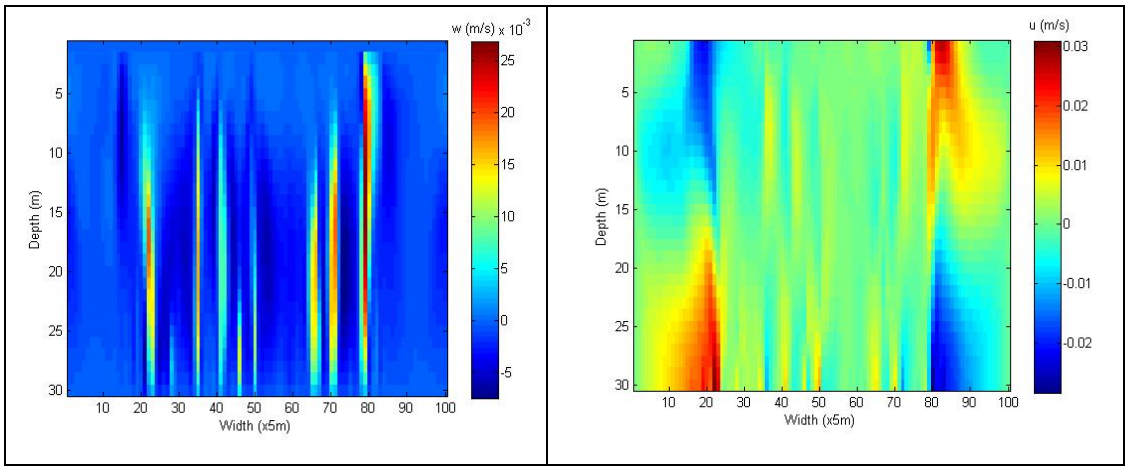

Figure 5.12
Vertical velocity for a hydrothermal plume with B_o=8.107·10^{-8} m^2/s^3 in the mixed period. The diameter of the source ranges from 20 (x5m) to 80 (x5m).

From the velocity contour, it can also be seen that the hydrothermal plume does not cross the thermocline, which base extends at 10 m depth (see the temperature profile in Figure 5.11). This in accordance with the fact that Ri is

larger than the critical value (Ri_c=11), Narimousa, 1996. The thermocline then acts as a barrier to the hydrothermal plume, as measured with the ADCP (Figures 5.11 and 5.14). Vertical development of the hydrothermal plume in scenario 2 is similar to the previous simulation. The hydrothermal plume does not cross the thermocline (Figure 5.14); rather, larger intrusions from hypolimnetic water are observed in the last iterations when compared to those obtained in scenario 1. In this scenario, the Ri is again larger than 11. Therefore, we expect that in scenario 2 the base of the metalimnion might be eroded. The upward velocity plotted in both cases shows that the hydrothermal plume does not reach a steady state. In order to verify how long the model should run, it has been taken into account that the characteristic time for a SP to reach the thermocline is around 1333.3 s ($\tau = \ell/u$ = 20 m / (0.015 m/s)). Therefore, the model has been run the number of iterations corresponding to 12 hours (which corresponds to nearly 32 times this characteristic time), which is enough to see how the single plumes generated change their position and upward velocity magnitude.

While the model is capable of generally predicting both the vertical and horizontal extension of the plume and the presence of single plumes, it fails to determine the absolute values of the velocities. From the model, vertical velocities are of the order of 0.015 m/s upward and 0.001 m/s downward (Figure 5.11), which should be measurable by the ADCP. In contrast, the ADCP was not able to measure them, indicating they may fall below its limit of detection (0.005 m/s). In that case, the model would overestimate at best three times the vertical velocity values in this scenario. In scenario 2, as the buoyancy flux is higher, vertical velocities are also higher, the upward velocity being ~0.033 m/s and the downward being ~0.046 m/s (see Figure 5.14). Again, we could not experimentally detect velocity values with the ADCP. Therefore, in this case the model overestimates the upward velocities as it did in scenario 1.

Positive horizontal velocity values (v) correspond to a flow towards the south, and positive horizontal velocity values (u) correspond to a flow towards the

east. As in the case of vertical velocities, horizontal velocities cannot be detected from the experimental data, although their theoretical values in scenario 1 ($u \in$(-0.026, 0.029) m/s and $v \in$(-0.035, 0.032) m/s, in Figure 5.13) and in scenario 2 ($u \in$(-0.084, 0.143) m/s and $v \in$(-0.161, 0.097) m/s, in Figure 5.15) should be measurable by the ADCP.

These differences between velocity values predicted by the model and values of the flow velocity measured around the source could be attributed to the fact that velocities might not be completely horizontal because of the V-shaped topography around the source in basin B1 and basin B2. It must be pointed out that model equations are derived for open convection from an isolated source without boundary constraints. The V-shape of the depressions might play a crucial role in determining the rim velocity and its direction.

In Figure 5.13 the detrainment at 15 m depth and the entrainment at 28 m depth can be seen (shown with black arrows), while in Figure 5.15 the detrainment occurs at 10 m, just below the thermocline. This can be caused by the fact that scenario 2 has a buoyancy flux one order of magnitude larger than that in scenario 1. It can also be seen how at the west side of the hydrothermal plume the flow direction is towards the south from the bottom to 15 m depth and then it changes its sense, being towards the north from that depth to the surface. At the east side the flow is directed towards the north from the bottom to 15 m depth and then changes being towards the south. Taking both horizontal components of velocity together, the circulation around the hydrothermal plume can be deduced. In accordance with theory, the circulation found on the forcing disk known as the rim current is cyclonic and that found at the spreading depth of the hydrothermal plume is anti-cyclonic. Although we had first expected a single vortex around the hydrothermal plume (as the values found of the Rossby plume number always are higher than 3), the number of vortices N_v found ranges between 0.6 and 1 (see equation 3.7 in Chapter 3), denoting that, although there is rotation around the source, it could be possible that the single vortex does not develop completely, this has been also found in

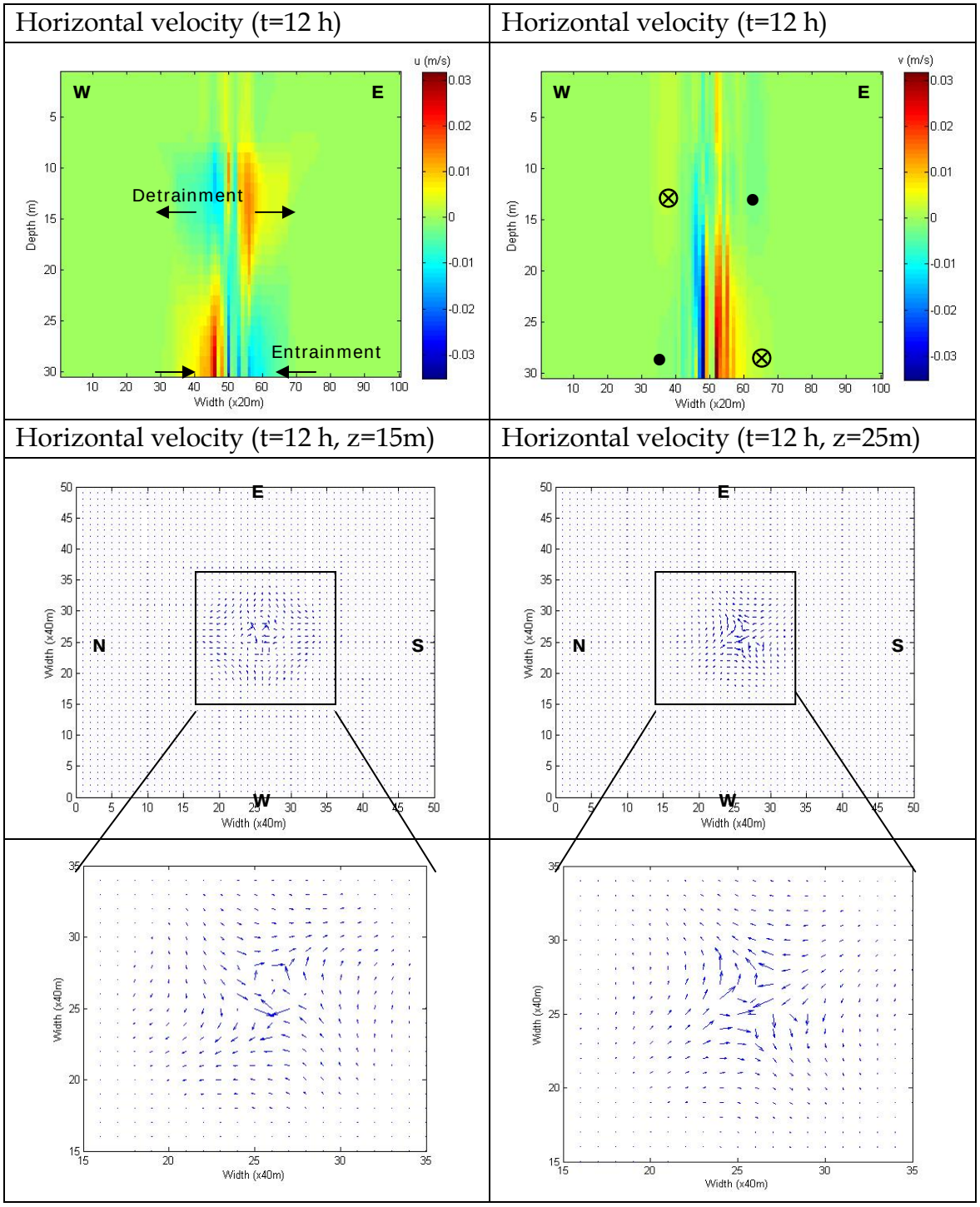

Figure 5.13
Horizontal velocity components (u>0: east direction; v>0 north direction) 12 hours after its initiation for a hydrothermal plume with $B_o=8.107 \cdot 10^{-8}$ m^2/s^3 in the stratified period (top). Horizontal velocity field run at 15 and 28 m depth (bottom), velocity values have been plotted in each 2 node grid.

laboratory experiments because of the formation of single plumes emanating from "convective holes" which forms beneath the source (Narimousa, 1996). In fact, data undertaken in the field campaigns are not enough to see if the

single vortex theoretically expected develops or not develops completely. This can be seen at 15 and 28 m depth in Figures 5.13 and 5.15 (scenario 1 and 2 respectively) and although the unique vortex can not be seen in these figures, there is a change in the direction of the current developed around the hydrothermal plume as it was expected, quasi cyclonic on the forcing disk and quasi anti-cyclonic at the spreading depth.

Simulations with entry parameters which could give N_v values larger than 1 have not been run because we wanted to study the hydrothermal dynamics of the plume developed in basin B1; therefore, B_o values have been taken near the real ones. Moreover, cases with N_v values higher than 1 have been widely studied by Okada et al., 2004, and as explained in Chapter 6, we are in another range of values.

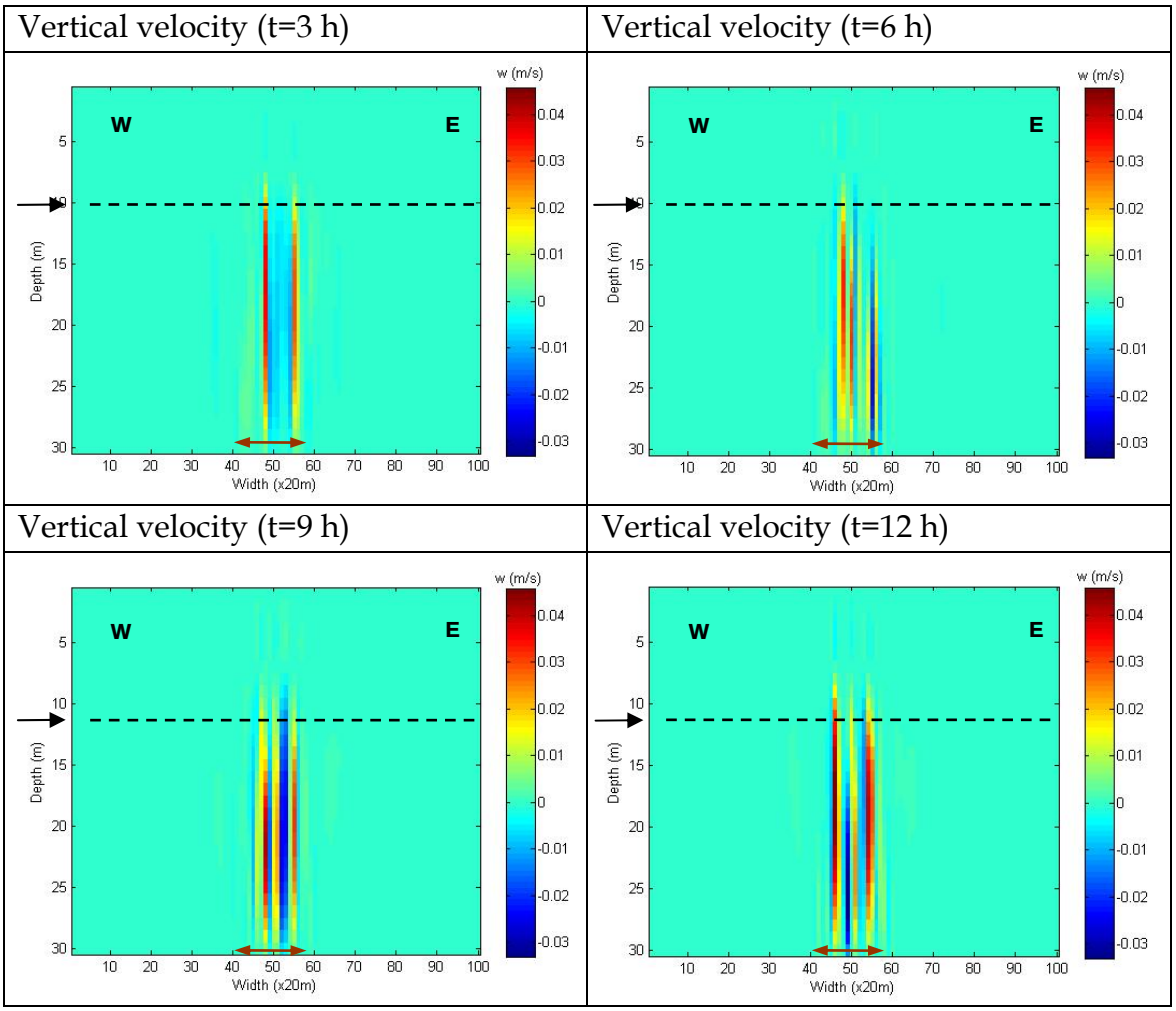

Figure 5.14
Temporal evolution of the vertical velocity for a hydrothermal plume with B_o=9.34·10^{-7} m^2/s^3 in the stratified period. The base of the thermocline (top of the hypolimnion) has been drawn as a dashed line. As shown in Figure 5.7, the diameter of the source ranges from 40 (x20m) to 60 (x20m) and it is drawn as a double arrow.

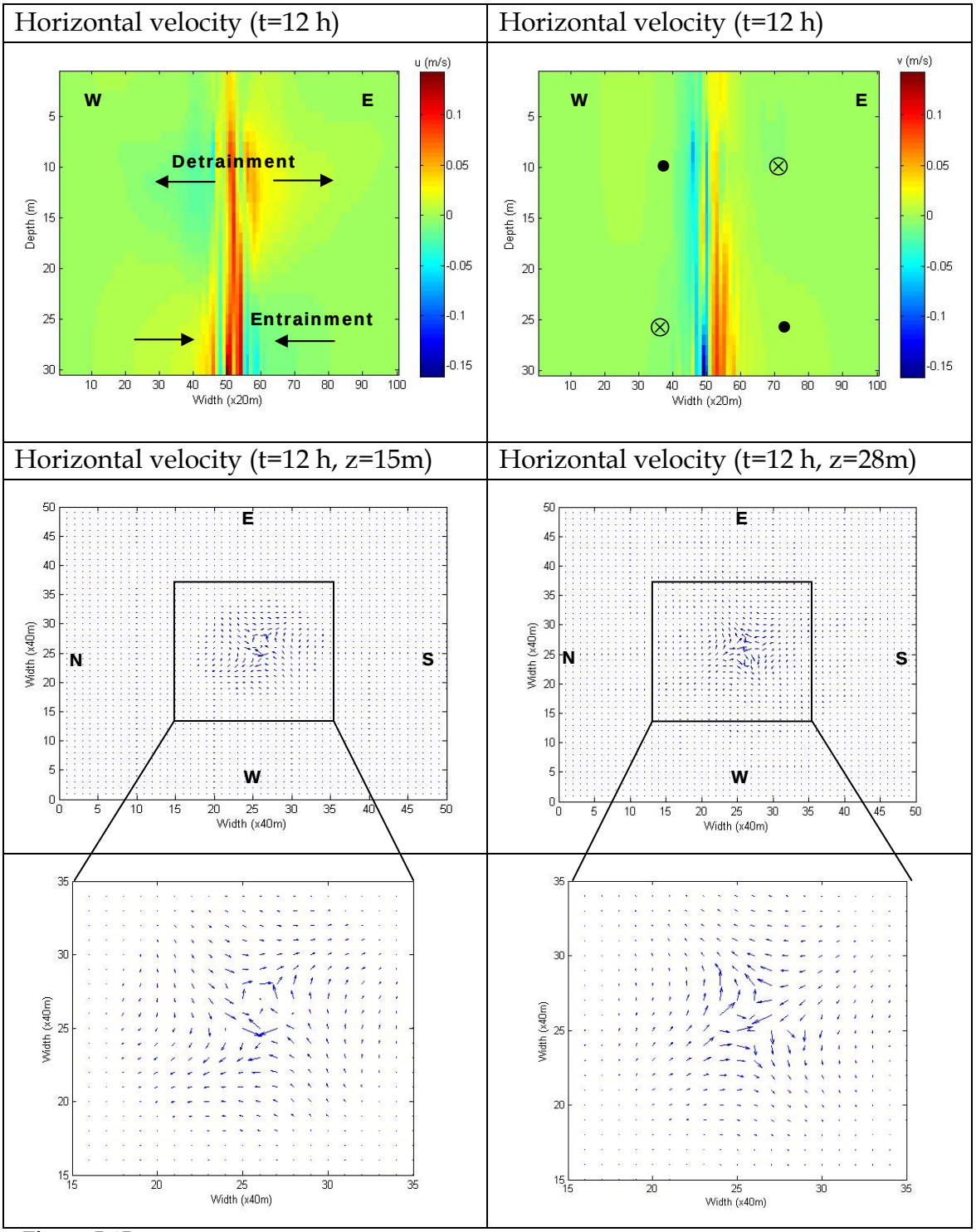

Figure 5.15
Horizontal velocity components (u>0: east direction; v>0 north direction) after 12 hours from its initiation for a hydrothermal plume with B_o=9.34·10^{-7} m^2/s^3 in the stratified period (top). Horizontal velocity field run at 15 and 28 m depth (bottom), velocity values have been plotted each 2 grid node.

7.4.1.2 Mixed period

In this period the water column is almost mixed, with a water temperature in the column almost constant at 10.15 ^{o}C (see Figure 5.16 top). This is the characteristic vertical profile of temperature for winter, with only a thin mixing layer situated at the surface of the water column and with a slight temperature gradient. Two cases will be studied, depending on the B_o values.

As shown in Figures 5.16 and 5.17, the hydrothermal plume is formed by several single plumes. From the vertical velocity counters the scales of SP are, as in previous cases, of the order of 20 m in the horizontal. The vertical extension depends on stratification. The number of SP formed has also been found to change with time.

In both scenarios (3 and 4), the hydrothermal plume easily crosses the diurnal thermocline (a weak thermocline produced by the diurnal temperature differences), and develops from the bottom to the surface. In that case, the weak stratification does not represent a barrier to the vertical development of the hydrothermal plume, which collapses at the lake surface (see Figures 5.16 and 5.18).

Vertical maximum velocity magnitudes, upward and downward, are 0.012 m/s and 0.026 m/s in scenario 3 (Figure 5.16) and in scenario 4 respectively, as the buoyancy flux is higher (~ 1 order of magnitude), the hydrothermal plumes vertical velocities are of 0.065 m/s upward and 0.048 m/s downward (Figure 5.18).

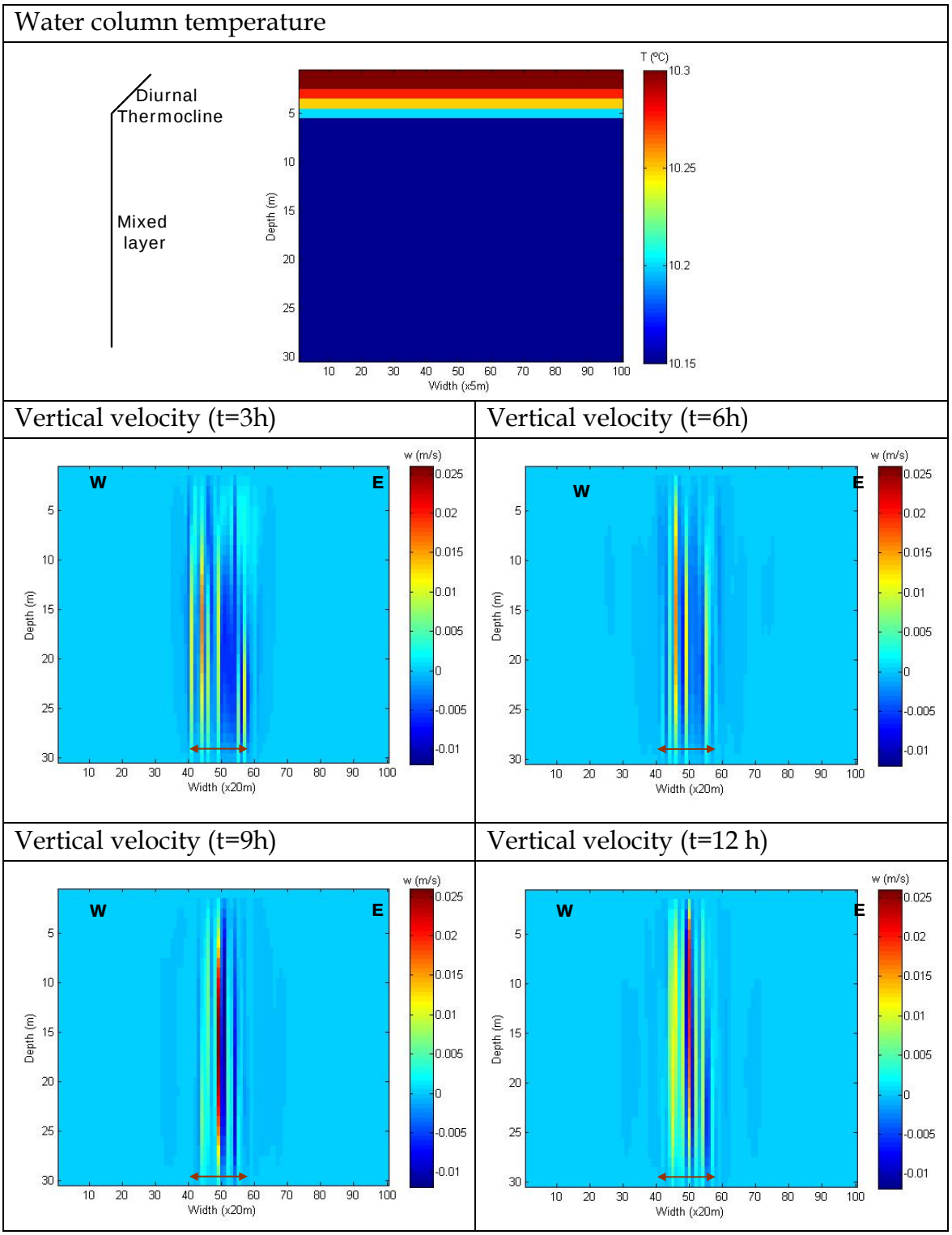

Figure 5.16
Temporal evolution of the vertical velocity for a hydrothermal plume with B_o=8.107·10^{-8} m^2/s^3 in the stratified period. Top panel presents the temperature profile of the water column. As was shown in figure 5.7 the diameter of the source ranges from 40(x20m) to 60 (x20m) and it is drawn as a brown double arrow.

Horizontal velocity values are u ∈(-0.031, 0.051) m/s and v ∈(-0.056, 0.062) m/s, in scenario 3 (Figure 5.17); and u ∈(-0.157, 0.170) m/s and v ∈(-0.112, 0.163) m/s in scenario 4 (Figure 5.19). There is still an overvaluation of velocities by the model.

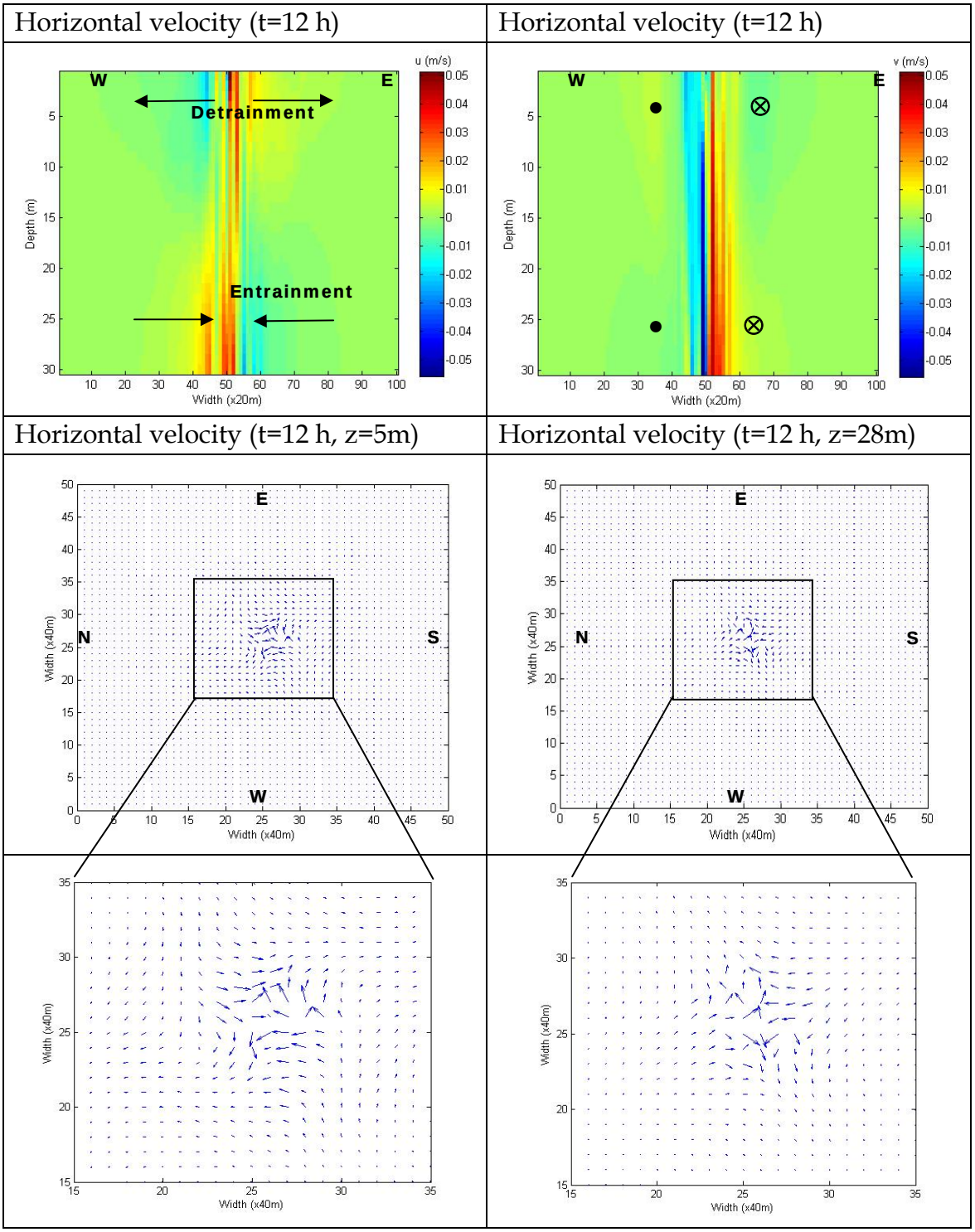

Figure 5.17
Horizontal velocity components after 12 hours from its initiation for a hydrothermal plume with B_o=8.107·10^{-8} m^2/s^3 in the stratified period (top). Horizontal velocity field run at 15 and 28 m depth (bottom), velocity values have been plotted each 2 grid node, velocity direction can be better seen with the zoom.

The entrainment for scenario 3 was found at 10 m depth above the forcing disk (Figure 5.17) and extended through a region from the lake surface down to 10 m depth. In contrast, for scenario 4, the entrainment zone is narrower than that in scenario 3, with a thickness of 5 m compared to that at 10 m depth for scenario 3. The detrainment zone, which was situated just below the lake surface, extended over a wide zone, 20 m depth (Figure 5.19) double that found in scenario 3. The difference can be attributed to the fact that scenario 4 has a buoyancy flux one order of magnitude higher and the intrusion of the plume in the lake water is larger, producing more entrainment of hypolimnetic water. In scenario 3, it can also be seen how the velocity has a southerly direction (at the west side of the hydrothermal plume) and northerly direction at the east side, from bottom to 16 m depth; and a northerly direction (at the west side of the hydrothermal plume) and southerly direction (at the east side), from 16 m depth to surface. Taking both horizontal components of velocity together, the circulation around the hydrothermal plume can be deduced; this can be seen at 15 and 28 m depth in Figures 5.17 and 5.19. Although we had first expected a single vortex around the hydrothermal plume as the values found of the Rossby plume number are always higher than 3, the number of vortex N_v found ranges between 0.6 and 1 (see 3.7 in Chapter 3), denoting the possibility that, despite rotation around the source, the single vortex does not develop at all.

A change in the direction of the current developed around the hydrothermal plume should be expected: cyclonic at the entrainment zone and anti-cyclonic at the detrainment zone. This circulation is in accordance with the theory and can also be seen in scenario 4, (Figure 5.18).

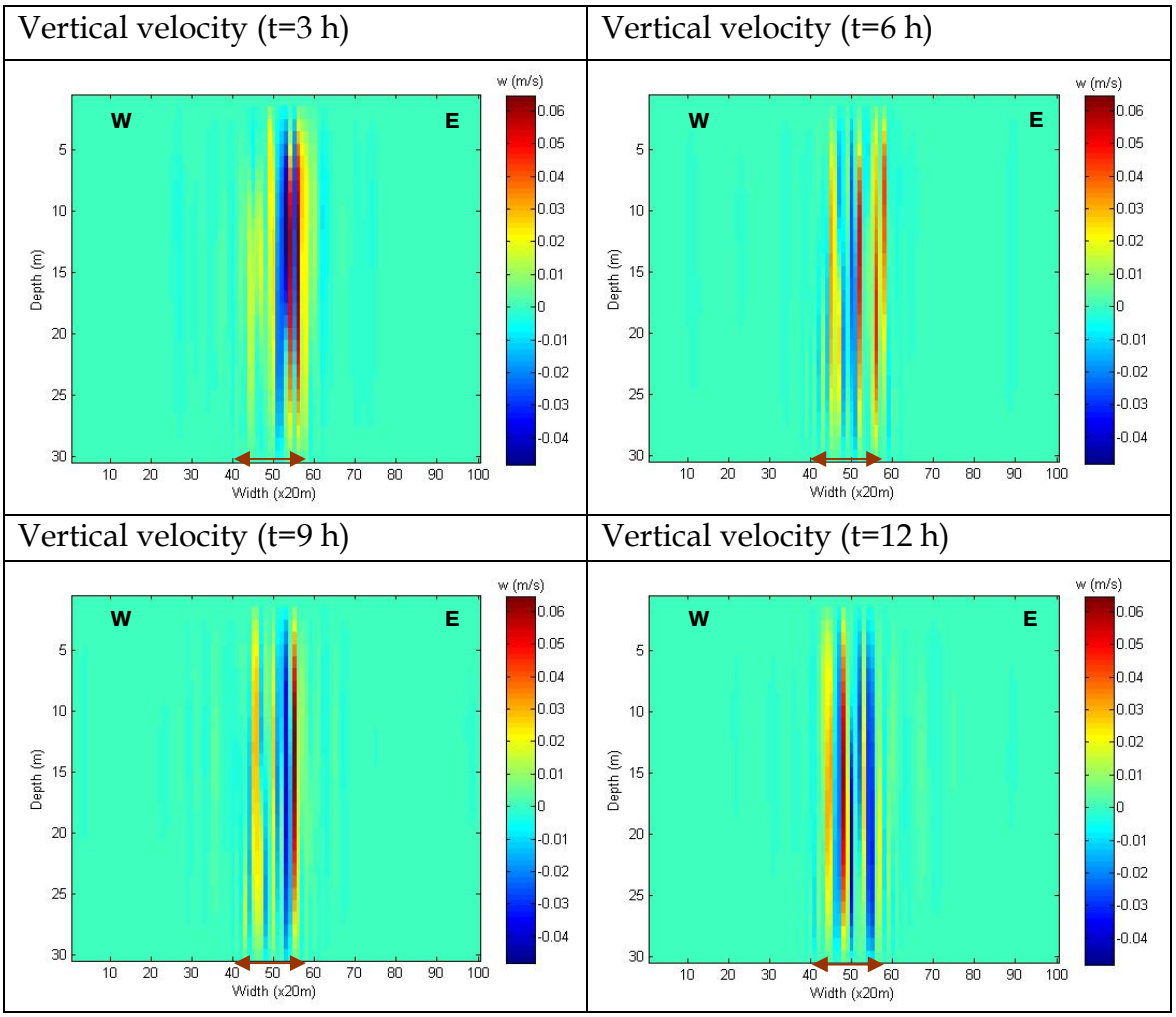

Figure 5.18
Temporal evolution of the vertical velocity for a hydrothermal plume with B_o=9.34 $\cdot 10^{-7}$ m^2/s^3 in the stratified period. As was shown in figure 5.7 the diameter of the source ranges from 40(x20m) to 60 (x20m) and it is drawn as a double arrow.

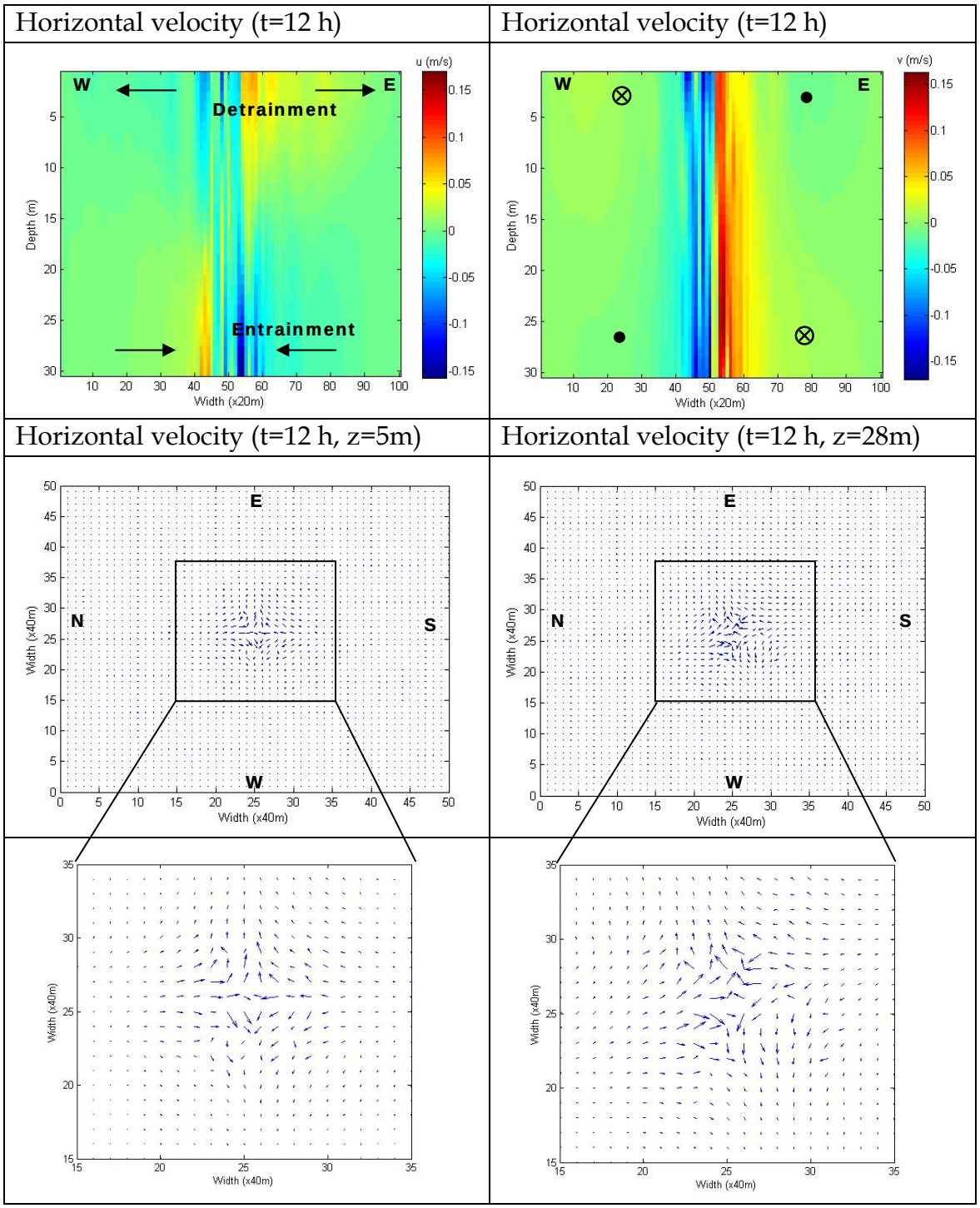

Figure 5.19
Horizontal velocity components (u>0: east direction; v>0 north direction) after 12 hours from its initiation for a hydrothermal plume with B_o=9.34·10^{-7} m^2/s^3 in the stratified period (Figure 5.15 top). Horizontal velocity field run at 5 and 28 m depth (bottom), velocity values have been plotted each 2 grid node.

5.4.2 Basin 2 (behaving as a single-plume)

We will focus now on the behaviour of the single plume found in basin B2. We will try to see if the present model is capable of reproducing the experimental results found. The next two simulations (scenarios 5 and 6) have different buoyancy flux values, B_o, with one order of magnitude of difference (see Table 5.2), and the same initial temperature profile because this particular convection process has only been found to develop during the mixed period. The temperature of the water column is almost constant at 16.8 ^oC.

	B_o (m^2s^{-3})	Period	Experimental case	Figures
Scenario 5	$1.12 \cdot 10^{-4}$	Mixed	November 2003	7.19, 7.20
Scenario 6	$1.12 \cdot 10^{-5}$	Mixed	-	7.21, 7.22

Table 5.2
Characteristics from the different scenarios run with the MITgcm to study the hydrothermal plume in basin B2.

Vertical velocities in the hydrothermal plume corresponding to scenario 5 are 0.456 m/s upward and 0.093 m/s downward (Figure 5.20). These values are nearly one order of magnitude higher than those found experimentally, as were the values found for the hydrothermal plume simulation in scenarios 1 to 4. For the single plume simulations, the model also overpredicts by one order of magnitude the vertical velocities of the plume. In scenario 6, maximum hydrothermal plume vertical velocities are higher than in the previous case: 0.202 m/s upward and 0.060 m/s downward (see Figure 5.22). The difference is not very large because the velocity values have only changed by a few units even though the difference between initial B_o was of one order of magnitude.

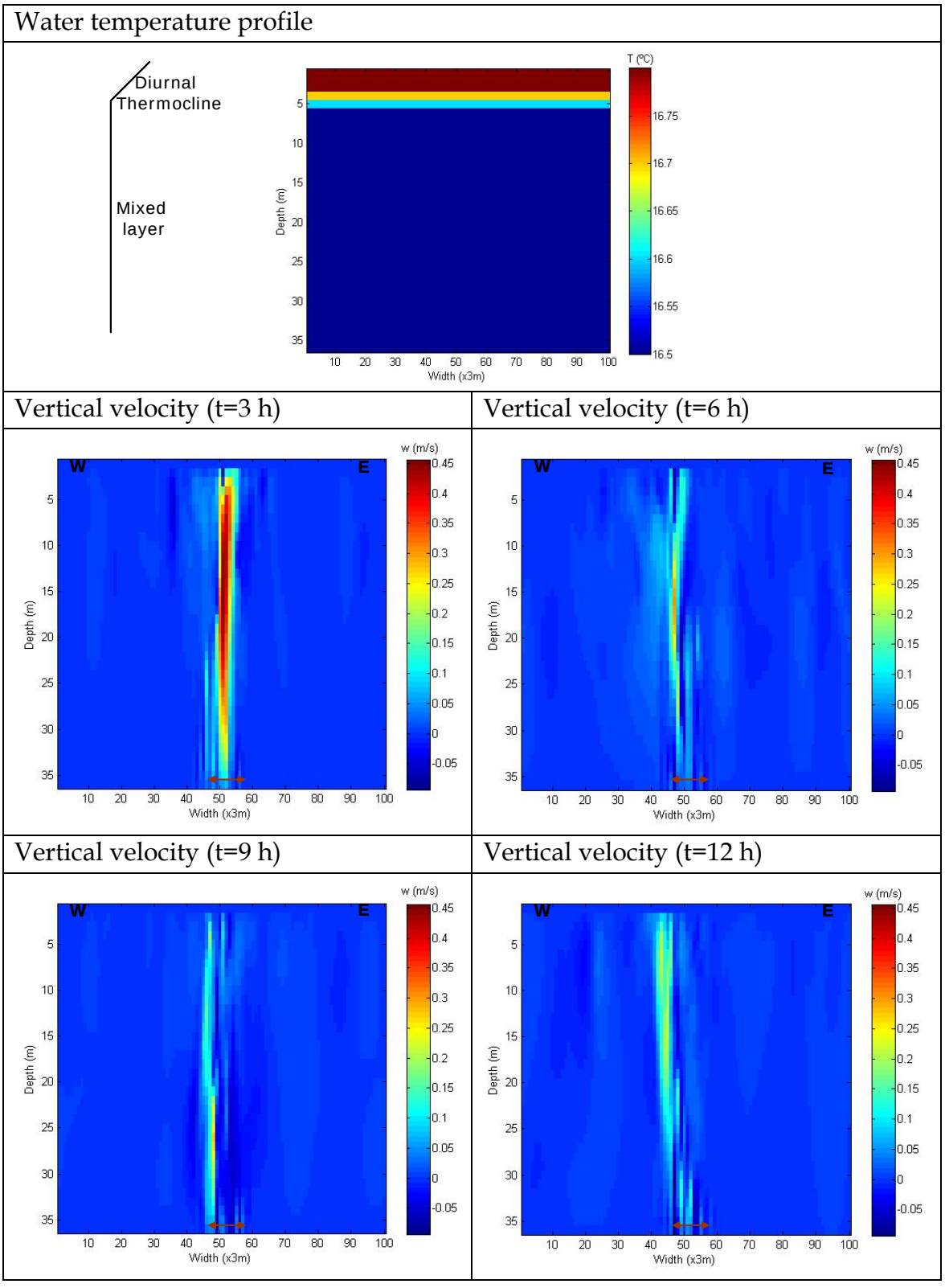

Figure 5.20
Temporal evolution of the vertical velocity for a hydrothermal plume with $B_o=1.12 \cdot 10^{-4}$ m^2/s^3 in the stratified period. Top panel presents the temperature stratification of the water column. As was shown in figure 5.7 the diameter of the source ranges from 45 (x3m) to 55 (x3m) and it is drawn as a double arrow.

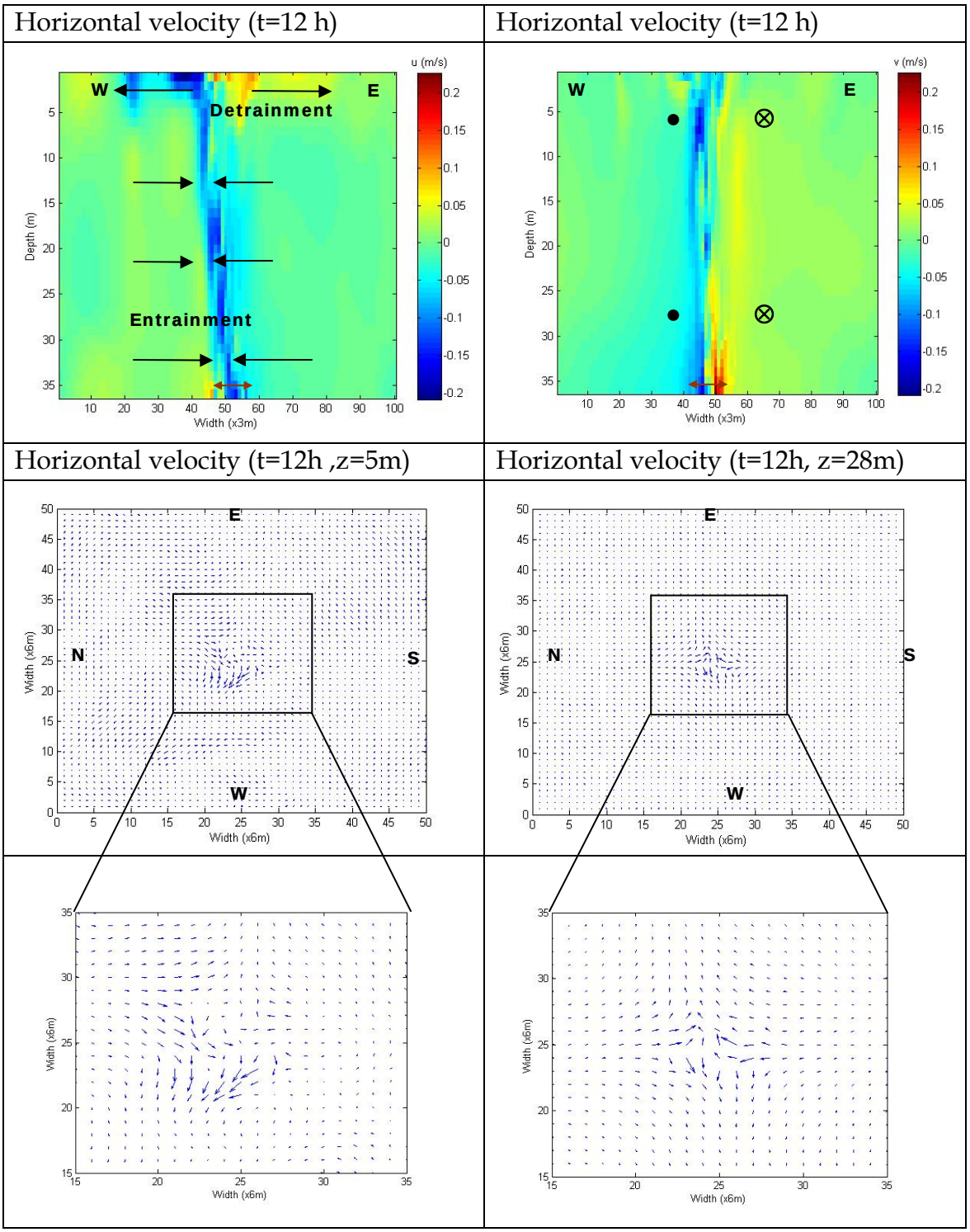

Figure 5.21
Horizontal velocity components (u>0: east direction; v>0 north direction) after 12 hours from its initiation for a hydrothermal plume with B_o=1.12·10^{-4} m^2/s^3 in the mixed period (Figure 5.19 top). Horizontal velocity field run at 5 and 28 m depth (bottom), velocity values have been plotted each 2 grid node.

In the single plume case, horizontal velocity values could be detected by the ADCP and the order of magnitude coincides with the values found with the model (u ∈(-0.209, 0.125) m/s and v ∈(-0.169, 0.227) m/s, in scenario 5, see Figure 5.21; and u ∈(-0.172, 0.141) m/s and v ∈(-0.1294, 0.101) m/s, in scenario 6, see Figure 5.23). Velocity values found in scenario 6 are smaller than those found in scenario 5 because of buoyancy flux value being ~1 order of magnitude lower.

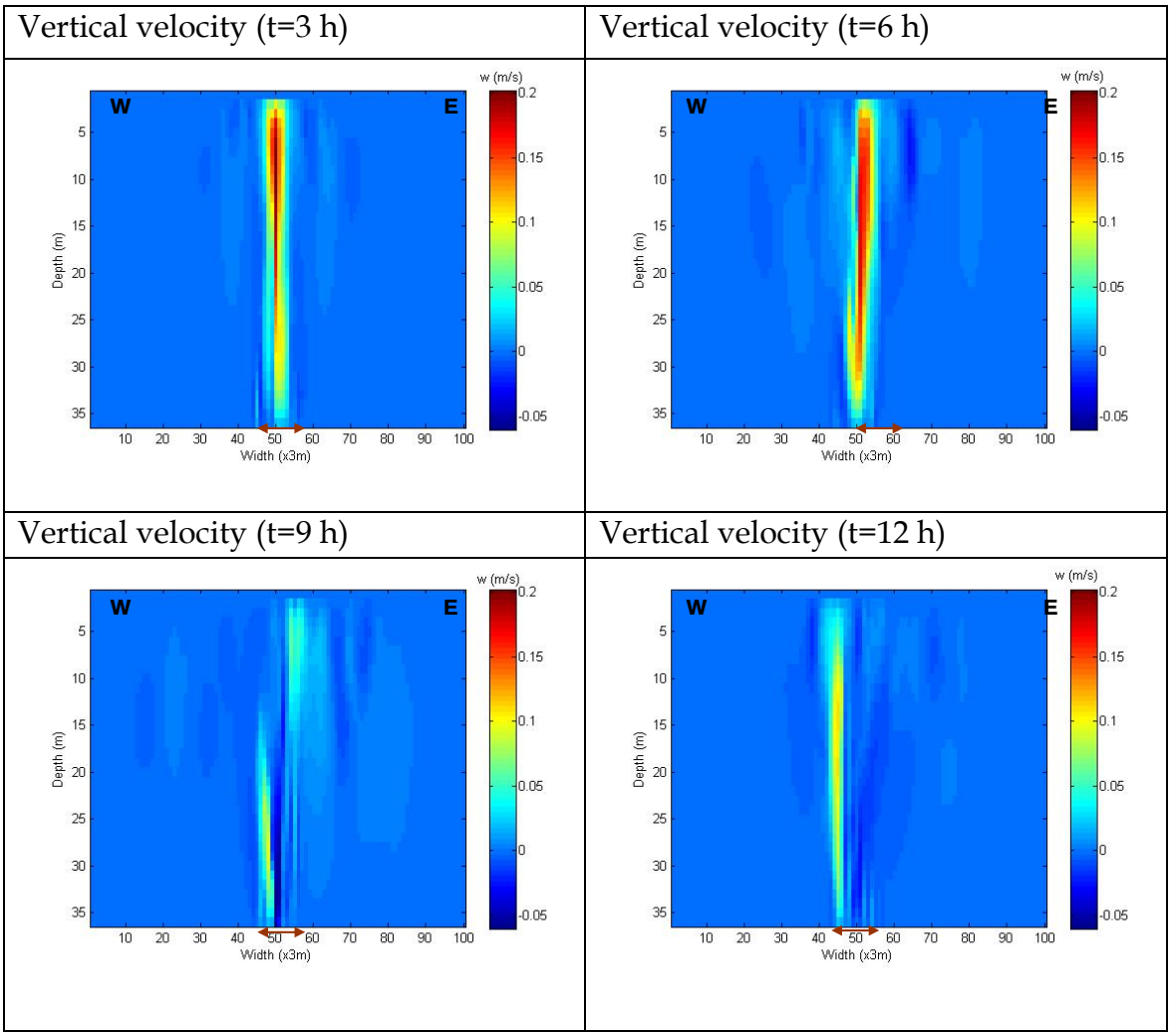

Figure 5.22
Temporal evolution of the vertical velocity for a hydrothermal plume with B_o=1.12·10^{-5} m^2/s^3 in the stratified period. As was shown in figure 5.7 the diameter of the source ranges from 45 (x3m) to 55 (x3m) and it is drawn as a double arrow.

In Figures 5.21 and 5.23, the entrainment was found all along the water column above the forcing disk upwards to ~5 m depth, and the detrainment was

reduced to the first 5 m below the surface of the lake. It can also be seen how along the whole column the velocity has northerly direction (at the west side of the hydrothermal plume) and a southerly one at the east side.

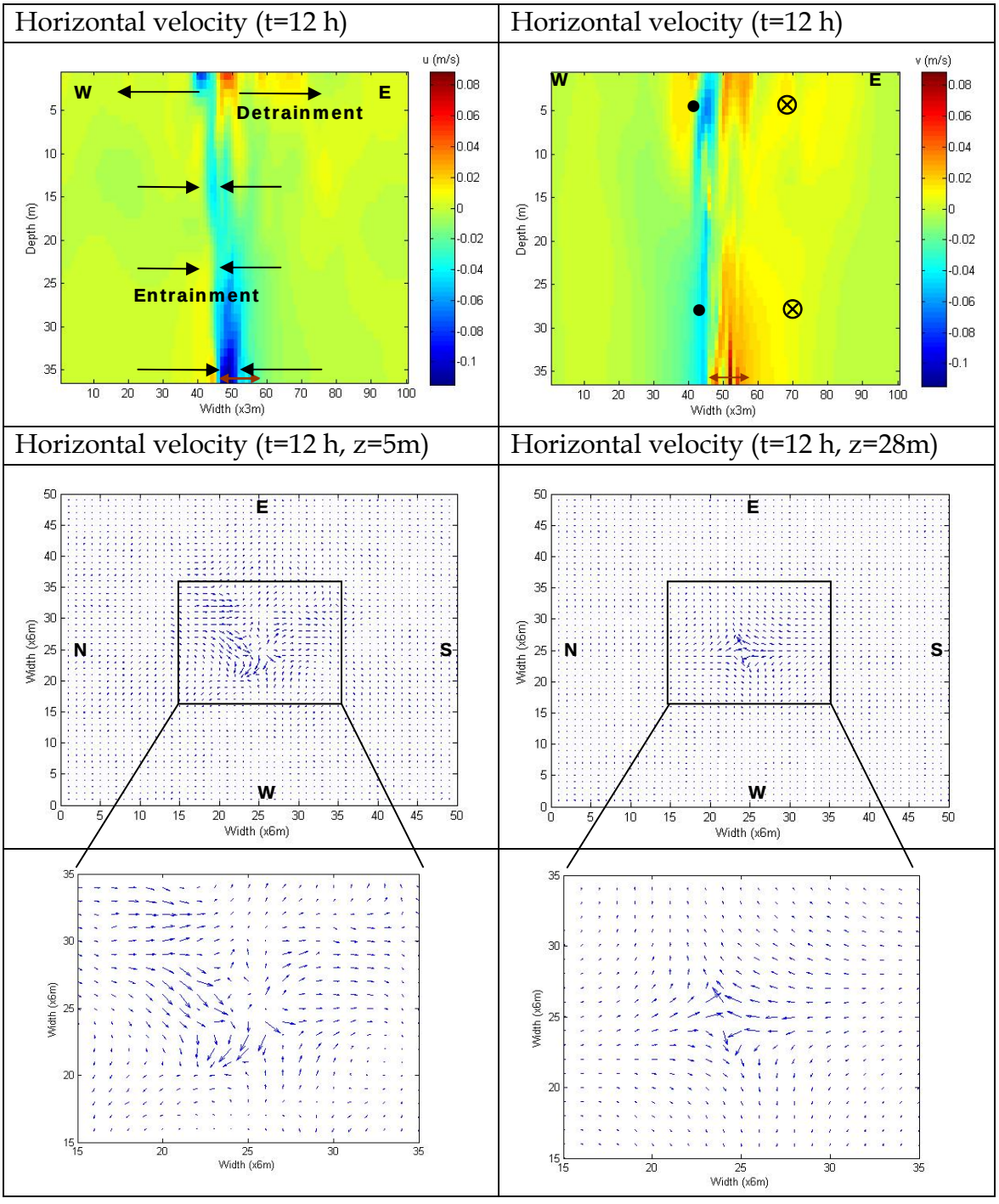

Figure 5.23
Horizontal velocity components (u>0: east direction; v>0 north direction) after 12 hours from its initiation for a hydrothermal plume with B_o=1.12·10^{-5} m^2/s^3 in the mixed period (Figure 5.19 top). Horizontal velocity field run at 15 and 28 m depth (bottom), velocity values have been plotted each 2 grid node.

Taking both horizontal components of velocity together, it can be seen that the circulation around the hydrothermal plume is cyclonic along the whole water column; this can be seen at 5 and 28 m depth in Figures 5.21 and 5.23. It can also be seen in both scenarios 5 and 6, how the single plume has a slight deviation to its west side all along the water column.

5.5 Conclusions

The hydrothermal plume developed in basin B1 is generated by a forcing disk with spatial inhomogeneity in the heat flux.

The hydrothermal plume is formed by several single plumes with independence of time. The number of these single plumes is highly variable with time and scenario.

In the stratified water column cases, when the Richardson number is higher than 11 the thermocline acts as a barrier to the vertical development of the hydrothermal plume.

In all the cases studied, while the model is capable of describing both the vertical and horizontal extensions of the hydrothermal plume, it generally overestimates the velocity values by at least one order of magnitude.

The same conclusions apply to the single plume in basin B2, while in that case, horizontal values found by the model are in agreement with those found experimentally.

The model gives the expected change in the sense of the current developed around the hydrothermal plume (cyclonic on the forcing disk and anti-cyclonic at the detrainment depth) although this could not be measured experimentally by the ADCP.

Model does not give a single vortex developed around the forcing disk because the number of vortices falls between 0.6 and 1. From the experimental results we can not state that a single vortex is formed.

More work should be done in order to better adjust the model results to the experimental data to see which are the input variables that affect the hydrothermal plume evolution in time.

Reference List

Adcroft, A., C. Hill, J-M. Campin and J. Marshall, 2005. Overview of the formulation and numerics of the MITgcm. M.I.T. Climate Modelling Initiative www-paoc.mit.edu/cmi/ECMWF2004-Adcroft.pdf

Legg, S., Jones, H. and M. Visbeck, 1996. A heton perspective of baroclinic eddy transfer in localized open ocean convection. *Journal of Physical Oceanography*, 26, 2 251-2 266.

Legg, S., Julien, K., Mc. Williams, J., and J. Werne, 2001. Vertical transport by convection plumes: Modification by rotation. *Physics and Chemistry of the Earth(B)*, 26 (4), 259-262.

Lowell, R.P., and L.N. Germanovich, 1995. Dike Injection and the Formation of Megaplumes at Ocean Ridges, *Science*, 267, 1804-1807.

Marshall, J., C. Hill, L. Perelman , C. Heisey and A. Adcroft, 1997. Hydrostatic, quasi-hydrostatic, and non-hydrostatic ocean modeling, *Journal of Geophysical Research,* 102(C3), 5753-5766.

Maxworthy, T. and S. Narimousa, 1994. Unsteady, turbulent convection into a homogeneous, rotating fluid, with oceanographic applications. *Journal of physical oceanography*, 24, 865-887.

Narimousa, S., 1996. Penetrative turbulent convection into a rotating two-layer fluid. *Journal of Fluid Mehanics*, 321, 299-313.

Okada, N., M. Ikeda, and S. Minobe (2004), Numerical Experiments of Isolated Convection under Polynya, *J. Oceanogr.*, *60*, 927-943.

Palmer, M.R., and Ernst, G.G.J., 1998. Generation of hydrothermal megaplumes by cooling of pillow basalts at mid-ocean ridges, *Nature*, 398, 643-647.

Pham, M.V., Plourde, F., Kim, S.D. and S. Balachandar, 2006. Large-eddy simulation of a pure thermal plume under rotating conditions. *Physics of fluids, 18,* (1), 015101.1-015101.15.

Serra, T., J. Colomer, R. Julià, M. Soler and X. Casamitjana, 2005. Behaviour and dynamics of a hydrothermal plume in Lake Banyoles, Catalonia, *Sedimentology 52*(4), 795-805.

Speer, K.G. and J. Marshall, 1995. The growth of convective plumes at sea floor hot springs. *Journal of Marine Research,* 53, 1025-1057.

6 Summary and conclusions

The aim of this PhD was to provide more insight into the convection processes that develop from finite sources in stratified and mixed environments. Experimental field data (taken from the hydrothermal sources B1 and B2 at Lake Banyoles), and computing simulations, were compared to the corresponding theoretical predictions for hydrothermal plumes. Field measurements were taken at Lake Banyoles as the lake affords uniquely suitable conditions for the present study. Whole field campaigns were programmed to show the main characteristics of hydrothermal sediment-laden plumes developing in the lake and their effects on water quality. The plumes were found to develop from warm sediment interfaces (lutoclines) whose evolution over time was also determined and found to be closely related to anomalous rainfall.

6.1 Relationship between sediment fluidization events and anomalous rainfall.

The characteristic rainfall, described by means of the atmospheric patterns over the recharge area of the aquifer that feeds water into Lake Banyoles, was analyzed. Among the 19 atmospheric circulation patterns identified by Romero et al. (1999) for the western Mediterranean area, seven were found to be responsible for the heavy or torrential rainfall over the recharge area and associated with sediment fluidization events in the lake. Three atmospheric patterns were Atlantic related, three were Mediterranean related types and the seventh had a dipolar pattern (with its high over the northern part of the area studied and its low over the southern part of the area). In Lake Banyoles, the sediment fluidizations at the bottom of basin B2 were analyzed from 1986 and 11 cases were described (from F1 to F11). Out of the 11 fluidization processes, 6 took place in the seasons of expected maximum rainfall, i.e. spring and autumn, 4 took place in winter, and only F6 initiated a fluidization in the summer season.

Two types of rainfall episodes were found to act as precursors of fluidizations:

a) Moderate to heavy rainfalls occurring over a few days, possibly of a torrential character on some days, as in fluidizations F3, F5, F6, F7, F9, F10 and F11.

b) Light to moderate rainfall, but extending –intermittently– over a sufficiently long period (months), as in F4 and F8.

In the fluidization process it was found that the lutocline of B2 migrated a maximum distance of 22-24 m and lasted for several months (in the order of 8 months). The largest fluidizations observed showed a vertical excursion of the lutocline that coincided with the depth of the B2 basin. Some fluidizations even flooded of the basin because at the south of Basin B2 the depth is about 20-22 m.

Finally, consecutive fluidizations were found. In such cases although in a small amount the input of water in the aquifer increased again, as a result, the water entering an already fluidized bed produced a secondary migration of the

lutocline that reached upper distances, i.e. less depth if measuring from the water surface, as in the cases of F3-F4 and F10-F11.

6.2 Basin B1

The development of the chronic hydrothermal plume in basin B1 was studied. It was found that changes in its vertical development depended on the seasonal meteorological conditions because of changes in the ambient stratification of the water column, where the thermocline acts as a barrier to vertical development. Hydrothermal plume height, calculated from the models, was in agreement with the experimental results found during the field campaigns.

Following the intensive field campaign carried out between October 2003 and November 2004, spatial inhomogeneities were found within the hydrothermal plume in B1. This spatial variability in hydrothermal plume development is produced by inhomogeneity in the lutocline temperature. This variation can be attributed to the inhomogeneity in the temperature lutocline, or also to the lateral entrainment of colder water above the lutocline (an increase in the density anomaly can produce an increase in buoyancy which in turn produces more lateral entrainment). Both mentioned processes can be responsible of the difference in buoyancy values which in turn resulted in different maximum spatial heights of the hydrothermal plume.

6.3 Basin B2

As was found from the ADCP velocity profiles, the fluidization in basin B2 presented time variability:

Period 1: At the beginning of the fluidization, a single plume develops, which is caused by the fact that the lutocline is still consolidated and the water springs flow through preferential paths. This regime, known as "single-plume convection", develops in a baroclinically stable regime (R_{oR}>0.2, where $R_{oR}=(B_o/(f^3\ R^2))^{1/4}$) when the ratio between the radius of the source and its height is smaller than 0.7, R/H<0.7 . This new regime, in which multiple convective plumes do not fully develop, has until now only been found in

numerical experiments, and it is found experimentally for the first time in this study.

Period 2: When subterranean springs in B2 have resuspended the confined and consolidated sediment at the bottom, its behavior is like the chronic plume in B1. Instead of entering through constrained paths, all the sediment below the lutocline is fluidized and a hydrothermal plume generates above it. This hydrothermal plume has the same characteristics like that in B1.

This change in B2 dynamics generates an important variation in the upward velocity. When water enters through preferential paths, the water pressure through small diameter sources causes a high mean upward velocity: w=0.05 m/s. After this, there is a transition period, when, as the incoming water resuspends the confined sediment, there is more than one preferential path. This causes water pressure to decrease and upward velocity also starts to decrease. Finally, when the sediments are totally fluidized, as can be found in basin B1, where the chronic hydrothermal plume develops, preferential paths disappear, and the sediment in B2 behaves like that in B1 which corresponds to the development of a hydrothermal plume from a finite source. The upward velocity, then, equals settling velocity, and although it is too small to be detected by the ADCP, values of $0.521 \cdot 10^{-5}$ m/s were found from the laboratory sediment analysis.

The experimental results in basin B2 of Lake Banyoles confirmed the presence of a single-plume convection (with aspect ratio $R/H < 0.7$ and large R_D/R values: $25.8 < R_D/R < 37.9$). In this regime, the density anomaly scales to $g' \sim B_o^{2/3}H^{-1/3}$ and the radial velocity scales to $U_r \sim B_o^{1/3}R\ H^{-2/3}$; according to the scaling proposed by Okada et al. (2004). In this scaling it is important to notice that the density anomaly is independent of the radius of the forcing region. The R_D/R values found experimentally are larger than those found by numerical simulations caused by the small scale of the convection process and the situation (mid latitudes).

In the single-plume convection, an upward current transports light water from the lake bottom to the surface. In the vicinity of the surface, the water should flow outward. We were not able to observe this circulation at the surface probably because the available ADCP data had lost the first 2 m of the water column. In our field measurements no outward velocity was found, probably because of mixing at the lake surface resulting from daily stratification that extended through the first few meters. In all measurements the convection retained a columnar shape with a ring or band shape, with entrainment from the sides. As a consequence, the density scale seemed to be determined by baroclinic circulation. The vertical flow direction showed a net upward transport, and only slight downward velocity values around the region where the main upward transport was located.

The single plume in basin B2 was found to affect the circulation in this basin and, as a consequence, the circulation in the lake. The single plume gives a vertical flow with a preferred upward direction and also horizontal flow entrainment from its sides to its centre. The presence of the single plume also affects the water quality of the lake and changes the Secchi depth from ~8 m (when the single plume is not active) to ~1 m or even lower. As is the case with the plume in basin B1 (Serra et al., 2002), we should expect that the single plume in basin B2 will change the sedimentary records in Lake Banyoles. These changes might be expected with the frequency of the fluidization events of B2 as described in Colomer et al. (2002) and Soler et al. (2007).

6.4 MITgcm numerical model

The Model gives a hydrothermal plume formed by several single plumes with independence of time in accordance with the experimental data. The number of these single plumes is highly variable with time and scenario. The vertical development of the hydrothermal plume is limited by the thermocline when the Richardson number is higher than 11, as it was expected.

In all the cases studied the model is capable of describing both the vertical and horizontal extensions of the hydrothermal plume and also it is able to reproduce the change in the direction of the current that developed. In accordance with theory, this was cyclonic on the forcing disk and produced entrainment and anti-cyclonic at the spreading depth of the hydrothermal plume, which produced detrainment. But model overestimates the horizontal component velocity values of the hydrothermal plume in B1; always giving values big enough to be detected by the ADCP, while there is no ADCP signal. We have concluded that the model gives values at least one order of magnitude higher than experimental data. In the simulation of the single plume that developed in B2, the horizontal velocity values that were found were in accordance with experimental data. This overestimation has been attributed to the fact that the model's equations are derived for open convection from an isolated source without boundary constraints and velocities might not be completely vertical because of the V-shaped topography around the source in basin B1 and basin B2.

6.5 Suggestions for further work.

1. Future work should include more field measurements to enable further study of the spatial inhomogeneity of thermal convection on shorter scales.

In basin B1 (where due to its chronic character field campaigns can be carried out at any time) and in B2 whenever it is active, data should be taken from along the entire basin source for the study of spatial inhomogeneity. Instruments should also be deployed for a period of time to study temporal inhomogeneity.

In basin B2, the 3D development of the single plume could be usefully studied in order to show water circulation around it.

2. The MITgcm model should be tested in order to study:

a) the interaction between both hydrothermal plumes.

b) the differences in Lake Banyoles dynamics caused by variations in its environment. Because of climate change it would be interesting to explore different possible scenarios and to investigate the affects of these, i.e.:

b.1) if water temperature increases as a result of an increase in air temperature (IPCC, 2007).

b.2) if the entry of water into the lake through the bottom of the basins (via subterranean springs) decreases as a result of the reduction of precipitation in the recharge area (IPCC, 2007).

c) the change in the hydrothermal plume behaviour in basin B2 as a result of the change in the relationship between the source radius (R) and the lutocline depth (H) at the entry parameters.

Hydrothermal plumes are efficient mixing agents, and their turbidity has an important role in water quality, especially when we consider where the public water supply for Banyoles comes from. Knowledge of the evolution and spatial extension of fluidizations procures tools for the management of this system. When there are fluidization events, the supply of nutrients to the lake must be considerably increased, which results in large phytoplankton blooms. Therefore, the effect of the fluidizations and the development of the hydrothermal plume in B2 are of interest not only because of the physics of circulation itself but also because of their impact on the whole ecosystem.

Finally, we hope that the insight gained into the convection process in Lake Banyoles, and the evolution and causes of fluidization events, will benefit future studies of a lake rich in scientific interest.

Annex A

Above they can be seen ADCP backscatter transects along the Basin B2 in the southern lobe of Lake Banyoles for different days.

11/3/2003

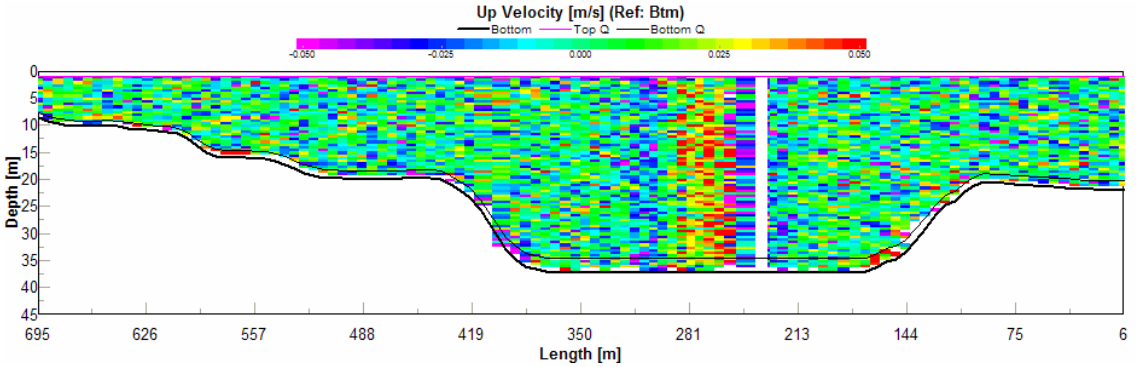

11/10/2003

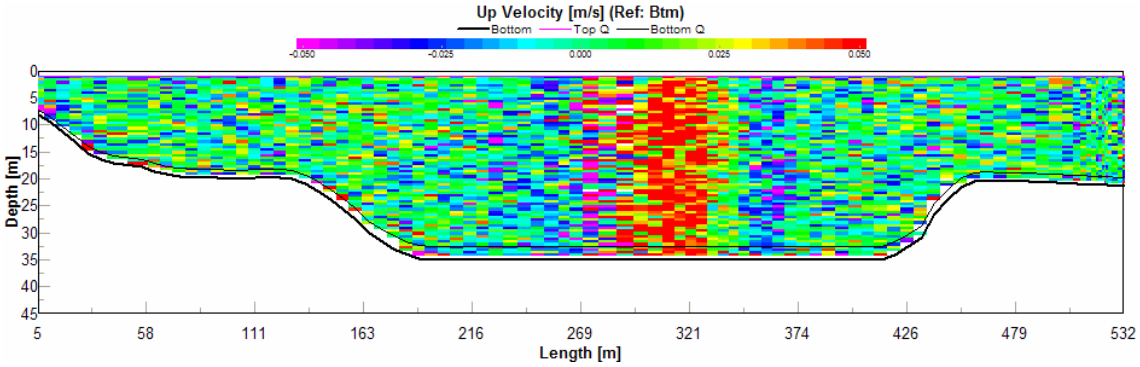

11/18/2003

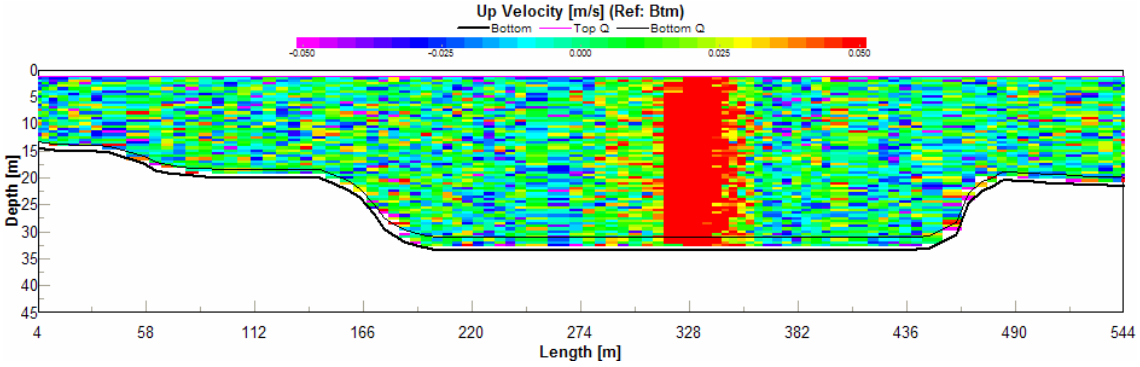

11/20/2003

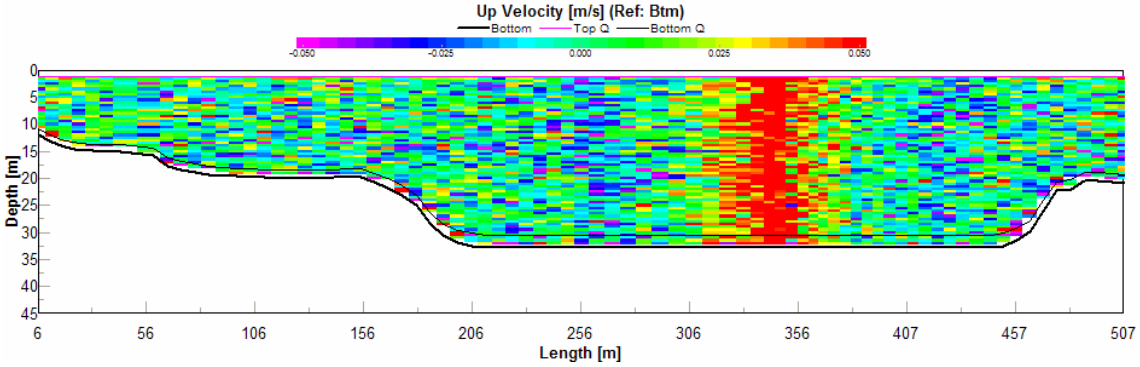

12/11/2003

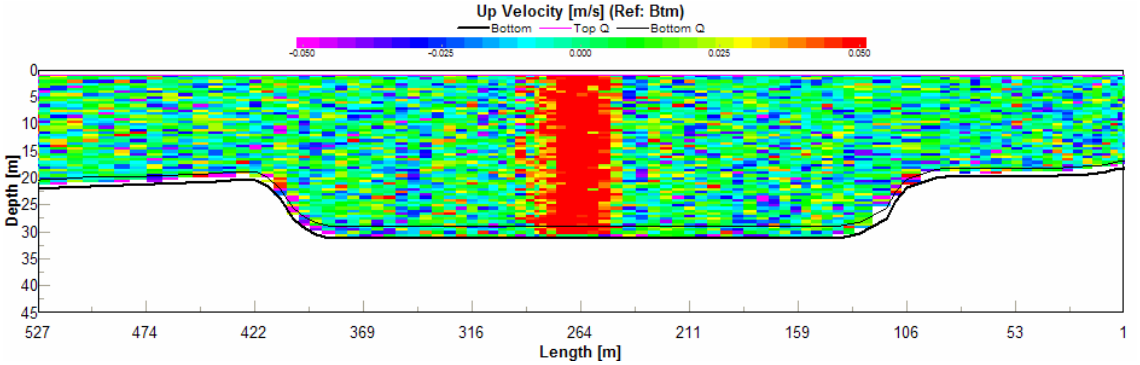

12/18/2003

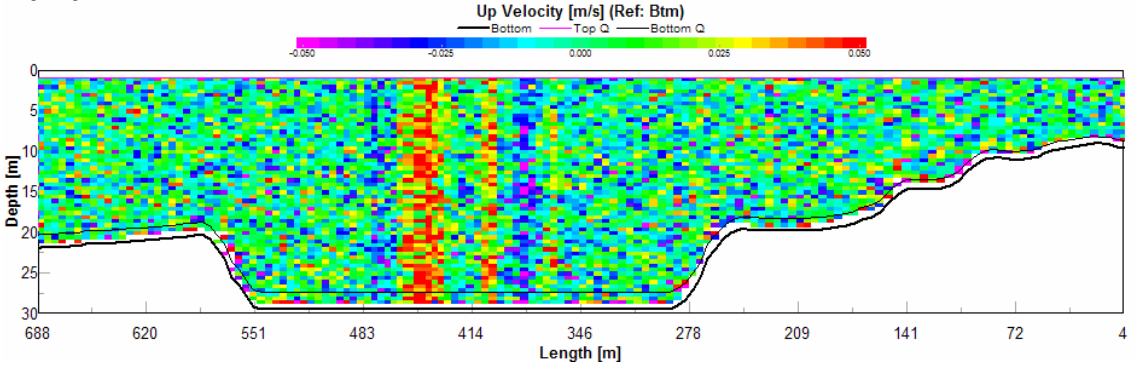

12/29/2003

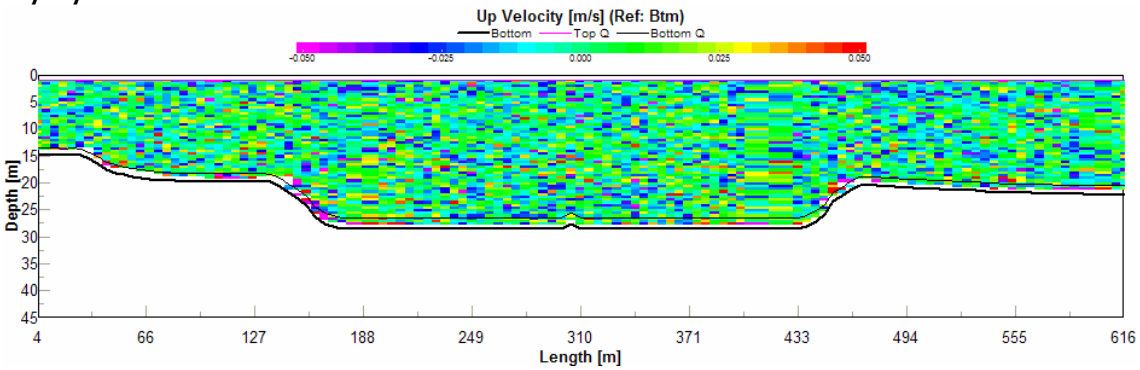

01/08/2004

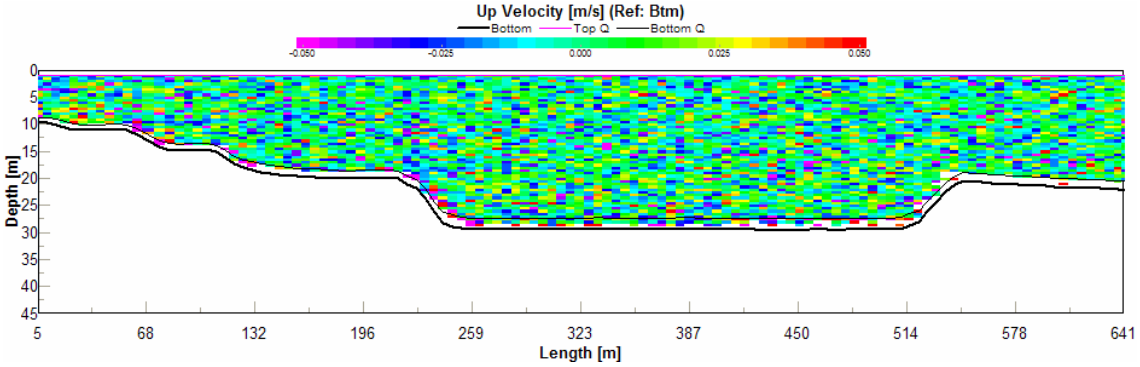
Up Velocity [m/s] (Ref: Btm)
Bottom
Top Q
Bottom Q
-0.050
-0.025
0.000
0.025
0.050
Depth [m]
0
5
10
15
20
25
30
35
40
45
5
68
132
196
259
323
387
450
514
578
641
Length [m]

Annex B

Oxygen (blue) and Chlorophyll (green) profiles in three points of the southern lobe of Lake Banyoles (basin 1, plain and basin 2) for a different days:

06/03/2004

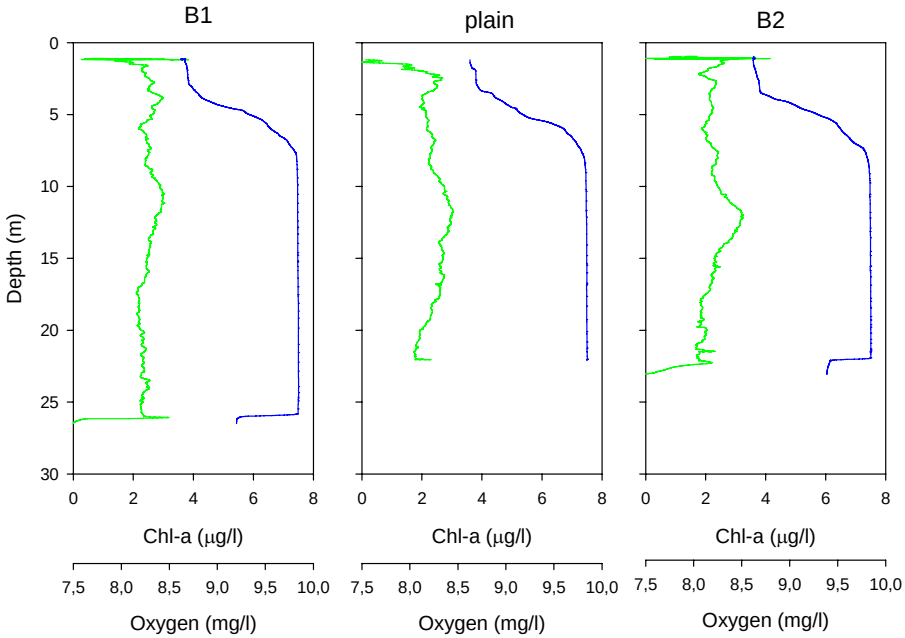

07/05/2004

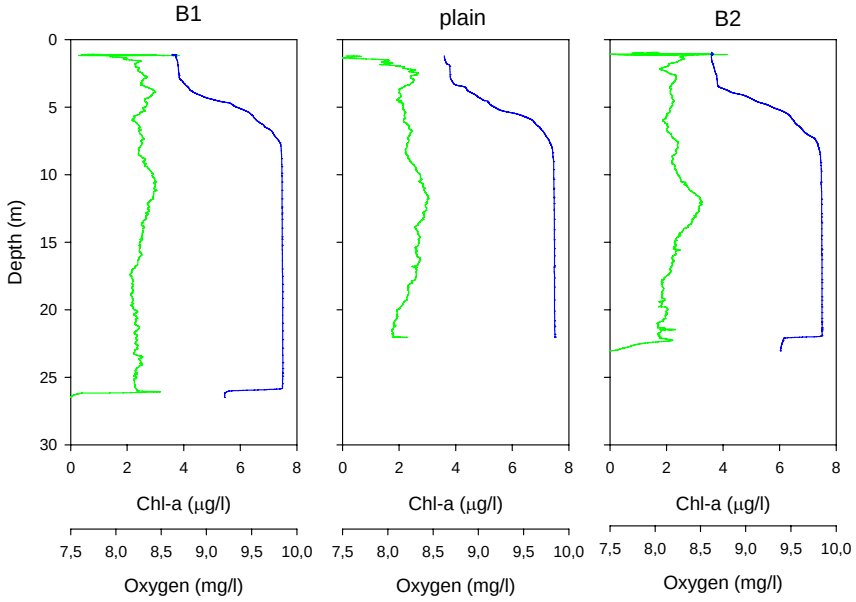

08/05/2004

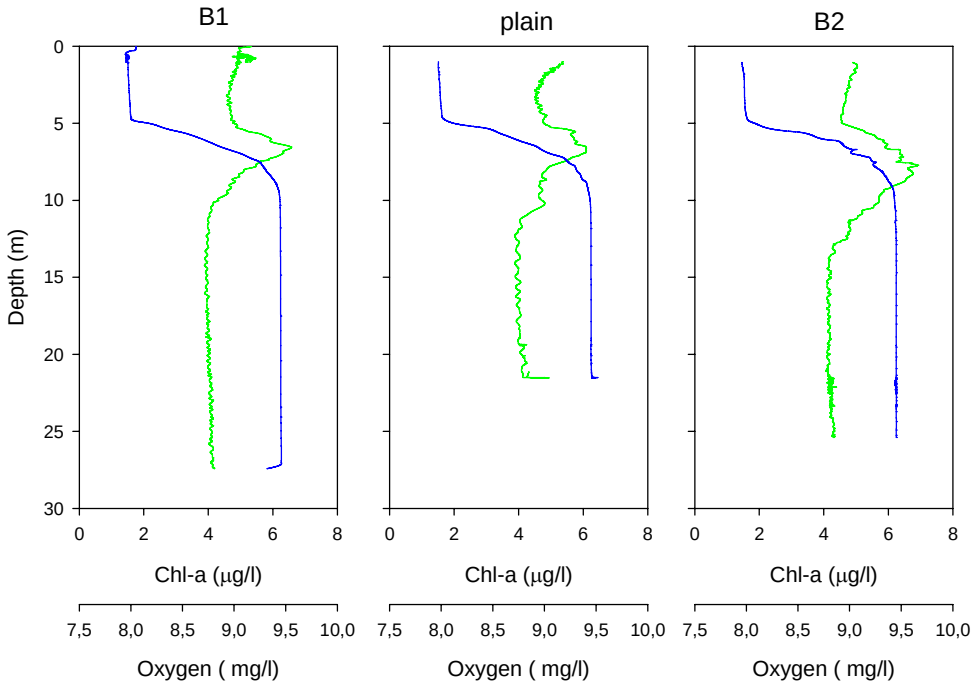
B1
plain
B2
Depth (m)
0
5
10
15
20
25
30
0
2
4
6
8
Chl-a (µg/l)
7,5
8,0
8,5
9,0
9,5
10,0
Oxygen (mg/l)